Manipulating Solubility and Dissolution through Multicomponent Crystallization

by

Zi Li

A dissertation submitted in partial fulfillment
of the requirements for the degree of
Doctor of Philosophy
(Chemistry)
in the University of Michigan
2016

Doctoral Committee:

Professor Adam J. Matzger, Chair
Assistant Professor Julie S. Biteen
Associate Professor Anne J. McNeil
Professor Naír Rodríguez-Hornedo

Acknowledgements

I would first like to thank my advisor, Professor Adam J. Matzger, for all his guidance and support all over my graduate studies at the University of Michigan. I am thankful for the way he teaches, and that I have learned so much, not only about chemistry but also in numerous other aspects, from his erudition, kindness, patience, frankness, and sense of humor. I cannot express how grateful I am for having such a great advisor throughout these years.

I am very thankful for all the members in the Matzger lab. I am thankful for Dr. Antek Wong-Foy, whose expertise in all instruments in the lab and willingness to help are indispensable for the normal operation of this lab. I am thankful for Dr. Onas Bolton, who kindly taught me so much about energetic materials and cocrystallization that greatly helped me in initiating my research on crystallization. I am thankful for Dr. Kira Landenberger, who kindly familiarized me with all aspects from research in the lab to life in Ann Arbor. I am thankful for Dr. Laura Pfund for her time helping me on instrument training, experiment instruction, and discussions over research. I am thankful to Jon for helping with TNT synthesis and discussions on crystallization. I am thankful to Jialiu for conducting the NMR examination of my cocrystal as well as being a caring friend. I am thankful for Dr. Rajesh Goud, Kortney, Kale, Rosalyn and Derek for all their helpful discussions and advice on my research and written work. Thanks to all the other members, from past to present including Jeremy, Rachel, Ping, Ananya, Jake, Chengcheng, Ren, Shantel, Zohaib, Ly, Saona, Yiyang, Nipuni, Ramanpreet, Matias, Nilanjana and Dr. Liu; I appreciate the time spent with all of you.

I would like to express my thanks to Professor Mark Meyerhoff for the great collaboration opportunity with his lab. Further thanks are due to my collaborator, Yaqi, with whom I had great time both doing research and having fun. I am thankful for Yaqi and Dr. Elizabeth Brisbois for making the SNAP/polymer materials and conducting the shelf-life studies. The collaboration experience was very valuable to me.

I am also very thankful to my committee members. I would like to thank Professor Na ŕ Rodr ǵuez-Hornedo for valuable discussion on cocrystal stability and dissolution experiments. I am thankful for Professor Anne McNeil for having discussions on polymers. I would like to thank Professor Julie Biteen, who was my advisor during my first rotation at University of Michigan, for helping me so much with my transition to the role of a graduate student.

I am thankful for Dr. Jeff W. Kampf for single crystal analysis of the CBZ/PABA 4:1 cocrystal. I am also thankful for Bing Fu for the help with the use of Matlab software in the SNAP solubility studies.

Thanks are extended to friends I met here in Ann Arbor. I would like to thank those people in the Department of Chemistry, including Yue (Sherry), Meng, Huiqing, Peipei, Chuan, Hang, Tao, Teppei, Laura, and Ted, for their help in both academics and other aspects. I would also like to thank Chuan and Xiaoyu, for inviting me to interesting activities as well as their wedding ceremony.

I am so grateful for my friends in China and other countries in the world, either those I met in school or online, for keeping the connection across the earth. I really cherish

the time they spend talking and listening to me. I am supported by their friendship all the time. Special thanks go to my favorite historical personage, by whom I have been encouraged to go forward throughout these years.

Last and the most important thanks are to my family, to whom I owe the most. There aren’t words to express my gratitude to my parents for all their love and support through all these years since I was born.

Table of Contents

List of Figures

List of Tables

Abstract

Chemical entities can be arranged into different packing motifs, leading to variation in properties of solid materials. Solid form optimization is a critical approach to material development and here crystallization systems with multiple components are investigated to improve performance in specific applications of biomedical relevance.

Cocrystallization is a technique to optimize solid forms by introducing a neutral coformer to form multicomponent crystal with the target molecule; this method shows great potential to improve the dissolution of poorly soluble compounds. In some systems, a compound can form cocrystals in multiple stoichiometries with the same coformer. A novel carbamazepine /p-aminobenzoic acid 4:1 cocrystal is discovered and structurally characterized. Phase stability data demonstrate that it is a thermodynamically unstable form. Dissolution experiments reveal that for cocrystallization pairs with multiple stoichiometries accessible, cocrystal stoichiometry is not the only factor that determines the dissolution rate; intermolecular interactions within the crystal play a vital role. This project answers the question how coformer stoichiometry influences dissolution.

Solid state studies of a class of *S*-nitroso-*N*-acetyl-D-penicillamine (SNAP)-doped polymer materials that achieve prolonged and localized delivery of nitric oxide (NO) for potential biomedical applications are conducted to investigate the mechanism of the long-term storage stability and sustained NO release. Crystalline SNAP is detected in polymers during solid state characterization and a crystallization based theory is

proposed wherein SNAP molecules are partially solubilized in polymers, and the excess SNAP beyond the solubility limit crystallizes and embeds in the polymer. Solubility of SNAP in polymer has been determined by PXRD analysis. It is proposed that the lattice energy of crystalline SNAP is the key to the stability improvement, while the solubilized SNAP is more reactive that decomposes and releases NO. It is the first time that the stability mechanism of this system has been investigated; this crystallization based hypothesis has been tested in other SNAP/polymer composites.

It is proposed that the unsuccessful cocrystallization between a target compound and a poorly soluble coformer can be a kinetic result of the coformer solubility limit, which favors the formation of single component crystals that compete with the hypothetical cocrystals. In order to retain a high degree of coformer supersaturation in solution favorable for cocrystallization, soluble polymeric additives were employed. It was demonstrated that solubility and metastable limit of poorly soluble compounds can be altered in presence of soluble polymers. Therefore, utilization of polymer additives is a feasible approach to adjust the metastable zone width which is a potential strategy to facilitate the growth of unattainable cocrystals.

Chapter 1 Introduction

1.1 The Variety of Crystalline Forms

Chemical entities, such as atoms, molecules and ions, can be arranged into more than one solid form. In contrast to glasses or amorphous solids which lack three-dimensional long-range order, a material is classified to be crystalline if it packs in an infinite three-dimensional array. Crystalline materials are commonly utilized in a wide range of fields because of their chemical and formulation stability. Another benefit to crystallinity is better ease of manufacturing.

For a given crystallizing component, various crystallization conditions (solvent, degree of supersaturation, crystallization temperatures, etc.) can lead to a different packing motif, which results in multiple polymorphs.[1-12] An example of polymorphism is the pentamorphic compound tolfenamic acid, a nonsteroidal anti-inflammatory drug (NSAID) with five polymorphs that can be visually distinguished under optical microscope by the morphology variation from needles, prisms to plates.[4] Flufenamic acid, another NSAID, possesses at least nine polymorphs with eight structurally characterized, has been a record holder for structurally characterized drug presenting polymorphism.[5] Polymorphism is a general crystallization behavior that is not exclusively detected in pharmaceuticals. For example, energetic materials can be polymorphic as well. Five polymorphs of a relatively new energetic compound 2,4,6,8,10,12-hexanitro-2,4,6,8,10,12-hexaazaisowurtzitane (CL-20) have been discovered.[14] For the benchmark energetic material 2,4,6-trinitrotoluene (TNT), two

polymorphs are reported (Figure 1.1).[13] The constituents of all polymorphs are the same. However, the properties of polymorphs vary due to their diverse packing motifs as a result of the differences in intermolecular interactions.

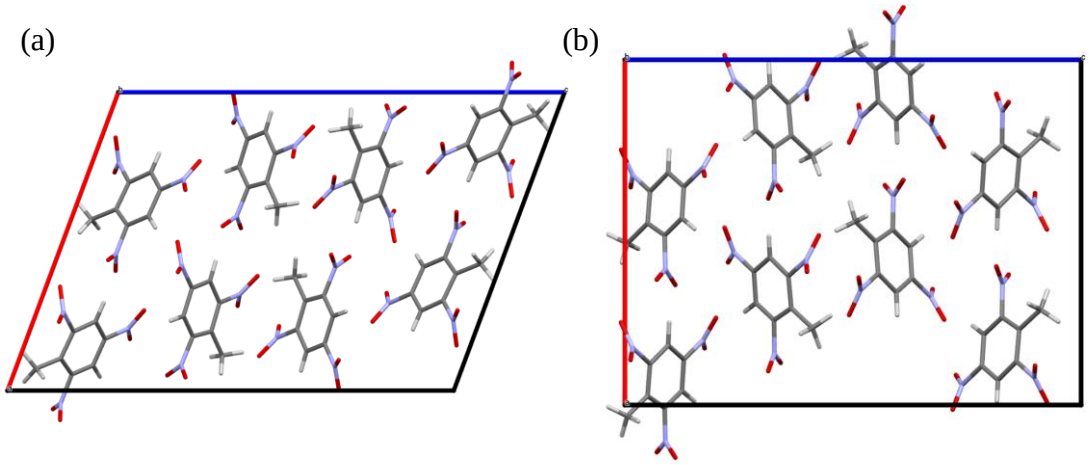

Figure 1. 1 Packing of (a) monoclinic and (b) orthorhombic TNT.[13]

Aside from single component polymorphs, crystals with two or more components can also be obtained (Figure 1.2). Salts are ionic multicomponent crystals consisting of at least two groups of oppositely charged ions that can pack into overall electrically neutral products.[15-20] In contrast to salts, cocrystals, consist of neutral molecular components that pack in a defined ratio.[6, 21-25] When a single component of a crystallizing unit is a liquid at room temperature, the multicomponent crystals formed are classified as solvates.[26] For instance, hydrates are the most commonly seen solvates, with water molecules included in the crystal lattices. With the introduction of one or more coformers that build intermolecular interactions with target chemical entities, the number of possible crystal structures can be greatly increased.

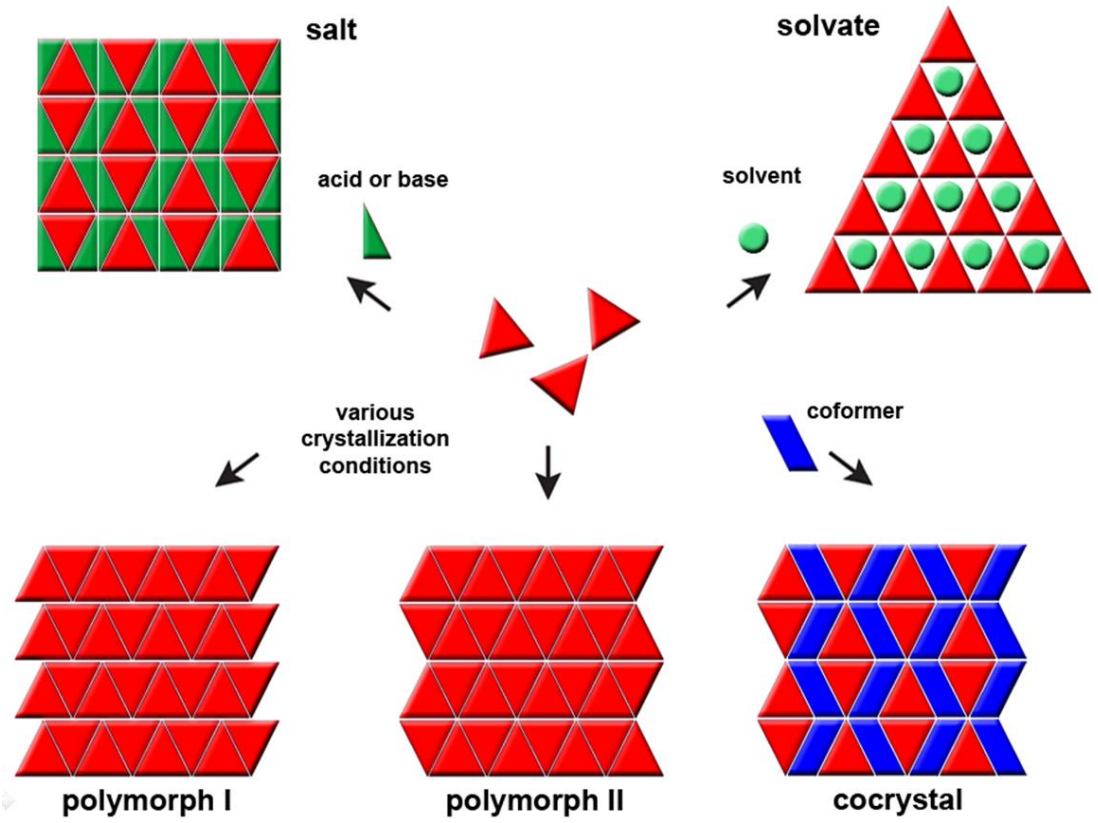

Figure 1. 2 Single component and multicomponent crystalline forms of a given chemical entity (represented by red triangles). Polymorphs consist of only one component packing into different motifs can be obtained under various crystallization conditions. By introducing ions (dark green triangles), solvents (light green circles) or coformers (blue parallelograms), multicomponent crystals including salts, solvates and cocrystals can be obtained.

Polymorphism can arise within multicomponent crystals as well (Figure 1.3).[27-29] Polymorphic cocrystals can be obtained from polymorphic coformers.[30] For instance, two polymorphs of carbamazepine-nicotinamide (CBZ-NCT) cocrystals and two polymorphs of carbamazepine-saccharin (CBZ-SAC) cocrystals can be grown by solvent evaporation in presence of various insoluble polymer heteronuclei, while carbamazepine is a pentamorphic compound.[6] Five anhydrous polymorphs of furosemide-nicotinamide 1:1 cocrystal have been discovered and characterized by powder X-ray diffraction (PXRD) and differential scanning calorimetry (DSC).[26] Although the reported number of cocrystal polymorphs is less than that of single

component crystal polymorphs, there is no statistical evidence that can prove reduced polymorphism in cocrystals.[31] The lack of knowledge of cocrystal polymorphism may be due to the incompatibility between current screening methods and the specific crystallization condition required for the target cocrystals formation. Taking polymorphism of multicomponent crystals into consideration, the options for crystalline form optimization can be expanded to a larger extent.

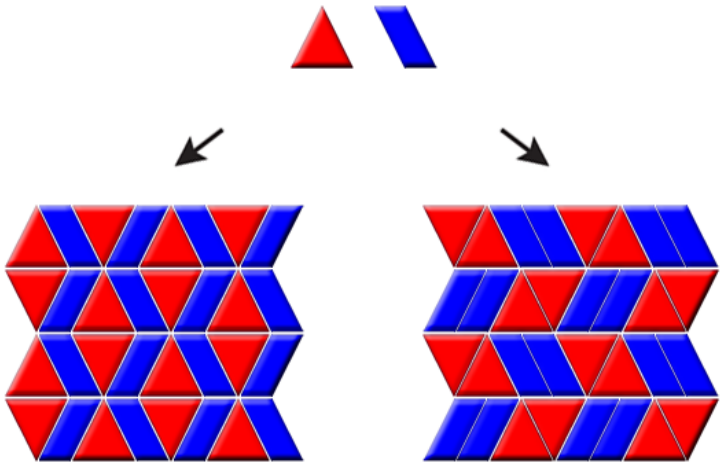

Figure 1. 3 Polymorphism in cocrystals. The two cocrystals are of the same constituents and stoichiometry, but the packing motifs are different.

1.2 Polymorph Selection and Multicomponent Crystal Development for Improved Solid Materials

All the variations in crystal structure, from packing motifs to constituent stoichiometry, result from differences in intermolecular interactions. Because crystalline material properties are highly dependent on the various intermolecular interactions between crystallizing components, knowledge of possible forms of target materials, as well as appropriate solid form selection, is essential for manufacturing.

Material properties that are crucial for application, such as density, hardness, melting point, stability, solubility, dissolution rate and color, can be vary in different

polymorphs.[1-5, 7, 9-12, 32] By altering the polymorph of a target chemical, the particular property of the solid material can be improved. Therefore, polymorphism has been extensively investigated for the sake of solid form optimization. Additionally, transformation from a metastable polymorph to other forms can occur during substance manufacturing, accompanied by undesirable changes in properties. A significant example is ritonavir, whose final drug product started failing the dissolution test after being introduced to the market. It was then recognized that the product converted to a thermodynamically more stable form which is much less soluble in the solvents used for formulation that precipitated out of solution. If the more stable form were discovered before putting ritonavir into market, such economic loss could have been prevented.[33] On the other hand, although metastable forms can suffer from undesired phase conversion, their relatively high solubility and weak stability can be beneficial in applications depends on the goal. Consequently, in order to avoid unexpected phase conversion and optimize material performance, it is of great importance to gain knowledge of all possible polymorphs before scaling up production.

Multicomponent crystal formation is an alternative strategy for new formulations of existing chemical entities when all single component polymorphs of the target compound fail to meet property requirements for an application. Salt formation has been established as a feasible approach to alter material properties.[15-20] There are vast examples of promoted solubility and dissolution rate of salts relative to the single component materials. However, for nonionizable entities that cannot form salts with counter ions, salt formation is not achievable. In such cases, cocrystallization becomes an attractive alternative.

Properties of cocrystals can differ greatly from those of their pure components. In some cases cocrystals combine the advantages of the pure components and, thus, can

meet application benchmarks that the pure component materials originally failed to meet.[21-25, 34-36] Cocrystallization has triggered interest in solubility and dissolution rate improvement for pharmaceutical materials.[37-39] Another good example is explosives: with the requirement of the rigid performance target and economical production, a new tactic to improve explosive materials is to develop formulations of existing energetic entities. By cocrystallization, it is possible to improve the stability of an energetic material without harming the explosive power. Despite the high density, desired oxygen balance and high explosive power, the energetic compound CL-20 is too sensitive for extensive applications. By cocrystallizing CL-20 with the explosive 1,3,5,7-tetranitro-1,3,5,7-tetrazacyclooctane (HMX) in a 2:1 stoichiometry, the obtained cocrystal presents low sensitivity which is comparable to the "safer" HMX. This stability has been attributed to the increased degree of hydrogen bonding in the cocrystal structure relative to the single component forms of either coformer. At the same time, the predicted detonation velocity of the cocrystal is still higher than the most powerful pure form of HMX.[22] The increased strength of intermolecular interactions with the introduced coformer allow for greater availability of solid state optimization.

1.3 Application of Polymers in Crystallization

There are multiple roles that can be played by polymers during crystallization process. Adjusting crystallization variables including temperature, solvent and degree of supersaturation are common strategies for crystalline form discovery and selection. However, these approaches do not explicitly target the vital nucleation step that determines the final solid state form. A variety of materials can be applied as heterogeneous particles or surfaces to facilitate nucleation by lowering the energy barrier.[40-44] Among them, polymer-induced heteronucleation (PIHn), a methodology developed to direct and control nucleation via interactions between a crystallizing component and functional groups of cross-linked insoluble polymer heteronuclei at

the interface (Figure 1.4), enables a high throughput modality that allows a large amount of experiments for polymorph discovery and selection to be run at the same time by replacing polymer heteronuclei without changes in solvent, temperature or degree of supersaturation. A phase-selection mechanism for PIHn has been proposed based on combined experimental and computational studies, indicating that the polymorph selection process is dependent on the affinity of the functional group on the surface of the polymer heteronucleants to the crystallizing components, which can be affected by both the polymer surface and the solvent media.[45] The compatibility between PIHn and several high throughput polymorph screening techniques is another plus. PIHn has been developed into a high density format of micro PIHn plate with 288 distinct polymers as the heteronuclei on a standard quartz microscope slide, which further decreases the total amount of materials used for polymorph screening.[46]

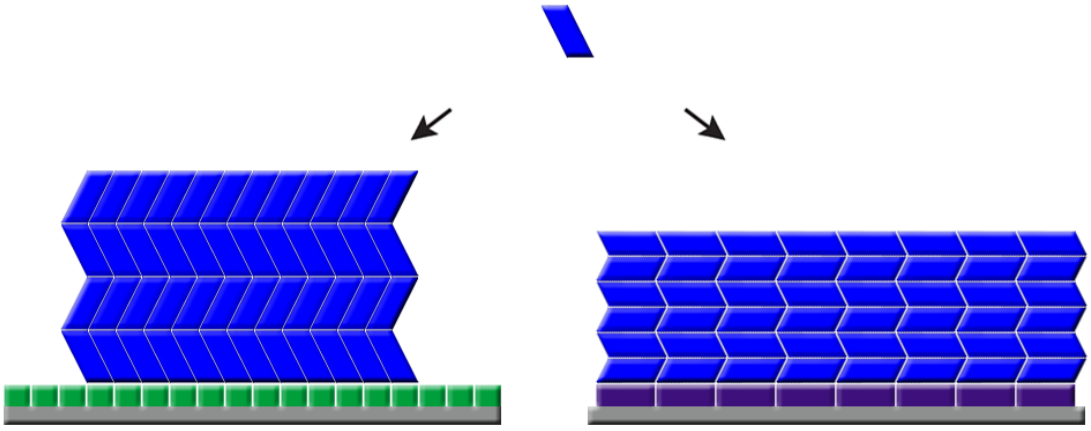

Figure 1. 4 Schematic representation of polymer induced heteronucleation (PIHn). Form selection of target molecule (blue parallelograms) is achieved by insoluble polymers with various functional groups (green squares and purple rectangles) at the solution-polymer interface to facilitate the formation of target nuclei.

In contrast to insoluble polymers that serve as heteronuclei to facilitate nucleation, soluble polymers can be utilized as crystallization inhibitors to prolong supersaturation in solution, as well as maintain the desired high energy amorphous forms of materials for the sake of solubility enhancement.[47-50] Unlike insoluble

heteronuclei that stabilize nuclei of a target polymorph, soluble polymers can adsorb onto specific faces of a crystal in solution, therefore preclude crystal growth perpendicular to that face (Figure 1.5). Such inhibition effect can be an alternative approach to solid form selection by impeding the formation of unintended forms.[51-55]

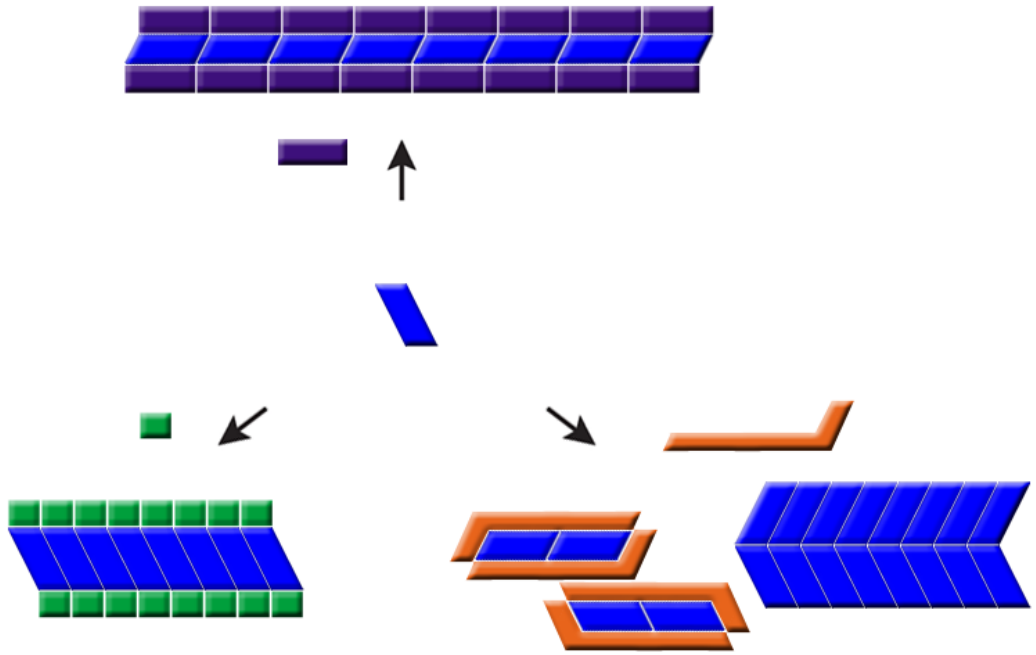

Figure 1. 5 Schematic representation of how soluble polymer additives influence crystallization in solution. Polymorph selection can be achieved by soluble polymer additives (green squares and purple rectangles) adsorbing onto specific faces of a crystal in solution, which preclude crystal growth perpendicular to that face. The formation of undesired form can be prevented by the polymeric inhibitor (orange polygons), allowing access to other forms that are slow to nucleate or grow.

The heteronucleation induced by insoluble polymer and the inhibition effect of soluble polymer additives are two sides of the same coin. If a soluble additive enables strong intermolecular interactions with a target crystallizing compound that lead to significant inhibition of crystal growth in solution, the specific functional group responsible for the interactions can be transformed into an insoluble heteronuclei which stabilizes the target nuclei on the interface and promote crystallization.[56] In addition, compounds can be incorporated onto polymer substrates to form

crystal/polymer composites.[57, 58] With all possibilities of various functionalities, non-crystalline polymers are predestined to be an indispensable part in the development of crystalline materials.

1.4 Organization of Thesis

Chapter 1 gives a brief introduction to select crystalline forms including single component polymorphic crystals and multicomponent crystals. Examples of crystalline material optimization by polymorph selection and multicomponent crystal formation are provided. The influences of both insoluble polymer heteronuclei and soluble polymer additives on crystallization are discussed with a brief discussion of mechanism.

Chapter 2 focuses on cocrystals with multiple stoichiometric ratios. A novel carbamazepine (CBZ)/p-aminobenzoic acid (PABA) 4:1 cocrystal has been discovered. The metastability of this 4:1 cocrystal has been elucidated by a series of characterization experiments. Dissolution experiments of CBZ/PABA cocrystals with three different stoichiometries have been conducted to elucidate the impact of cocrystal stoichiometry on compound dissolution.

Chapter 3 discusses solid state studies of a series of nitric oxide releasing materials: *S*-nitroso-*N*-acetylpenicillamine (SNAP)/polymer composites. The improved material stability is attributed to SNAP crystallization within the polymer, which has been verified using solid state characterization methods. Calculation of SNAP solubility in polymers is also demonstrated. The crystalline based stability mechanism has been verified by composites prepared with different polymers or by different methods.

Chapter 4 proposes a cocrystallization approach by using soluble polymer additives that can adjust coformer metastable zone to overcome kinetic barriers. It is shown that soluble polymers successfully alter the solubility and metastable limit of select compounds. Various effects of polymeric additives on cocrystallization are discussed.

1.5 References

(1) Khoshkhoo, S.; Anwar, J. Crystallization of polymorphs: the effect of solvent. *Journal of Physics D: Applied Physics* **1993,** *26*, B90.

(2) Threlfall, T. Crystallisation of polymorphs: Thermodynamic insight into the role of solvent. *Organic Process Research and Development* **2000,** *4*, 384-390.

(3) Price, C. P.; Grzesiak, A. L.; Lang, M.; Matzger, A. J. Polymorphism of Nabumetone. *Crystal Growth & Design* **2002,** *2*, 501-503.

(4) López-Mejías, V.; Kampf, J. W.; Matzger, A. J. Polymer-Induced Heteronucleation of Tolfenamic Acid: Structural Investigation of a Pentamorph. *Journal of the American Chemical Society* **2009,** *131*, 4554-4555.

(5) López-Mejías, V.; Kampf, J. W.; Matzger, A. J. Nonamorphism in Flufenamic Acid and a New Record for a Polymorphic Compound with Solved Structures. *Journal of the American Chemical Society* **2012,** *134*, 9872-9875.

(6) Porter Iii, W. W.; Elie, S. C.; Matzger, A. J. Polymorphism in Carbamazepine Cocrystals. *Crystal Growth & Design* **2008,** *8*, 14-16.

(7) Chen, S.; Guzei, I. A.; Yu, L. New Polymorphs of ROY and New Record for Coexisting Polymorphs of Solved Structures. *Journal of the American Chemical Society* **2005,** *127*, 9881-9885.

(8) Han, G.; Chow, P. S.; Tan, R. B. H. Growth Behaviors of Two Similar Crystals: The Great Difference. *Crystal Growth & Design* **2015,** *15*, 1082-1088.

(9) Lang, M.; Kampf, J. W.; Matzger, A. J. Form IV of carbamazepine. *Journal of Pharmaceutical Sciences* **2002,** *91*, 1186-1190.

(10) Grzesiak, A. L.; Lang, M.; Kim, K.; Matzger, A. J. Comparison of the Four Anhydrous Polymorphs of Carbamazepine and the Crystal Structure of Form I*. *Journal of Pharmaceutical Sciences* **2003,** *92*, 2260-2271.

(11) Snider, D. A.; Addicks, W.; Owens, W. Polymorphism in generic drug product development. *Advanced Drug Delivery Reviews* **2004,** *56*, 391-395.

(12) Pfund, L. Y.; Chamberlin, B. L.; Matzger, A. J. The Bioenhancer Piperine is at Least Trimorphic. *Crystal Growth & Design* **2015,** *15*, 2047-2051.

(13) Vrcelj, R. M.; Sherwood, J. N.; Kennedy, A. R.; Gallagher, H. G.; Gelbrich, T. Polymorphism in 2-4-6 Trinitrotoluene. *Crystal Growth & Design* **2003,** *3*, 1027-1032.

(14) Xu, J.; Tian, Y.; Liu, Y.; Zhang, H.; Shu, Y.; Sun, J. Polymorphism in hexanitrohexaazaisowurtzitane crystallized from solution. *Journal of Crystal Growth* **2012,** *354*, 13-19.

(15) Jin, S.; Lin, Z.; Wang, D.; Chen, G.; Ji, Z.; Huang, T.; Zhou, Y. Crystal and molecular structure of four organic salts from benzylamine and carboxylic acids. *Journal of Chemical Crystallography* **2015,** *45*, 159-168.

(16) Berge, S. M.; Bighley, L. D.; Monkhouse, D. C. Pharmaceutical salts. *Journal of Pharmaceutical Sciences* **1977,** *66*, 1-19.

(17) Jin, S.; Feng, C.; Wen, X.; Wang, D. Crystal Structures of Two Salts from Piperidine, Naphthalene-1,5-Disulfonic Acid, and 4-Nitrophthalic Acid. *Journal of Chemical Crystallography* **2016,** *46*, 21-27.

(18) Morris, K. R.; Fakes, M. G.; Thakur, A. B.; Newman, A. W.; Singh, A. K.; Venit, J. J.; Spagnuolo, C. J.; Serajuddin, A. T. M. An integrated approach to the selection of optimal salt form for a new drug candidate. *International Journal of Pharmaceutics* **1994,** *105*, 209-217.

(19) Gould, P. L. Salt selection for basic drugs. *International Journal of Pharmaceutics* **1986,** *33*, 201-217.

(20) De Melo, C. C.; Da Silva, C. C. P.; Pereira, C. C. S. S.; Rosa, P. C. P.; Ellena, J. Mechanochemistry applied to reformulation and scale-up production of Ethionamide:

Salt selection and solubility enhancement. *European Journal of Pharmaceutical Sciences* **2016,** *81*, 149-156.

(21) Bolton, O.; Matzger, A. J. Improved Stability and Smart-Material Functionality Realized in an Energetic Cocrystal. *Angewandte Chemie International Edition* **2011,** *50*, 8960-8963.

(22) Bolton, O.; Simke, L. R.; Pagoria, P. F.; Matzger, A. J. High Power Explosive with Good Sensitivity: A 2:1 Cocrystal of CL-20:HMX. *Crystal Growth & Design* **2012,** *12*, 4311-4314.

(23) Landenberger, K. B.; Bolton, O.; Matzger, A. J. Two Isostructural Explosive Cocrystals with Significantly Different Thermodynamic Stabilities. *Angewandte Chemie International Edition* **2013,** *52*, 6468-6471.

(24) Landenberger, K. B.; Matzger, A. J. Cocrystal Engineering of a Prototype Energetic Material: Supramolecular Chemistry of 2,4,6-Trinitrotoluene. *Crystal Growth & Design* **2010,** *10*, 5341-5347.

(25) Landenberger, K. B.; Matzger, A. J. Cocrystals of 1,3,5,7-Tetranitro-1,3,5,7-tetrazacyclooctane (HMX). *Crystal Growth & Design* **2012,** *12*, 3603-3609.

(26) Ueto, T.; Takata, N.; Muroyama, N.; Nedu, A.; Sasaki, A.; Tanida, S.; Terada, K. Polymorphs and a Hydrate of Furosemide–Nicotinamide 1:1 Cocrystal. *Crystal Growth & Design* **2012,** *12*, 485-494.

(27) Bevill, M. J.; Vlahova, P. I.; Smit, J. P. Polymorphic Cocrystals of Nutraceutical Compound p-Coumaric Acid with Nicotinamide: Characterization, Relative Solid-State Stability, and Conversion to Alternate Stoichiometries. *Crystal Growth & Design* **2014,** *14*, 1438-1448.

(28) Powell, K. A.; Bartolini, G.; Wittering, K. E.; Saleemi, A. N.; Wilson, C. C.; Rielly, C. D.; Nagy, Z. K. Toward Continuous Crystallization of Urea-Barbituric Acid: A Polymorphic Co-Crystal System. *Crystal Growth & Design* **2015,** *15*, 4821-4836.

(29) Llinas, A.; Barbas, R.; Font-Bardia, M.; Quayle, M. J.; Velaga, S.; Prohens, R. Two New Polymorphic Cocrystals of Zafirlukast: Preparation, Crystal Structure, and Stability Relations. *Crystal Growth & Design* **2015,** *15*, 4162-4169.

(30) Lemmerer, A.; Adsmond, D. A.; Esterhuysen, C.; Bernstein, J. Polymorphic Co-crystals from Polymorphic Co-crystal Formers: Competition between Carboxylic Acid ··Pyridine and Phenol ··Pyridine Hydrogen Bonds. *Crystal Growth & Design* **2013,** *13*, 3935-3952.

(31) Vishweshwar, P.; McMahon, J. A.; Peterson, M. L.; Hickey, M. B.; Shattock, T. R.; Zaworotko, M. J. Crystal engineering of pharmaceutical co-crystals from polymorphic active pharmaceutical ingredients. *Chemical Communications* **2005**, 4601-4603.

(32) Price, C. P.; Grzesiak, A. L.; Matzger, A. J. Crystalline Polymorph Selection and Discovery with Polymer Heteronuclei. *Journal of the American Chemical Society* **2005,** *127*, 5512-5517.

(33) Chemburkar, S. R.; Bauer, J.; Deming, K.; Spiwek, H.; Patel, K.; Morris, J.; Henry, R.; Spanton, S.; Dziki, W.; Porter, W.; Quick, J.; Bauer, P.; Donaubauer, J.; Narayanan, B. A.; Soldani, M.; Riley, D.; McFarland, K. Dealing with the Impact of Ritonavir Polymorphs on the Late Stages of Bulk Drug Process Development. *Organic Process Research & Development* **2000,** *4*, 413-417.

(34) Hickey, M. B.; Peterson, M. L.; Scoppettuolo, L. A.; Morrisette, S. L.; Vetter, A.; Guzmán, H.; Remenar, J. F.; Zhang, Z.; Tawa, M. D.; Haley, S.; Zaworotko, M. J.; Almarsson, Ö. Performance comparison of a co-crystal of carbamazepine with marketed product. *European Journal of Pharmaceutics and Biopharmaceutics* **2007,** *67*, 112-119.

(35) Shan, N.; Zaworotko, M. J. The role of cocrystals in pharmaceutical science. *Drug Discovery Today* **2008,** *13*, 440-446.

(36) Desikan, S.; Parsons, R. L.; Davis, W. P.; Ward, J. E.; Marshall, W. J.; Toma, P. H. Process Development Challenges to Accommodate A Late-Appearing Stable Polymorph: A Case Study on the Polymorphism and Crystallization of a Fast-Track Drug Development Compound. *Organic Process Research & Development* **2005,** *9*, 933-942.

(37) Thakuria, R.; Delori, A.; Jones, W.; Lipert, M. P.; Roy, L.; Rodr ǵuez-Hornedo, N. Pharmaceutical cocrystals and poorly soluble drugs. *International Journal of Pharmaceutics* **2013,** *453*, 101-125.

(38) Roy, L., Co-crystal Solubility and Thermodynamic Stability. 2012; p 247.

(39) Good, D. J., Cocrystal Eutectic Constants and Prediction of Solubility Behavior. American Chemical Society: 2010; 'Vol.' 10, p 1028.

(40) Capacci-Daniel, C.; Gaskell, K. J.; Swift, J. A. Nucleation and Growth of Metastable Polymorphs on Siloxane Monolayer Templates. *Crystal Growth & Design* **2010,** *10*, 952-962.

(41) Mitchell, C. A.; Yu, L.; Ward, M. D. Selective Nucleation and Discovery of Organic Polymorphs through Epitaxy with Single Crystal Substrates. *Journal of the American Chemical Society* **2001,** *123*, 10830-10839.

(42) Kang, J. F.; Zaccaro, J.; Ulman, A.; Myerson, A. Nucleation and Growth of Glycine Crystals on Self-Assembled Monolayers on Gold. *Langmuir* **2000,** *16*, 3791-3796.

(43) Lee, A. Y.; Ulman, A.; Myerson, A. S. Crystallization of Amino Acids on Self-Assembled Monolayers of Rigid Thiols on Gold. *Langmuir* **2002,** *18*, 5886-5898.

(44) Ulman, A.; Kang, J. F.; Shnidman, Y.; Liao, S.; Jordan, R.; Choi, G.-Y.; Zaccaro, J.; Myerson, A. S.; Rafailovich, M.; Sokolov, J.; Fleischer, C. Self-assembled monolayers of rigid thiols. *Reviews in Molecular Biotechnology* **2000,** *74*, 175-188.

(45) López-Mejías, V.; Knight, J. L.; Brooks, C. L.; Matzger, A. J. On the Mechanism of Crystalline Polymorph Selection by Polymer Heteronuclei. *Langmuir* **2011,** *27*, 7575-7579.

(46) Pfund, L. Y.; Matzger, A. J. Towards Exhaustive and Automated High-Throughput Screening for Crystalline Polymorphs. *ACS Combinatorial Science* **2014,** *16*, 309-313.

(47) Rimer, J. D.; An, Z.; Zhu, Z.; Lee, M. H.; Goldfarb, D. S.; Wesson, J. A.; Ward, M. D. Crystal Growth Inhibitors for the Prevention of l-Cystine Kidney Stones Through Molecular Design. *Science* **2010,** *330*, 337-341.

(48) Ilevbare, G. A.; Liu, H.; Edgar, K. J.; Taylor, L. S. Impact of Polymers on Crystal Growth Rate of Structurally Diverse Compounds from Aqueous Solution. *Molecular Pharmaceutics* **2013,** *10*, 2381-2393.

(49) Ozaki, S.; Kushida, I.; Yamashita, T.; Hasebe, T.; Shirai, O.; Kano, K. Inhibition of crystal nucleation and growth by water-soluble polymers and its impact on the supersaturation profiles of amorphous drugs. *Journal of Pharmaceutical Sciences* **2013,** *102*, 2273-2281.

(50) Ilevbare, G. A.; Liu, H.; Edgar, K. J.; Taylor, L. S. Maintaining Supersaturation in Aqueous Drug Solutions: Impact of Different Polymers on Induction Times. *Crystal Growth & Design* **2013,** *13*, 740-751.

(51) Kitamura, M.; Ishizu, T. Kinetic effect of L-phenylalanine on growth process of L-glutamic acid polymorph. *Journal of Crystal Growth* **1998,** *192*, 225-235.

(52) Davey, R. J.; Blagden, N.; Potts, G. D.; Docherty, R. Polymorphism in Molecular Crystals: Stabilization of a Metastable Form by Conformational Mimicry. *Journal of the American Chemical Society* **1997,** *119*, 1767-1772.

(53) He, X.; Stowell, J. G.; Morris, K. R.; Pfeiffer, R. R.; Li, H.; Stahly, G. P.; Byrn, S. R. Stabilization of a Metastable Polymorph of 4-Methyl-2-nitroacetanilide by Isomorphic Additives. *Crystal Growth & Design* **2001,** *1*, 305-312.

(54) Thallapally, P. K.; Jetti, R. K. R.; Katz, A. K.; Carrell, H. L.; Singh, K.; Lahiri, K.; Kotha, S.; Boese, R.; Desiraju, G. R. Polymorphism of 1,3,5-Trinitrobenzene Induced by a Trisindane Additive. *Angewandte Chemie International Edition* **2004,** *43*, 1149-1155.

(55) Farmanesh, S.; Ramamoorthy, S.; Chung, J.; Asplin, J. R.; Karande, P.; Rimer, J. D. Specificity of Growth Inhibitors and their Cooperative Effects in Calcium Oxalate Monohydrate Crystallization. *Journal of the American Chemical Society* **2014,** *136*, 367-376.

(56) Pfund, L. Y.; Price, C. P.; Frick, J. J.; Matzger, A. J. Controlling Pharmaceutical Crystallization with Designed Polymeric Heteronuclei. *Journal of the American Chemical Society* **2015,** *137*, 871-875.

(57) Brisbois, E. J.; Handa, H.; Major, T. C.; Bartlett, R. H.; Meyerhoff, M. E. Long-Term Nitric Oxide Release and Elevated Temperature Stability with S-Nitroso-N-acetylpenicillamine (SNAP)-Doped Elast-eon E2As Polymer. *Biomaterials* **2013,** *34*, 6957-6966.

(58) Wo, Y.; Li, Z.; Brisbois, E. J.; Colletta, A.; Wu, J.; Major, T. C.; Xi, C.; Bartlett, R. H.; Matzger, A. J.; Meyerhoff, M. E. Origin of Long-Term Storage Stability and Nitric Oxide Release Behavior of CarboSil Polymer Doped with S-Nitroso-N-acetyl-d-penicillamine. *ACS Applied Materials & Interfaces* **2015,** *7*, 22218-22227.

Chapter 2 Influence of Coformer Stoichiometric Ratio on Pharmaceutical Cocrystal Dissolution

Li, Z.; Matzger, A. J. "Influence of Coformer Stoichiometric Ratio on Pharmaceutical Cocrystal Dissolution: Three Cocrystals of Carbamazepine/4-Aminobenzoic Acid" *Mol. Pharm.*, **2016**, *13* (3), pp 990-995

2.1 Introduction

According to the Biopharmaceutics Classification System (BCS), drug substances can be classified into four classes based on their solubility and permeability. Among them, Class II and Class IV refer to poorly soluble drugs with high permeability and low permeability, respectively.[1] Active pharmaceutical ingredients (APIs) that suffer from low aqueous solubility display slow dissolution rates, and in many cases this slow drug release from dosage forms hinders the bioavailability of the compounds.[2] It is estimated that about 40% of the drugs on the market display poor solubility. For potential drug candidates, the proportion of BCS class II and IV drugs can be as much as 80-90%.[3] Low efficacy, as the result of poor bioavailability in many cases, is a common cause of development failure. Therefore, solving solubility and dissolution issues is an important aspect of drug development.

Multiple approaches aimed at optimizing the solid forms of existing APIs to overcome solubility-limited bioavailability have been investigated due to the increasing proportion of poorly soluble drugs being developed. Although amorphous solid dispersions have exhibit great promise for solubility and dissolution rate enhancement,

the most common route to deliver APIs is still by crystalline dosage, because of the stability and considerable processing advantages in production.[4-8]

For crystalline drugs, the neutral single component API forms as well as multicomponent crystals, such as salts, solvates and cocrystals, can be considered for development into a dosage.[6-13] Not all drugs are polymorphic, and there can be situations where none of the achievable polymorphs meet the requirement for properties in application. Among the approaches of multicomponent crystallization, cocrystallization is an attractive option for solid form optimization of non-ionizable drugs for which salt formation is not applicable.[14-16] Cocrystallization can dramatically alter the properties of neutral compounds by introducing a neutral coformer that interacts with the target API in a defined stoichiometric ratio through intermolecular interactions. Even for ionizable drugs, the number of coformer candidates for cocrystallization can exceed the number of counterions for salt formation.[17] Therefore, this approach presents great potential to adjust API solubility.

Similar to salt formation, cocrystallization can increase both solubility and dissolution rate of drugs.[13] The overall effect of a coformer which is introduced to a pharmaceutical compound for cocrystallization on the dissolution of obtained cocrystal is dependent on both the solvation energies of the added cocrystallizing components and the cocrystal lattice energy.[18] With the introduction of a soluble coformer, besides changes in the strength of the crystal lattice because of the different intermolecular interactions that construct the packing motif, the strong solvent-solute interactions between the coformer component and the solvent formed from cocrystal solvation can also promote drug dissolution (Figure 2.1). As a result, the enhanced dissolution by cocrystallization can improve the bioavailability of poorly soluble drugs.[19] An example is furosemide, that the dissolution rate of the cocrystals can be visibly improved compared to the single component form.

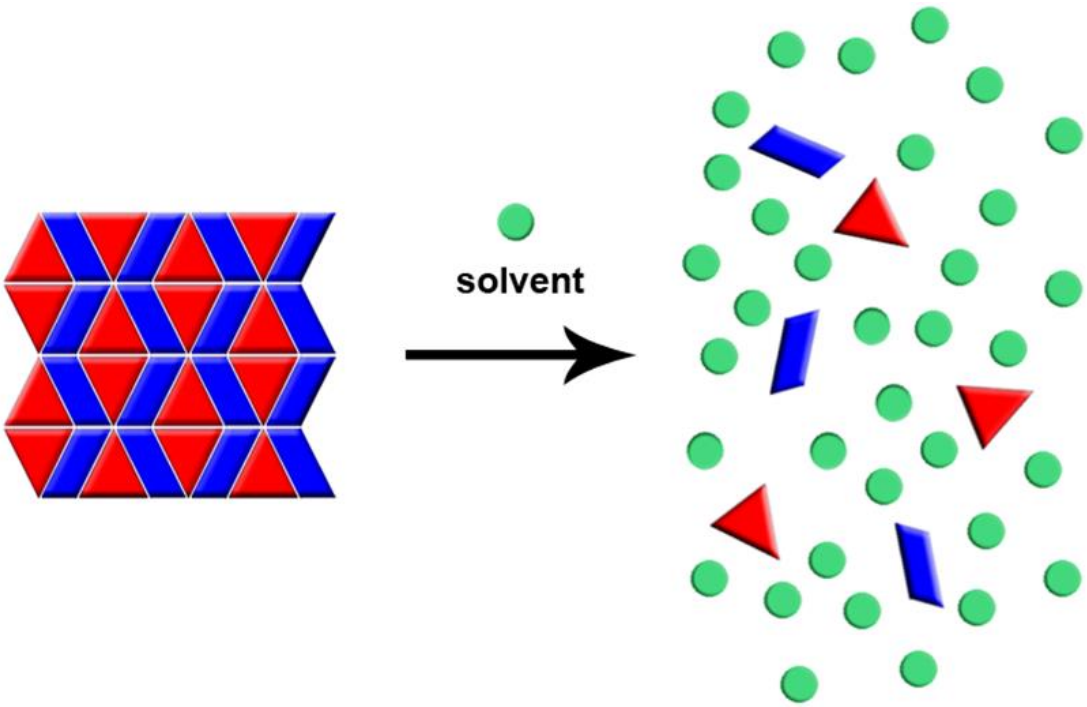

Figure 2. 1 Drug dissolution can be improved by introducing a soluble coformer, which can influence the lattice energy of the cocrystal and possesses strong solvent affinity that can drive cocrystal dissolution.

In some cocrystallization systems, there can be multiple cocrystal stoichiometries available for a target API to be packed with a specific coformer introduced to form multicomponent crystals for solid form optimization (Figure 2.2), which, in principle, provides more opportunities to engineer dissolution behavior. Studies on the synthons in such systems as well as the conversion between different cocrystal stoichiometries have been reported.[20-27] It was revealed that cocrystals of different stoichiometric ratios can coexist in solution at a eutectic point, and the conversion between cocrystal stoichiometries in solution is dependent on the coformer concentration. What is not understood is how cocrystal stoichiometry influences API performance.

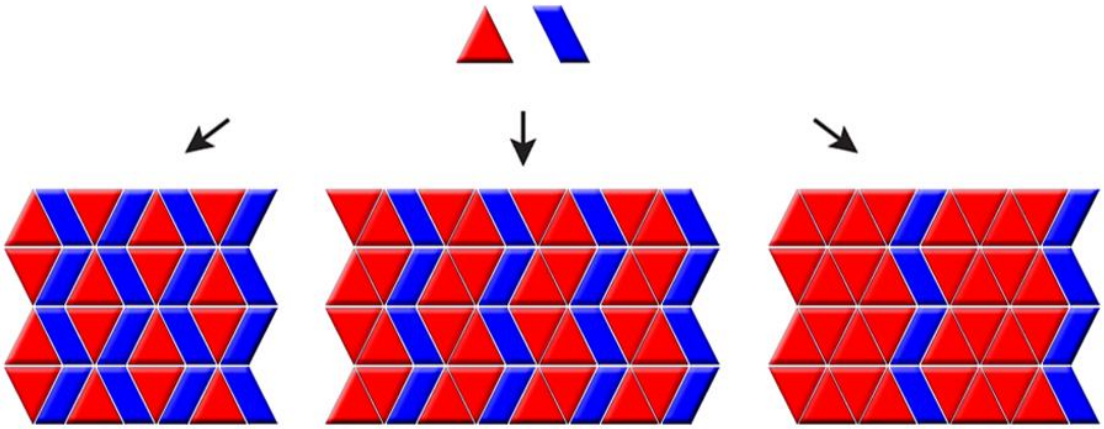

Figure 2. 2 Multiple stoichiometries can be available for a given cocrystallizing component pair. The cocrystallizing components can pack into more than one motif, with different ratios of the coformers corresponding to various intermolecular interactions in each structure.

For cocrystals consisting of only two components, the dissolution process of the cocrystals is determined by the cocrystal lattice energy and the interactions between each crystallizing component and the solvent. When multiple cocrystal stoichiometries are available with a specific coformer (without formation of solvates), given that the coformer is more soluble than the drug, as the proportion of the coformer in cocrystal increases, the enhanced strong affinity between the coformer and the solvent molecules is expected to favor cocrystal dissolution.[28] On the other hand, as an analogue of the common ion effect in salts, the drug concentration of cocrystals at equilibrium decreases as a function of increasing cocrystallizing component concentration in solution.[21, 29] Consequently, for cocrystals with greater coformer stoichiometry, the coformer concentration in solution is higher for a given drug concentration, which may favor drug precipitation in alternative stoichiometries. Another property of cocrystals with higher coformer stoichiometry is the greater mass of material required to reach the same API concentration. The above analysis indicates that there are multiple factors imposed by coformer stoichiometry that influence cocrystal dissolution and the relative influence of each of these is not well defined. These are, however, not the only factors of significance as intermolecular interactions

among the cocrystals may vary in both strength and abundance (vide infra). Multiple coformer stoichiometries have previously been observed to lead to changes in drug solubilization albeit in a system where the changes in coformer stoichiometry are accompanied by changes in cocrystal solvation (both solvent identity and stoichiometry) thus convoluting the coformer stoichiometry effects with solvation effects (Figure 2.3).[30] To elucidate the impact of coformer stoichiometric ratio on cocrystal dissolution without the interferences of molecules other than the selected drug, coformer and dissolution medium, a system with more than 2 stoichiometric ratio of non-solvate cocrystal is desired.

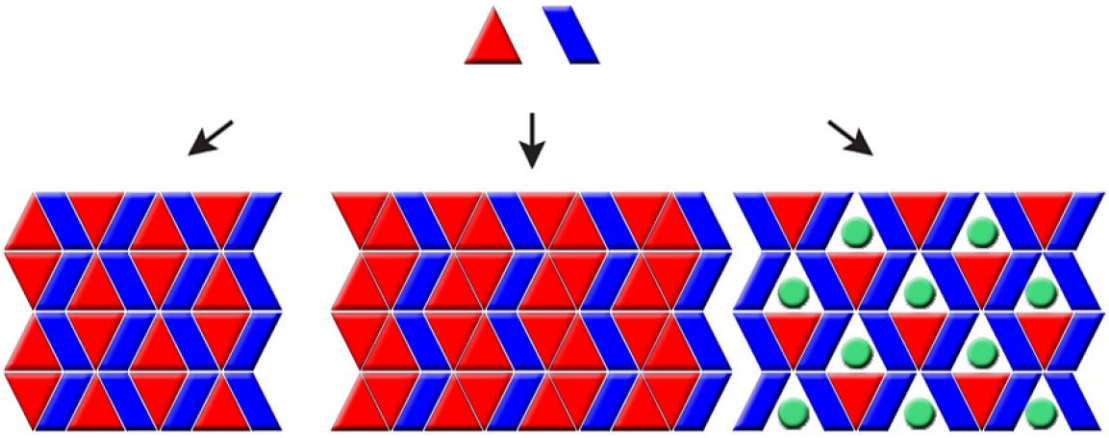

Figure 2. 3 Multiple cocrystal stoichiometry can be achieved with changes in cocrystal solvation (the solvate with the green circles representing solvent molecules possesses a drug – coformer stoichiometry different from the other two cocrystals). Except for coformer stoichiometry and cocrystal lattice energy, the interactions between the solvent molecules in the solvate and in the dissolution medium bring in extra interferences that complicate the dissolution process.

Carbamazepine (CBZ, Figure 2.4) is a polymorphic anti-epileptic BCS Class II compound and therefore exhibits low aqueous solubility and high permeability.[2, 31] Efforts have been made to optimize CBZ solid form solubility and dissolution rate through cocrystallization.[32-34] *p*-Aminobenzoic acid (PABA, Figure 2.4) is a coformer exhibiting an aqueous solubility of ~5.0 g/L at 24 °C, a value much higher than CBZ (17.7 mg/L).[35, 36] A CBZ/PABA 1:1 cocrystal and a CBZ/PABA 2:1 cocrystal have

been described previously.[21, 37, 38] Here, a new stoichiometry CBZ/PABA 4:1 cocrystal is reported. With more than two different cocrystal stoichiometries structurally characterized, a result rarely found in cocrystallized pharmaceuticals,[26, 27] CBZ/PABA is an attractive system to study the influence of multiple stoichiometric ratios on materials properties and, in particular, how the stoichiometric ratio of a soluble coformer affects the dissolution of a drug.

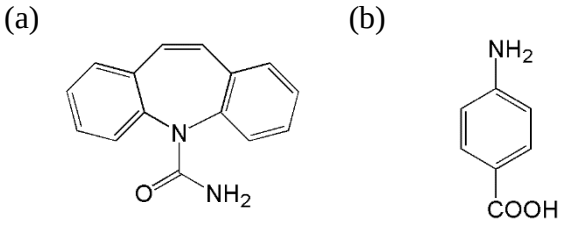

Figure 2. 4 Chemical structures of (a) CBZ and (b) PABA.

2.2 Results and Discussion

2.2.1 CBZ/PABA 4:1 Cocrystal Characterization

Clusters of needles were obtained by solvent evaporation of CBZ/PABA ethanolic solutions of various stoichiometric ratios (Figure 2.5). Due to the similarities in morphology of the known CBZ I, CBZ II, PABA I, and CBZ/PABA 1:1 cocrystal there is no reliable way to visually distinguish among the needle-shaped crystals; therefore powder X-ray diffraction (PXRD) characterization was performed for form identification of obtained needles. From samples crystallized out of a 0.2 M CBZ:0.1 M PABA ethanol solution, as well as a 0.1 M CBZ:0.1 M PABA ethanol solution, a unique PXRD pattern was observed, with characteristic lines at $2\theta = 6.63$, 8.71, and 13.30° (Figure 2.6), indicating a novel crystalline form.

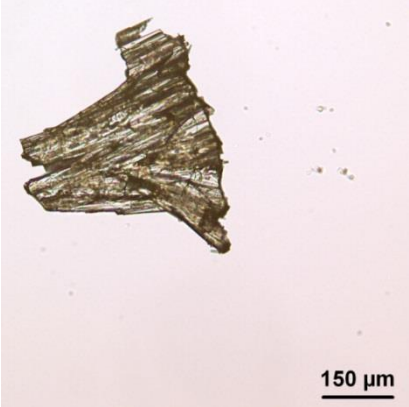

Figure 2. 5 Optical image of CBZ/PABA 4:1 cocrystal clusters. Since multiple crystals consist of CBZ and/or PABA are needle-shaped crystals, it is not reliable to visually distinguish this forms.

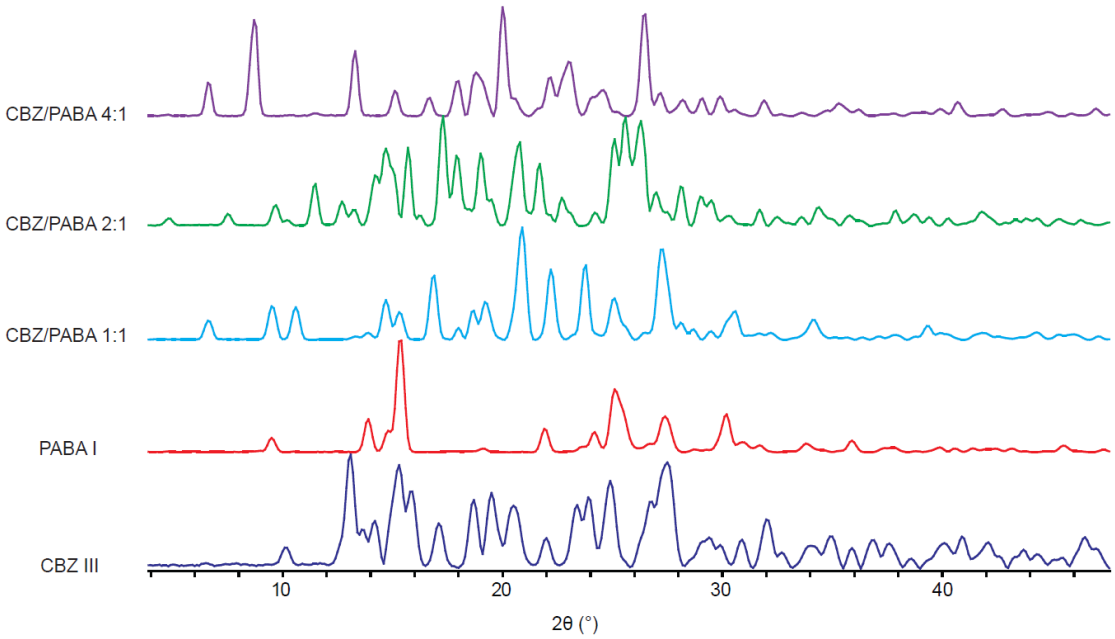

Figure 2. 6 Powder X-ray diffraction patterns of CBZ III, PABA I, CBZ/PABA 1:1, CBZ/PABA 2:1 and CBZ/PABA 4:1 cocrystals. The 4:1 cocrystal presents a unique PXRD pattern distinct from all the other reported forms, with characteristic lines at 2θ = 6.63, 8.71, and 13.30°.

Raman spectroscopy characterization was conducted to determine the constituents of the new form. Similar to the known CBZ/PABA cocrystals, the Raman spectrum of the

new form exhibits peaks in regions where CBZ or PABA single component crystals show characteristic peaks, but these peak positions are distinguishable from the spectra of all the previously reported forms (Figure 2.7). These features led to the speculation that the new form is a novel CBZ/PABA cocrystal.

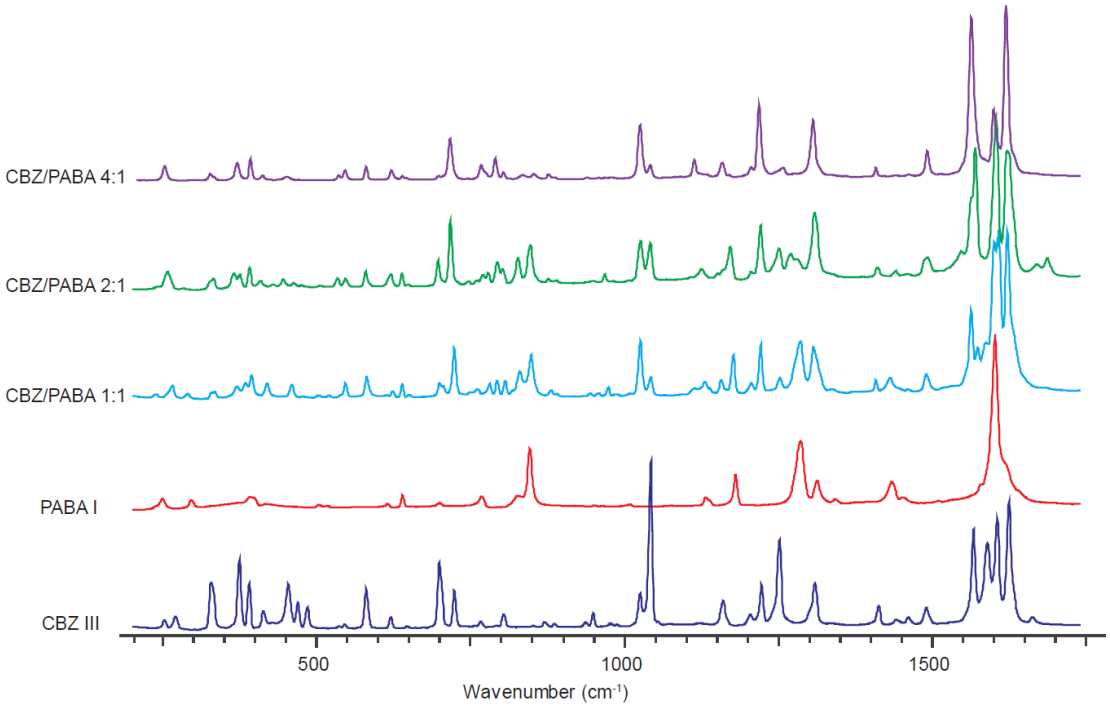

Figure 2. 7 Raman spectra of CBZ III, PABA I, CBZ/PABA 1:1, CBZ/PABA 2:1 and CBZ/PABA 4:1 cocrystals. In the CBZ/PABA 4:1 cocrystal spectrum, the PABA characteristic peak features are relatively weak compared to the 1:1 and 2:1 cocrystals.

To determine the stoichiometry of the newly discovered cocrystal of CBZ/PABA, proton NMR spectroscopy was carried out and a 4:1 CBZ:PABA ratio was measured (Figure 2.8). This new phase is CBZ-rich relative to the previously reported CBZ/PABA 1:1 and 2:1 forms, and this result agrees with the Raman spectrum of the new form in which the features of PABA at 846 cm^{-1}, 1180 cm^{-1}, 1285 cm^{-1} and 1601 cm^{-1} are relatively weak compared to those of CBZ/PABA 1:1 and 2:1 cocrystals.

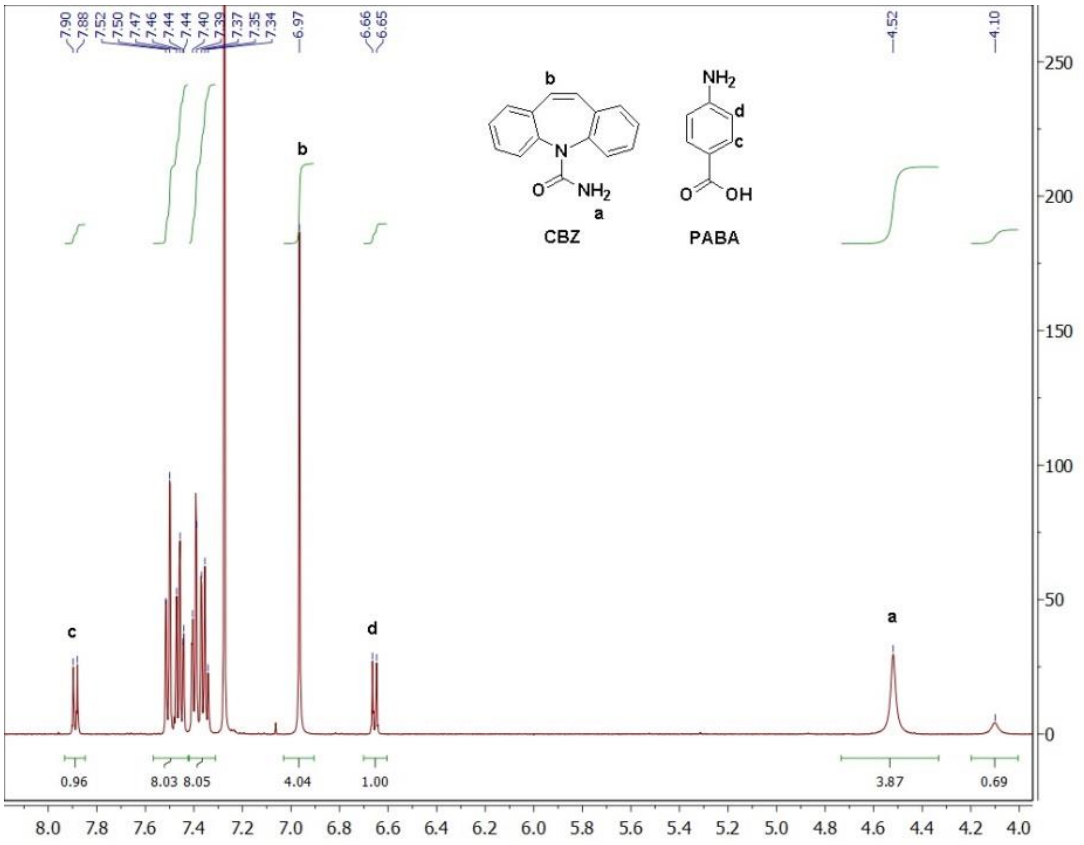

Figure 2. 8 ^{1}H NMR spectroscopic data for CBZ/PABA 4:1 cocrystal. The integration indicates a 4:1 CBZ:PABA stoichiometry for the cocrystal discovered in this work.

Single crystal samples of CBZ/PABA 4:1 cocrystals were grown by slow evaporation of dilute 4:1 CBZ:PABA ethanol solution in order to determine the 4:1 cocrystal structure (Figure 2.9). Single crystal XRD reveals the CBZ/PABA 4:1 cocrystal is monoclinic in the space group C 2/c (Table 2.1). Although severe PABA disorder makes detailed analysis of intermolecular interactions between the components in the 4:1 cocrystal impossible, packing of the three cocrystals are sufficiently different that motifs responsible for each stoichiometry are easily discerned. The 4:1 cocrystal packing features infinite PABA chains occupying channels between isolated homodimers of CBZ; all CBZ molecules are symmetry equivalent and this is distinct from the previously reported forms where interactions between CBZ and PABA are present. The 1:1 cocrystal is characterized by infinite chains of CBZ homodimers connected to PABA homodimers by interaction by N—H donation from PABA to CBZ

carbonyls. All CBZ molecules are symmetry equivalent in the 1:1 cocrystal. The 2:1 cocrystal is characterized by finite groups of two hetero-dimerized CBZ—PABA pairs connected to one CBZ homodimer by N—H (PABA)/carbonyl (CBZ) interactions. This leads to two symmetry inequivalent CBZ molecules (Figure 2.10).

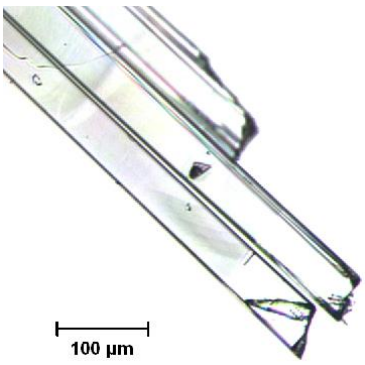

Figure 2. 9 Thin prism-shaped single crystal samples of CBZ/PABA 4:1 cocrystal.

Table 2. 1 Crystal lattice comparison of CBZ/PABA cocrystals

CBZ/PABA Cocrystal Stoichiometry	1:1	2:1	4:1
Lattice System	Monoclinic	Monoclinic	Monoclinic
Space Group	P 2_1/n	C 2/c	C 2/c
a (Å)	5.1909(4)	37.013(3)	20.3857(6)
b (Å)	18.4126(13)	12.1319(9)	5.10210(10)
c (Å)	19.0481(14)	13.5991(10)	26.5935(19)
β (˚)	97.7740(10)	99.1730(10)	95.583(9)
V (Å^3)	1803.85	6028.42	2752.87

Lattice parameters of CBZ/PABA 1:1 and 2:1 are from references.[21, 37]

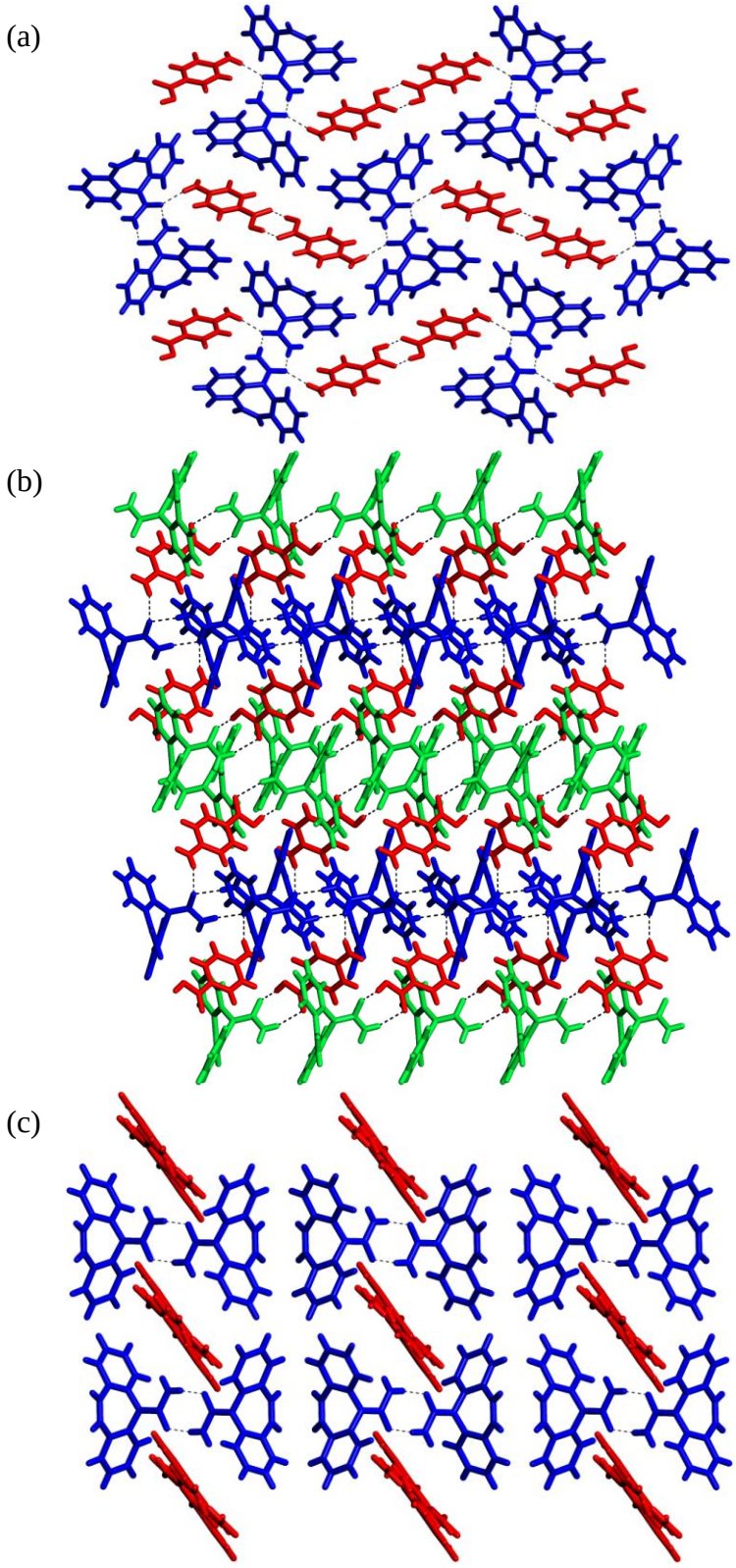

Figure 2. 10 Packing of (a) CBZ/PABA 1:1, (b) CBZ/PABA 2:1 and (c) CBZ/PABA 4:1 cocrystals. Blue color corresponds to symmetry equivalent homo-dimerized CBZ. Green color corresponds to symmetry equivalent hetero-dimerized CBZ. Red color corresponds to PABA.

2.2.2 CBZ/PABA Cocrystal Stability

The CBZ/PABA 4:1 cocrystal shows behavior consistent with a metastable form. CBZ/PABA 1:1 and 2:1 cocrystals can be prepared on large scale by neat grinding, solvent-assisted grinding with ethanol, or by slurring CBZ with corresponding stoichiometric ratio equivalents of PABA. These Raman spectroscopy and PXRD characterization results are consistent with the notion that CBZ/PABA 1:1 and 2:1 cocrystals are thermodynamically stable forms of the corresponding CBZ/PABA stoichiometries. On the other hand, by neat grinding, solvent-assisted grinding, and slurring of CBZ with 0.25 molar equivalents of PABA, the desired CBZ/PABA 4:1 cannot be obtained, and instead physical mixtures of CBZ III and CBZ/PABA 2:1 cocrystal form (Figure 2.11). This holds true either in the absence or presence of seeds of the 4:1 cocrystal indicating that the result is not kinetic, and the 4:1 cocrystal is less stable relative to its alternative stoichiometries.

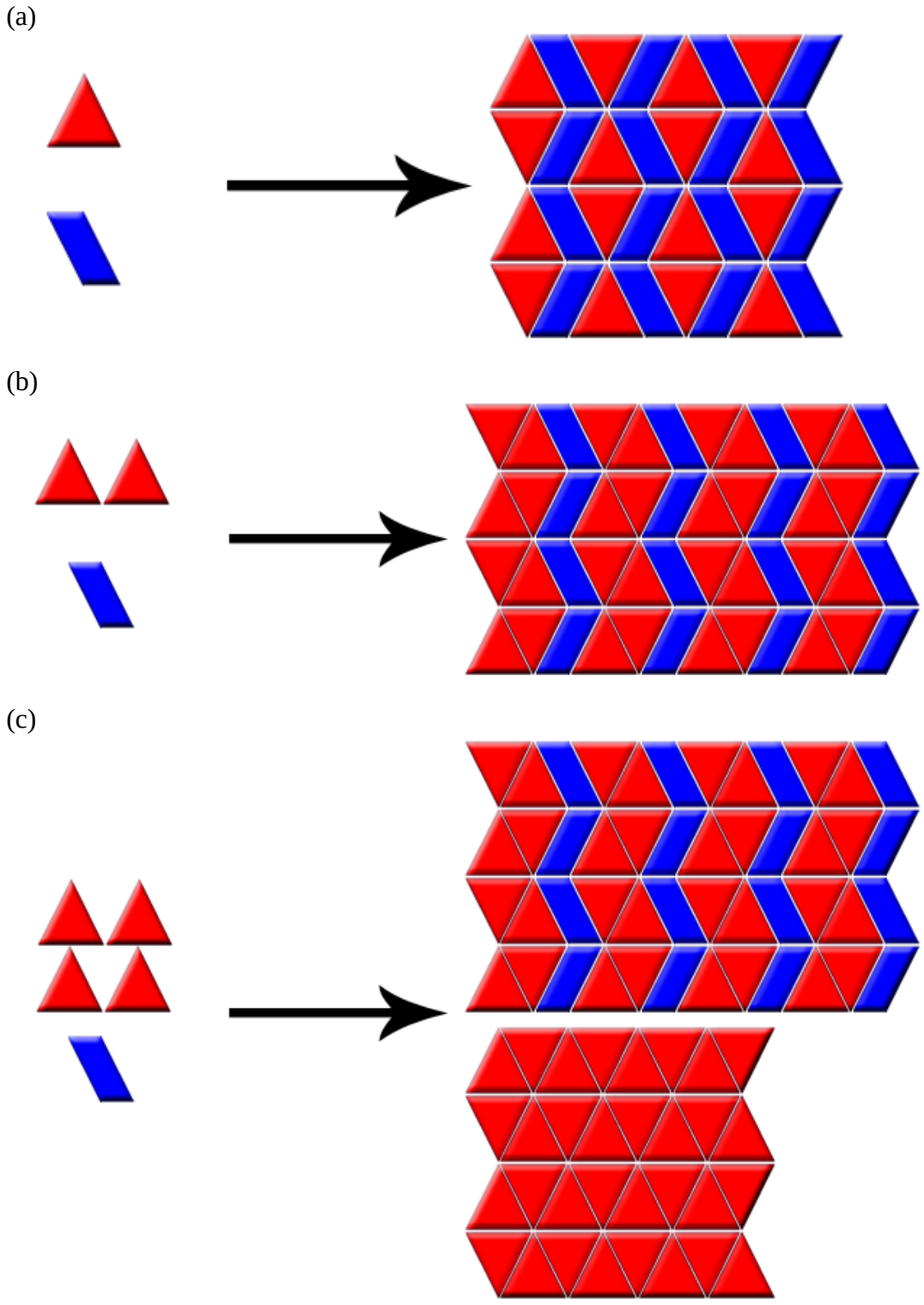

Figure 2. 11 CBZ/PABA (a) 1:1 and (b) 2:1 cocrystals can be obtained by slurrying or grinding CBZ and PABA of corresponding stoichiometries, while (3) initial 4:1 CBZ:PABA reactants give mixed product of CBZ III and CBZ/PABA 2:1 cocrystal.

Additionally, wetted by a minimum amount of either pure solvent or filtered solution cosaturated with CBZ and CBZ/PABA 2:1 cocrystal, 4:1 cocrystals also convert to physical mixtures of CBZ III and CBZ/PABA 2:1 (Figure 2.12). The spontaneous conversion of 4:1 samples to crystals of alternative stoichiometry again suggests that, unlike the 1:1 and 2:1 cocrystals, the 4:1 cocrystal is not a thermodynamically favored form relative to the physical mixture of CBZ/PABA 2:1 and CBZ III. Despite the fact that CBZ/PABA 4:1 cocrystals cannot be obtained from grinding or slurring, once they are formed, the metastable cocrystals can be stored without decomposition or conversion to other forms under ambient temperature and humidity, and only convert once solvent is present.

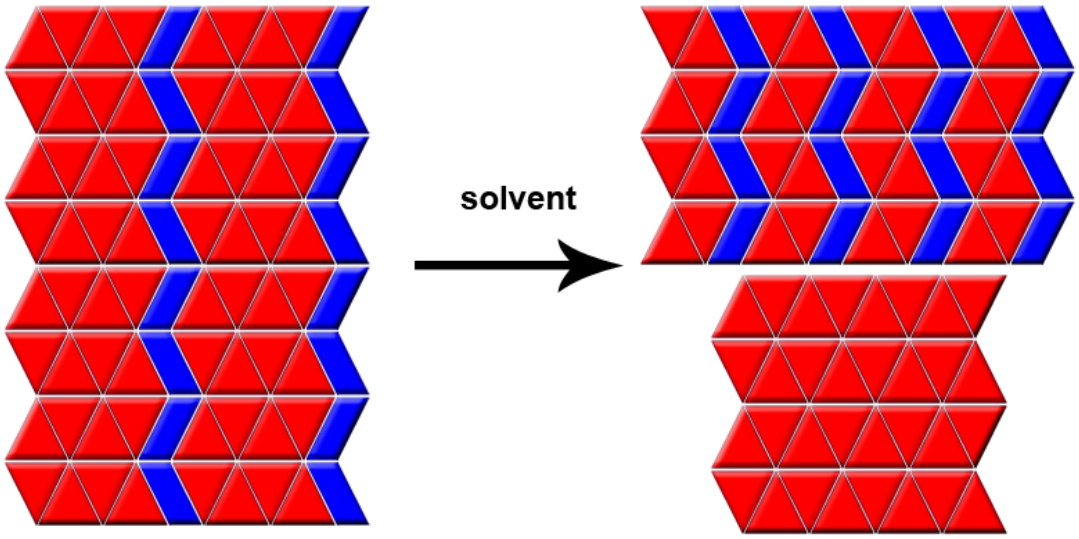

Figure 2. 12 The CBZ/PABA 4:1 cocrystals spontaneously convert to physical mixture of CBZ III and CBZ/PABA 2:1 cocrystal with the existence of solvent media.

In the reported phase diagram for the CBZ/PABA/ethanol system, the CBZ/PABA 1:1 cocrystal has invariant points with either CBZ/PABA 2:1 or PABA, and the CBZ/PABA 2:1 cocrystal has invariant points with either CBZ or CBZ/PABA 1:1.[21] If the 4:1 cocrystal is present on this phase diagram, it would be in a region somewhere between pure CBZ and pure CBZ/PABA 2:1. However, all CBZ/PABA 4:1 cocrystals suspended in slurries of pure CBZ, pure CBZ/PABA 2:1 or mixtures of CBZ and

CBZ/PABA 2:1 dissolved in agreement with experiments of CBZ/PABA 4:1 conversion to CBZ and CBZ/PABA 2:1 described above; thus CBZ/PABA 4:1 does not have a stable region on the ternary phase diagram. A similar situation has been reported with a caffeine/maleic acid 2:1 cocrystal obtained by neat and solvent-assisted grinding but unattainable by crystallization from solvent; the form is metastable and converts to a mixture of caffeine and 1:1 cocrystal with the addition of acetone.[17] A ciprofloxacin succinate (2:1) tetrahydrate has also been implicated to be metastable.[23, 39] A final example is a diacetone diperoxide/1,3,5-tribromo-2,4,6-trinitrobenzene cocrystal that decomposes to the pure forms of its constituents at room temperature.[40] The term "schizophilic" has been applied to describe such a cocrystal that is unstable relative to its pure components. Hence, the new CBZ/PABA 4:1 cocrystal is a schizophilic cocrystal that, instead of being unstable relative to its pure components, yields a mixture of one pure component (CBZ) and a second stoichiometry of cocrystal (CBZ/PABA 2:1).

Thermal stabilities of the three CBZ/PABA cocrystal stoichiometries were examined by differential scanning calorimetry (DSC). Both CBZ/PABA 1:1 and 2:1 cocrystals presented only one major endothermic peak, at 148 ℃ and 157 ℃ respectively, corresponding to their melting points. By contrast, the 4:1 cocrystal DSC profiles revealed a phase transition at 100 ℃, followed by multiple endothermic peaks (Figure 2.13). The transformation products at 100 ℃ were identified by applying hot stage Raman microspectroscopy. Changes in cocrystal morphology from prisms with smooth surfaces to rough crystals with small needles attaching to the surfaces were observed. Raman spectroscopy showed that the 4:1 cocrystal gradually disappeared at the conversion temperature and peaks of CBZ I, the preferred CBZ polymorph at high temperature, appeared. Due to the strong CBZ I Raman characteristic peaks and fluorescence that conceal the relatively weak CBZ/PABA 1:1 Raman characteristic peaks, the conversion products of both CBZ I and CBZ/PABA 1:1 are confirmed by PXRD analysis (Figure 2.14). The DSC results indicate that CBZ/PABA 4:1 has

weaker thermal stability than CBZ/PABA 1:1 and 2:1 cocrystals, and undergoes phase conversion before reaching its melting point (Figure 2.15), which is again suggestive of relatively weak intermolecular interactions in the 4:1 cocrystal compared to the previously known forms.

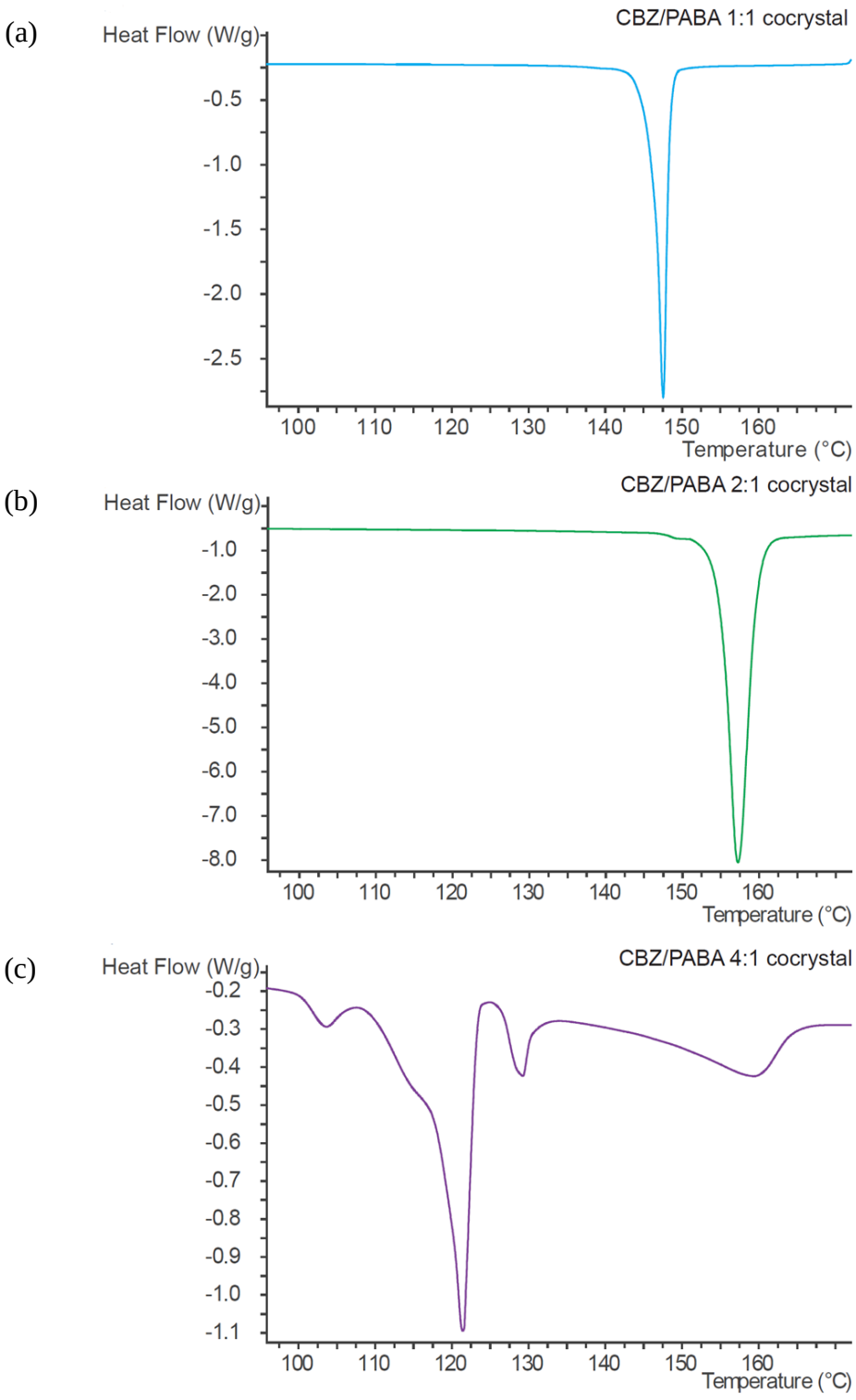

Figure 2. 13 Differential scanning calorimetry profile of CBZ/PABA 1:1, 2:1 and 4:1 cocrystals. CBZ/PABA 1:1 and 2:1 cocrystals present one major endothermic peak, corresponding to their melting points, which indicates a higher thermal stability than CBZ/PABA 4:1 that undergoes phase conversion before reaching its melting point.

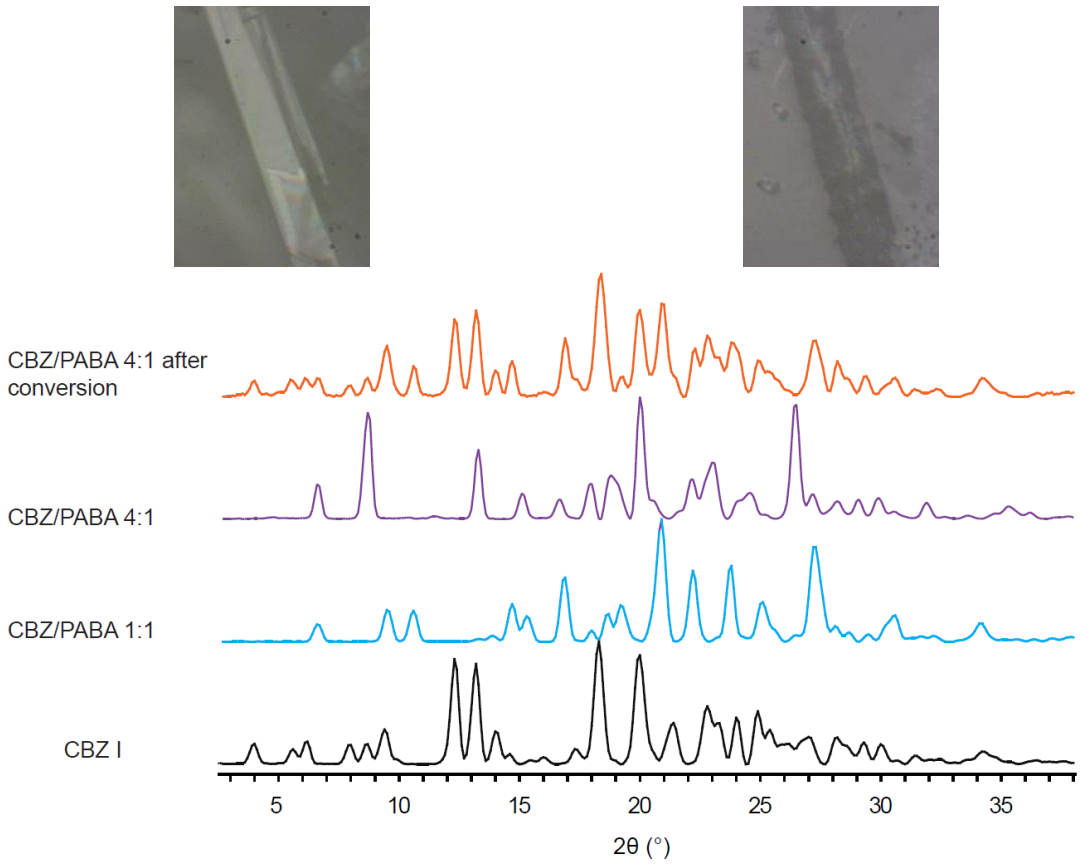

Figure 2. 14 Powder X-ray diffraction patterns of CBZ I, CBZ/PABA 1:1, CBZ/PABA 4:1 before and after phase conversion at 100 ℃. The insets are images of CBZ/PABA 4:1 (a) before and (b) after conversion.

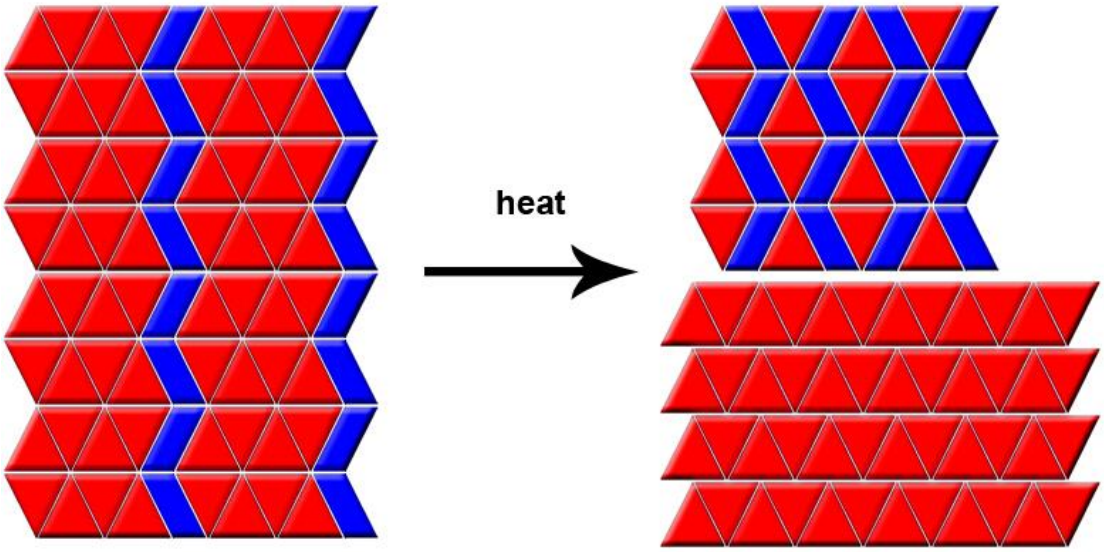

Figure 2. 15 The CBZ/PABA 4:1 cocrystals convert to physical mixture of CBZ I and CBZ/PABA 1:1 cocrystal at 100 °C.

2.2.3 CBZ/PABA Cocrystal Dissolution

Ultimately the goal of cocrystallization for most APIs is to improve dissolution and the question being addressed here is how stoichiometry influences this property. Because CBZ/PABA 4:1 is metastable and converts easily to other forms in solution, dissolution rate rather than the drug concentration in the saturated solution was applied to assess the influence of coformer on solubilization. Here the dissolution investigation started with the hypothesis that the drug dissolution can benefit from the increasing stoichiometry of a more soluble coformer, and that the CBZ/PABA cocrystallization system, with three different non-solvate cocrystal stoichiometries accessible, serves as a model system for the investigation of this proposal.

Both CBZ and PABA solutes enter the solution during cocrystal dissolution. Therefore, the dissolution behaviors of all cocrystals are described by the changes in concentration of both components in the dissolution media, which are calculated based on the UV-vis spectra applied to monitor the dissolution process. Possible phase conversion can be detected by simultaneous Raman spectroscopy and ex-situ PXRD characterization (Figure 2.16).

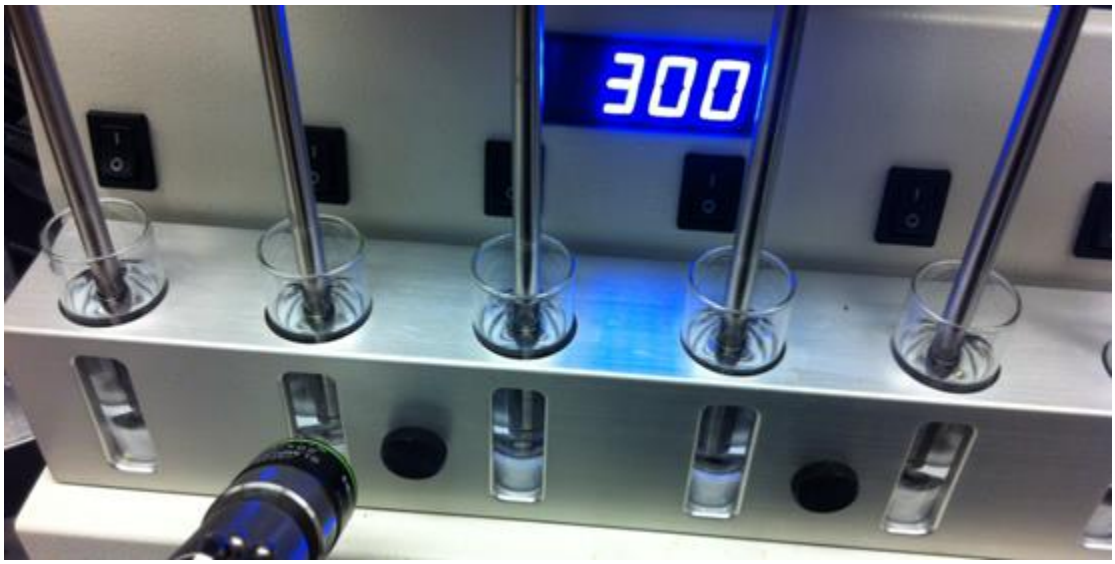

Figure 2. 16 Instrumental setup for in-situ UV-vis spectroscopy and simultaneous Raman spectroscopy monitoring dissolution process. The dissolution was monitored by both the UV-vis spectra measured by probes immerged in the solution and the Raman spectra recorded by the 20× objective pointing in the second dissolution channel.

2.2.3.1 Formula Derivation for Cocrystal Dissolution

For all CBZ/PABA cocrystals, since two components coexist in the solution during dissolution, and the absorption of CBZ and PABA overlaps throughout the UV-Vis spectra in selected solvents, CBZ and PABA concentrations in solution cannot be expressed by the absorbance at only one specific wavelength. Alternatively, equation sets combining the absorbance at two different wavelengths λ_1 and λ_2 have been set up for calculation.

According to the Beer-Lambert Law

$$A_{\lambda_1} = \sum_{i=1}^{N} \varepsilon_i c_i l$$

For a dissolution system with 2 solutes, at a specific time frame, the absorption A_{λ_1} and A_{λ_2} at wavelength λ_1 and λ_2 can be expressed as:

$$A_{\lambda_1} = \varepsilon_{1\lambda_1} c_1 l + \varepsilon_{2\lambda_1} c_2 l = a_1 c_1 + a_2 c_2$$

$$A_{\lambda_2} = \varepsilon_{1\lambda_2} c_1 l + \varepsilon_{2\lambda_2} c_2 l = b_1 c_1 + b_2 c_2$$

where the variables a_1 and b_1 correspond to the absorbance of CBZ solution with a unit concentration at wavelength λ_1 and λ_2, and a_2 and b_2 correspond to the absorbance of PABA solution with a unit concentration at wavelength λ_1 and λ_2, which all can be determined from calibration of standard solution. Therefore, the concentration of CBZ and PABA in solution c_1 and c_2 at a given time can be expressed as:

$$c_1 = \frac{a_2 A_{\lambda_2} - b_2 A_{\lambda_1}}{a_2 b_1 - a_1 b_2}, c_2 = \frac{b_1 A_{\lambda_1} - a_1 A_{\lambda_2}}{a_2 b_1 - a_1 b_2}$$

As a result of the calculation, the dissolution behaviors of CBZ/PABA cocrystals can be described by the concentration change of CBZ and PABA in dissolution media separately.

2.2.3.2 Dissolution Experiments in Phosphate-Buffered Saline (PBS)

With PBS that has a pH of 7.0 as the aqueous dissolution medium, it was noted that in all experiments of samples containing CBZ, including CBZ III, CBZ dihydrate and all CBZ/PABA cocrystals, the dissolution rates, represented by the slope of the concentration-time profiles, kept decreasing over time during the dissolution process (Figure 2.17). Additionally, congruent dissolution of CBZ/PABA cocrystals was never observed during the dissolution process, and cocrystal dissolution behavior can only be described by the concentration of both components separately. Therefore, the dissolution behavior of CBZ III, CBZ hydrate, CBZ/PABA 1:1, CBZ/PABA 2:1, and CBZ/PABA 4:1 in PBS is described by the initial CBZ and PABA dissolution rates and the dissolution rates after 1 hour (Table 2.2).

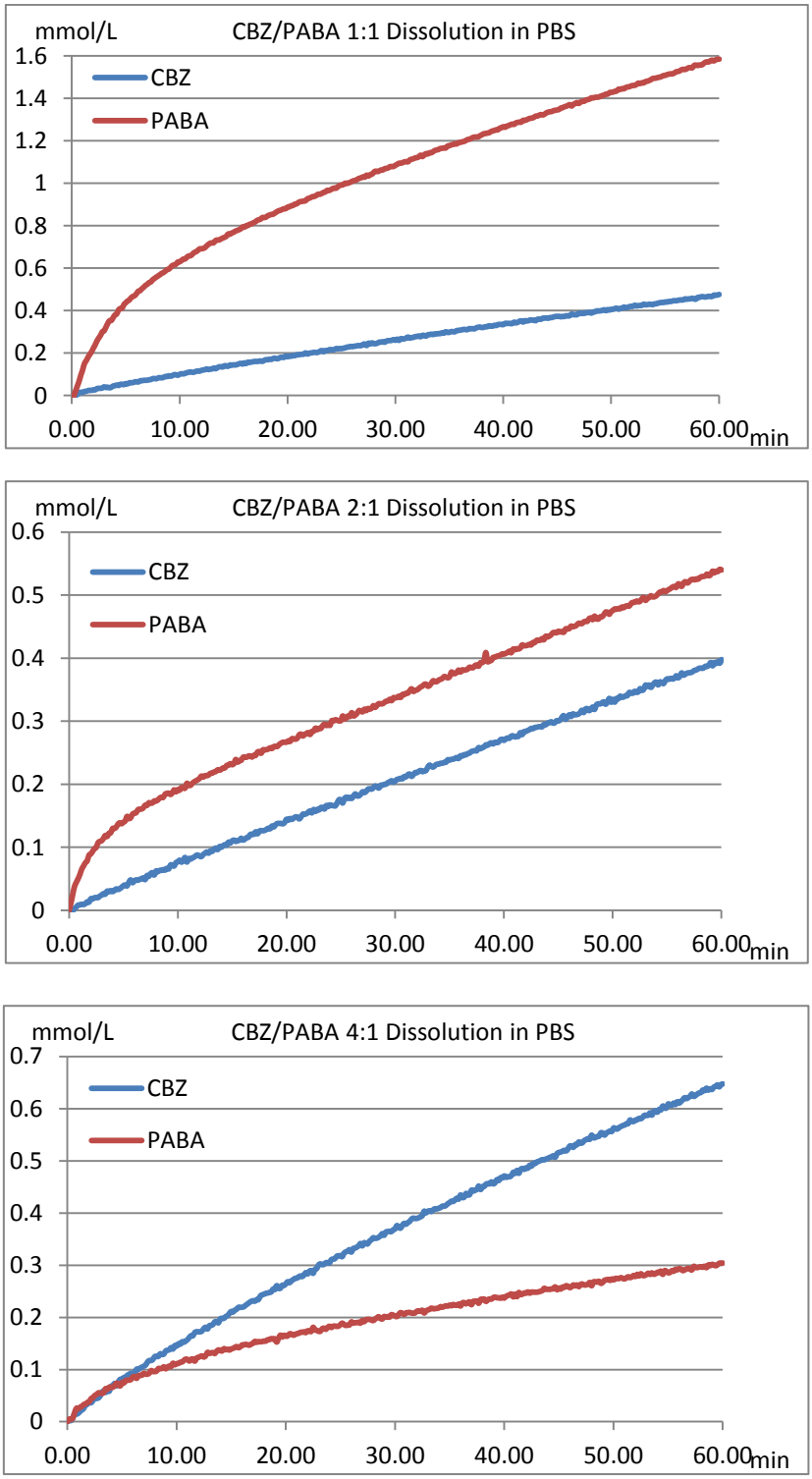

Figure 2. 17 Representative CBZ/PABA cocrystal dissolution profiles in PBS. Incongruent stoichiometry of CBZ and PABA in solution is observed throughout the dissolution process.

Table 2. 2 CBZ/PABA dissolution rates (average ± standard error of the mean) in PBS

Rate of Dissolution (μmol/min/cm^2)	CBZ After 1 Hour	CBZ Initial	PABA After 1 Hour	PABA Initial
CBZ III	7.22 ± 0.24	21.0 ± 0.4	—	—
CBZ dihydrate	6.49 ± 0.10	12.6 ± 0.7	—	—
PABA I	—	—	—	765 ± 9
CBZ/PABA 1:1	6.45 ± 0.18	19.4 ± 1.8	15.9 ± 1.2	131 ± 9
CBZ/PABA 2:1	6.14 ± 0.15	15.7 ± 0.8	6.28 ± 0.29	64.1 ± 2.3
CBZ/PABA 4:1	7.90 ± 0.21	23.1 ± 1.3	2.61 ± 0.14	22.2 ± 1.4

All units are in μmol/min/cm^2. Presented data are average values of 10 trials for each form. Pure PABA samples were fully dissolved before 1 hour. The initial rates of dissolution are determined from the first minute. The dissolution rates after 1 hour are determined between 55 minutes and 60 minutes.

In opposition to the notion that an increase of the PABA stoichiometry would promote drug dissolution, although the PABA dissolution rates of cocrystals presented positive correlation with PABA stoichiometry, CBZ/PABA 4:1, the cocrystal with the lowest PABA stoichiometric ratio, exhibited the highest CBZ dissolution rate at all times, whereas CBZ/PABA 2:1 showed the lowest CBZ dissolution rate among the three cocrystals. Notably, for all CBZ/PABA cocrystal samples, the ratios of CBZ dissolution rates compared to PABA dissolution rates are always lower than the CBZ:PABA cocrystal stoichiometry. This result indicates that CBZ/PABA cocrystal dissolution in PBS is not a simple one-step process; either the two cocrystal components do not dissolve congruently, or form conversion and/or precipitation occur during dissolution.

In order to elucidate possible solid form conversion during dissolution, in-situ Raman spectroscopy and ex-situ PXRD characterization were applied to examine solid form present in the dissolution pellet. Formation of CBZ dihydrate on the surface of CBZ III

and all CBZ/PABA cocrystals was observed by in-situ Raman spectroscopy during dissolution (Figure 2.18). These observations can be rationalized by generation of CBZ supersaturation with respect to CBZ dihydrate in the dissolution layer leading to precipitation on the sample surface; such observations mirror those reported in the cases of CBZ/nicotinamide and CBZ/saccharin cocrystals.[33, 41] This outcome is supported by analysis of the remaining samples after 1 hour of dissolution in which physical mixtures of the original form and CBZ dihydrate were identified by both Raman spectroscopy and PXRD. With CBZ dihydrate covering the sample surface, a smaller effective dissolution surface area of the original form is obtained, resulting in a drop in CBZ III and CBZ/PABA cocrystal dissolution rates. For the same reasons, the CBZ and PABA dissolution rates measured do not track the cocrystal stoichiometry, since part of the dissolved CBZ in the dissolution layer precipitates on the pellet surface as CBZ dihydrate. This is not the sole effect reducing dissolution rate with time as the concentration of CBZ in the dissolution medium is sufficient to be influencing the dissolution rates (this is evident for CBZ dihydrate). These effects are smaller during initial dissolution and so the behavior of the CBZ component more closely mirrors the intrinsic properties of samples. In these case CBZ dissolution rates increase in the order: CBZ/PABA 2:1 < CBZ/PABA 1:1 < CBZ/PABA 4:1. Clearly there is no correlation between the cocrystal stoichiometry and drug dissolution rate.

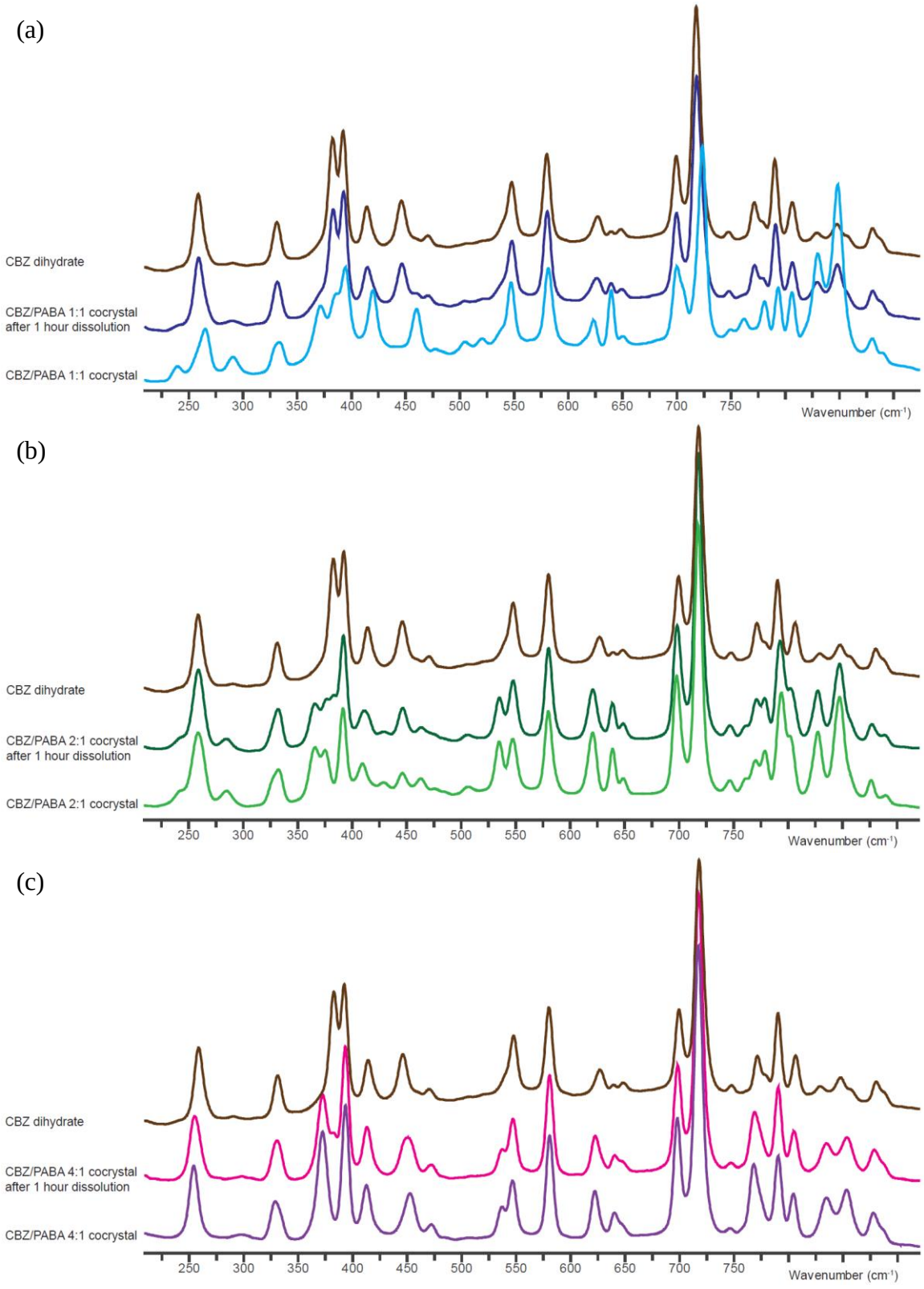

Figure 2. 18 In-situ Raman spectra for CBZ/PABA (a) 1:1, (b) 2:1 and (c) 4:1 cocrystal dissolution. Formation of CBZ dihydrate on all CBZ/PABA cocrystal surfaces during dissolution was detected. The CBZ dihydrate was featured by the characteristic peaks between 370 cm^{-1} and 400 cm^{-1}.

2.2.3.3 Dissolution Experiments in Acetonitrile

In order to obtain dissolution profiles directly mirroring sample properties without the disturbance of phase conversion to CBZ dihydrate, dissolution experiments of all samples were conducted in acetonitrile. In acetonitrile at 20 °C the solubility of CBZ III is 35.2 g/L and that of PABA I is 62.2 g/L.[42, 43] PABA still exhibits higher solubility than CBZ, but compared to the case in PBS the differences in solubility is much smaller. In contrast to observations in PBS, the CBZ and PABA dissolution profiles in acetonitrile were linear with constant slope (within the limit of instrument linearity) corresponding to the dissolution rate indicating constant dissolution behavior (Figure 2.19). In addition, CBZ and PABA dissolution rates of all cocrystal samples in acetonitrile mirror the cocrystal stoichiometric ratios (Table 2.3), indicating that both components dissolved congruently. The hypothesis that CBZ dissolution can be improved by the increase of PABA stoichiometry was again disproved, since CBZ/PABA 4:1, the cocrystal with the lowest PABA stoichiometric ratio, again presented the highest drug dissolution rate. The dissolution rate of CBZ in CBZ/PABA 2:1, which might be expected to be higher than pure CBZ III because the presence of PABA coformer, turns out to be the lowest among all samples.

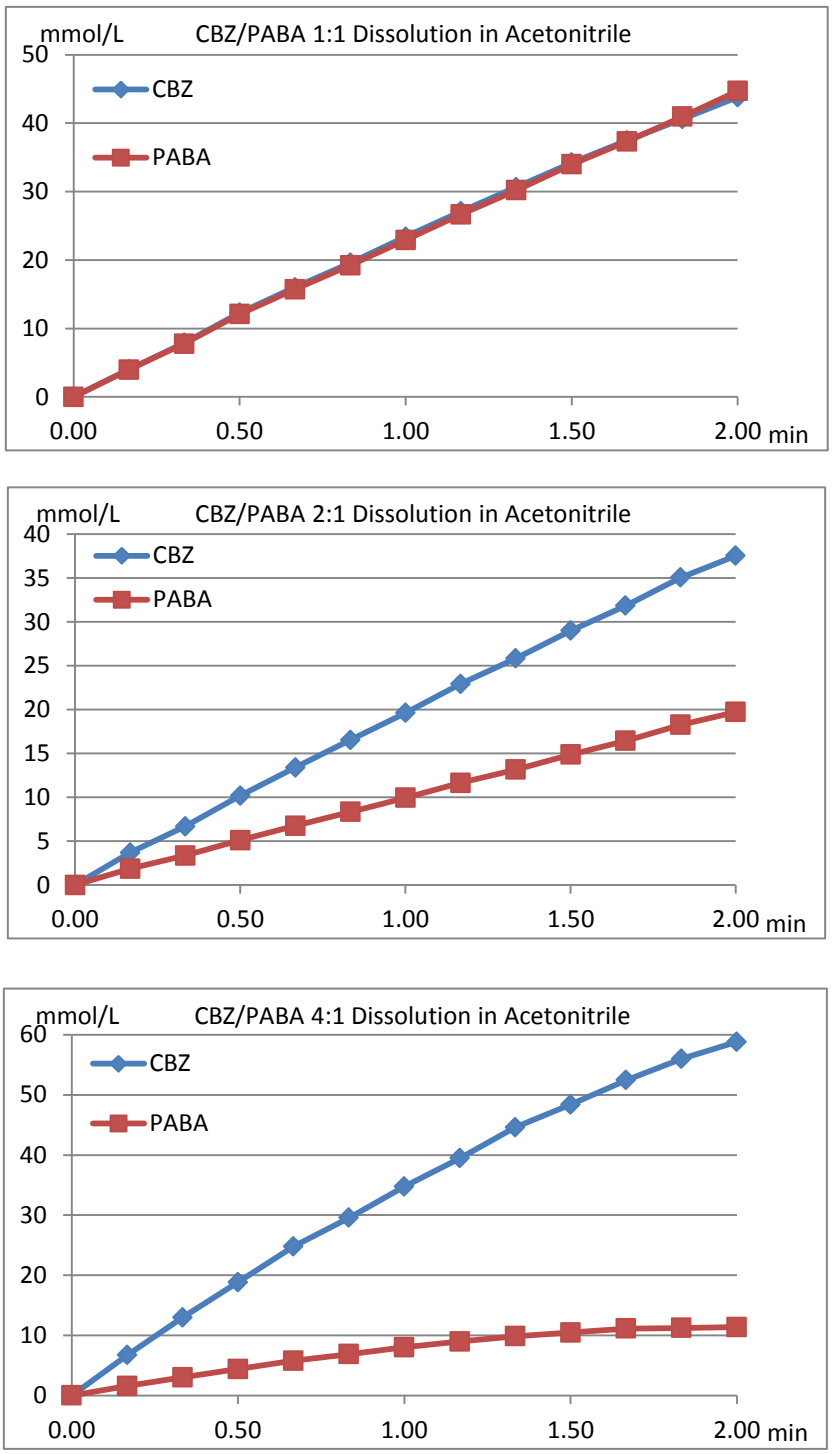

Figure 2. 19 Representative CBZ/PABA cocrystal dissolution profiles in acetonitrile. Only data of the first 2 minutes are presented to avoid the region of strongly saturated UV-Vis absorption.

Table 2. 3 CBZ/PABA dissolution rates (average ± standard error of the mean) in acetonitrile

Rate of Dissolution (mmol/min/cm^2)	CBZ	PABA
CBZ III	4.62 ± 0.06	—
CBZ dihydrate	7.31 ± 0.08	—
PABA I	—	11.4 ± 0.1
CBZ/PABA 1:1	5.65 ± 0.13	5.62 ± 0.13
CBZ/PABA 2:1	4.31 ± 0.04	2.17 ± 0.02
CBZ/PABA 4:1	8.89 ± 0.13	2.27 ± 0.04

The dissolution rates are much higher compared to those in PBS, and all units are in mmol/min/cm^2.

With regard to the dissolution behavior of CBZ/PABA cocrystals in acetonitrile, CBZ/PABA 4:1 showed the highest CBZ dissolution rate, which is attributed to the relatively weak intermolecular interactions implied by its schizophilic behavior. CBZ/PABA 2:1 presented the lowest dissolution rate in both PBS and acetonitrile dissolution experiments. In fact CBZ/PABA 2:1 does not display improved drug dissolution in acetonitrile relative to CBZ III. It was also noticeable that unlike the incongruent dissolution in PBS, where dissolution rates of the more soluble PABA in cocrystals were in positive correlation with PABA stoichiometry (regardless of the CBZ dissolution rate), the PABA dissolution rates of all three cocrystals in acetonitrile no longer follow the order of PABA proportion in cocrystal. This result can be attributed to the fact that PABA solubility in acetonitrile is not significantly higher than that of CBZ (minimal differential driving force for dissolution) and thus the dissolution disadvantage resulting from the strong intermolecular interactions in the 2:1 cocrystal could not be overcome by the small advantage imparted by improved PABA solubility.

2.3 Conclusions

A CBZ/PABA cocrystal of 4:1 stoichiometry has been discovered and structurally characterized. Stability studies showed that the novel form is schizophilic and converts readily to a mixture of pure CBZ and alternative stoichiometries of CBZ/PABA upon being wetted by solvent. CBZ/PABA cocrystallization system is an uncommon case where 3 non-solvate cocrystal stoichiometries can be achieved. Although cocrystallization is known to be an applicable technique to improve the solubility and dissolution properties of poorly soluble drugs, in the dissolution experiments of CBZ/PABA cocrystals in PBS and acetonitrile, it is demonstrated here that the factors influencing the cocrystal dissolution behavior are complex, and cocrystallization with a more soluble coformer does not necessarily improve drug dissolution. In particular when the difference in solubility between the drug and the coformer is not large (in acetonitrile), the intermolecular interactions within the crystal lattice are a critical factor influencing cocrystal dissolution. Therefore, the stoichiometry of a soluble coformer cannot be used as a straightforward criterion to estimate the cocrystal dissolution behavior, and consequently, increasing coformer stoichiometry in a cocrystal is not a reliable approach to optimizing drug solubility and dissolution. On the other hand, greater attention to kinetic growth methods should be paid for cocrystal screening in attempt to optimize bioavailability of poorly soluble drugs, since crystal dissolution can benefit from the weak intermolecular interactions in the thermodynamically unstable forms.

2.4 Experimental

2.4.1 Materials

Carbamazepine (99%) and PABA (99%) were purchased from Acros Organics (New Jersey, USA). Ethanol was purchased from Decon Laboratories, Inc. Chloroform,

methanol and acetonitrile were obtained from Fisher Scientific (Pittsburgh, PA). $NaH_2PO_4 \cdot H_20$ and $Na_2HPO_4 \cdot 7H_20$ were purchased from Sigma (St. Louis, MO). NaH_2PO_4/Na_2HPO_4 10 mM phosphate-buffered saline (PBS) at pH 7.0 was prepared by dissolving 0.584 g $NaH_2PO_4 \cdot H_2O$ and 1.547 g $Na_2HPO_4 \cdot 7H_2O$ in 1 L deionized water.

2.4.2 Crystallization Methods

The known CBZ/PABA 1:1 and 2:1 cocrystals were synthesized by solution-mediated phase conversion from slurries prepared by adding CBZ and PABA in corresponding stoichiometries to filtered co-saturated CBZ-PABA-ethanol solution and stirring the samples for 2 days; the cocrystals can be obtained after filtration. The CBZ/PABA 4:1 cocrystal was first found by slow evaporation of a 0.2 M CBZ:0.1 M PABA ethanol solution at room temperature. The solution was prepared by dissolving 47.2 g/L CBZ and 13.7 g/L PABA in 1 mL ethanol at 70 °C. Pure samples of CBZ/PABA 4:1 for characterization and dissolution experiments were prepared by slowly evaporating an anhydrous methanol solution of 23.63 g/L CBZ and 3.43 g/L PABA.

2.4.3 Powder X-Ray Diffraction

Powder X-ray diffraction (PXRD) patterns were collected using a Rigaku R-Axis Spider diffractometer with an image plate detector and graphite monochromated Cu-Kα radiation (λ = 1.54187 Å) at 40 kV and 44 mA. Samples were mounted on a CryoLoop^{TM} using heavy mineral oil for data collection. Images were collected for ten minutes with a 0.3 mm collimator. The ω-axis was oscillated between 120° and 180° at 1°/sec, the ϕ-axis was rotated at 10°/sec, and χ-axis was fixed at 45°. The obtained images were integrated from 2.5 to 70° with a 0.1° step size in AreaMax 2.0 (Rigaku). All powder patterns were processed using Jade 9 XRD Pattern Processing,

Identification & Quantification analysis software from Materials Data, Inc. The simulated powder patterns of reported forms were calculated in Mercury 3.3 from the CCDC, and were compared with the experimental powder patterns in Jade 9.

2.4.4 Raman Microspectroscopy

Raman spectra were collected by using a Renishaw inVia Raman system equipped with a Leica microscope, a RenCam CCD detector and a 633 nm laser employing an 1800 lines/nm grating and a 50 μm slit. Spectra were obtained using the WiRE 3.4 software package. Calibration was performed with a silicon standard in static mode. Full spectra were collected through an Olympus SLMPlan 20× objective in extended scan mode in the range of 100-4000 cm^{-1}, and further analyzed by ACD/SpecManager Version 12.01 software from Advanced Chemistry Development, Inc.

2.4.5 Nuclear Magnetic Resonance (NMR) Spectroscopy Analysis

^{1}H NMR spectroscopy was conducted by dissolving the obtained new form into chloroform-d. NMR data were obtained using a 500 MHz Varian Inova NMR spectrometer.

2.4.6 Single Crystal X-Ray Diffraction (XRD)

Colorless single crystal needles of CBZ/PABA 4:1 cocrystals were grown by evaporation of an ethanol solution of 23.63 g/L CBZ and 3.43 g/L PABA concentration. A crystal of dimensions 0.28 × 0.02 × 0.02 mm was mounted on a Rigaku AFC10K Saturn 944+ CCD-based X-ray diffractometer equipped with a low temperature device and Micromax-007HF Cu-target micro-focus rotating anode (λ = 1.54187 A) operated at 1.2 kW power (40 kV, 30 mA). The X-ray intensities were measured at 85(1) K with the detector placed at a distance 42.00 mm from the crystal. A total of 4214 images

were collected with an oscillation width of 1.0° in ω. The exposure times were 15 sec. for the low angle images, 60 sec. for high angle. The integration of the data yielded a total of 39336 reflections to a maximum 2θ value of 136.44° of which 2509 were independent and 1932 were greater than 2σ(I). The final cell constants (Table 2.1) were based on the xyz centroids 15040 reflections above 10σ(I). Analysis of the data showed negligible decay during data collection; the data were processed with CrystalClear 2.0 and corrected for absorption. The structure was solved and refined with the Bruker SHELXTL (version 2014/6) software package, using the space group C2/c with Z = 8 for the formula ($C_{14}H_{12}N_2O$), 0.25($C_7H_7NO_2$). All non-hydrogen atoms were refined anisotropically with the hydrogen atoms placed in idealized positions. The PABA moiety is poorly ordered and was placed as a variable metric rigid group in two orientations further disordered by being located near an inversion center. Full matrix least-squares refinement based on F^2 converged at R1 = 0.1624 and wR2 = 0.4071 [based on I > 2sigma(I)], R1 = 0.1811 and wR2 = 0.4235 for all data. Additional details are presented in Table 2.1 and are given as Supporting Information in a CIF file. Acknowledgement is made for funding from NSF grant CHE-0840456 for X-ray instrumentation.

2.4.7 Grinding and Solvent-Assisted Grinding Experiments

CBZ and PABA were combined in 1:1, 2:1 or 4:1 stoichiometric ratio, with 2 drops of solvent (methanol, ethanol or acetonitrile) added in solvent-assisted grinding experiments, and mixed in a 1 inch stainless steel grinding jar with a 6.25 mm stainless steel grinding ball by a DENTSPLY BY RINN CRESCENT 3110-3A Wig-L-Bug mixer mill at the rate of 60 Hz for 30 min. For grinding experiments of 4CBZ:1PABA, seeds of CBZ/PABA 4:1 were added in 3 trials to overcome possible kinetic barriers. The obtained crystals were characterized by both Raman spectroscopy and PXRD analysis.

2.4.8 Solution-mediated Phase Conversion

Solvent (methanol, ethanol and acetonitrile) were added to CBZ and PABA with 1:1, 2:1 and 4:1 stoichiometries to scale up corresponding cocrystals, and the slurries were stirred by magnetic stir bars. The solids were characterized both after 1 day and after 1 week. After CBZ/PABA 2:1 and CBZ III present as the stable forms in the slurries of excess 4CBZ:1PABA in filtered ethanol, acetonitrile and chloroform solution co-saturated by both CBZ/PABA 2:1 and CBZ, CBZ/PABA 4:1 cocrystals were added to the slurries, which dissolved into solution and formed CBZ/PABA 2:1 and CBZ III, rather than driving the conversion of the existing mixtures to CBZ/PABA 4:1.

2.4.9 Differential Scanning Calorimetry (DSC)

Thermograms of all samples were recorded on a TA Instruments Q20 DSC. The thermal properties of the cocrystal samples, which were placed in hermetically-sealed aluminum pans, was tested under nitrogen purge and with a heating rate of 10 °C min^{-1} from 40 °C to 200 °C. The instrument was calibrated with an indium standard.

2.4.10 Hot Stage Experiment Combined with Raman Spectroscopy

CBZ/PABA cocrystal samples were placed on a LTS350 hotstage from Linkam Scientific Instruments Ltd equipped on the Renishaw inVia Raman microscope. Samples were heated from 80 °C to 110 °C with a 1 °C min^{-1} heating rate. The exposure time for Raman spectroscopy was 5 seconds with a static scan centered at 520 cm^{-1}.

2.4.11 Dissolution Experiments

2.4.11.1. Dissolution Monitored by In-situ UV-Vis Spectra with Simultaneous Raman Spectra

A Pion Rainbow Dynamic Dissolution Monitor® System, which can simultaneously collect UV-vis spectra from different solutions during dissolution, was utilized to investigate the dissolution behavior of CBZ III, CBZ dihydrate, PABA I, CBZ/PABA 1:1, 2:1 and 4:1 cocrystals. The path length of the probe tips was 2 mm. To draw standard curves for calibration, UV-vis spectra of a series of CBZ and PABA solutions with various concentrations in corresponding solvent (phosphate-buffered saline or acetonitrile) were collected by immersing probes into jars with 150 mL standard solutions agitated by magnetic stir bars. Pellets for dissolution experiments were prepared by compressing samples of approximately 2 mm thickness in dies at 200 psi for 5 minutes to form a smooth 0.0707 cm^2 disk. The dies were then set in FO miniBath magnetic stir bars such that only the smooth sample surface was in contact with the solution. All dissolution experiments were conducted by rotating the compressed pellets at a 300 rpm speed in 10 mL PBS or acetonitrile at room temperature. The probes were held above the top of the rotating samples without direct contact. For experiments in PBS, 120 UV-vis spectra with 10 second collection intervals were first collected, followed by 8 spectra with 5 minutes intervals. For experiments in acetonitrile, 100 UV-vis spectra with 10 seconds intervals were collected. Simultaneous Raman spectra were taken to monitor phase conversion during the dissolution process in PBS with a Kaiser Raman RXN System equipped with an Invictus™ 785 nm NIR laser and a non-contact optics with a 20× objective. All spectra were taken with 10 acquisitions with 1 s exposure time for each acquisition.

2.4.11.2 Dissolution Experiments in PBS

To resist pH decrease resulting from PABA dissolving into the solution, a 10 mM PBS solution with pH 7.0 was applied as the medium for the dissolution experiments, and pH meter measurements before and after dissolution showed that the changes in pH

were smaller than 0.1. In-situ UV-Vis and Raman spectroscopy were applied to monitor the dissolution process of all samples. Spectra of standard solution with known concentration prepared by dissolving CBZ and PABA in buffer respectively have been collected ahead for calibration. The absorbance at 268 nm and 284 nm was selected for calculating CBZ and PABA concentration in PBS. Formation of CBZ dihydrate was observed on the surfaces all CBZ/PABA cocrystal samples by in-situ Raman spectroscopy.

2.4.11.3 Dissolution Experiments in Acetonitrile

Since the UV-Vis absorption spectra of CBZ and PABA in acetonitrile is different from that in PBS, the absorbance at 240 nm and 284 nm instead of 268 nm and 284 nm has been selected for calculation.

2.5 References

(1) Amidon, G.; Lennernäs, H.; Shah, V.; Crison, J. A Theoretical Basis for a Biopharmaceutic Drug Classification: The Correlation of in Vitro Drug Product Dissolution and in Vivo Bioavailability. *Pharm Res* **1995,** *12*, 413-420.

(2) Zakeri-Milani, P.; Barzegar-Jalali, M.; Azimi, M.; Valizadeh, H. Biopharmaceutical classification of drugs using intrinsic dissolution rate (IDR) and rat intestinal permeability. *European Journal of Pharmaceutics and Biopharmaceutics* **2009,** *73*, 102-106.

(3) Thayer, A. M. FINDING SOLUTIONS. *Chemical & Engineering News Archive* **2010,** *88*, 13-18.

(4) Murdande, S. B.; Pikal, M. J.; Shanker, R. M.; Bogner, R. H. Solubility Advantage of Amorphous Pharmaceuticals: II. Application of Quantitative Thermodynamic Relationships for Prediction of Solubility Enhancement in Structurally Diverse Insoluble Pharmaceuticals. *Pharm Res* **2010,** *27*, 2704-2714.

(5) Hancock, B. C.; Parks, M. What is the True Solubility Advantage for Amorphous Pharmaceuticals? *Pharm Res 17*, 397-404.

(6) Babu, N. J.; Nangia, A. Solubility Advantage of Amorphous Drugs and Pharmaceutical Cocrystals. *Crystal Growth & Design* **2011,** *11*, 2662-2679.

(7) Blagden, N.; de Matas, M.; Gavan, P. T.; York, P. Crystal engineering of active pharmaceutical ingredients to improve solubility and dissolution rates. *Advanced Drug Delivery Reviews* **2007,** *59*, 617-630.

(8) Byrn, S. R.; Pfeiffer, R. R.; Stephenson, G.; Grant, D. J. W.; Gleason, W. B. Solid-State Pharmaceutical Chemistry. *Chemistry of Materials* **1994,** *6*, 1148-1158.

(9) Berge, S. M.; Bighley, L. D.; Monkhouse, D. C. Pharmaceutical salts. *Journal of Pharmaceutical Sciences* **1977,** *66*, 1-19.

(10) Rodríguez-Spong, B.; Price, C. P.; Jayasankar, A.; Matzger, A. J.; Rodríguez-Hornedo, N. r. General principles of pharmaceutical solid polymorphism: A supramolecular perspective. *Advanced Drug Delivery Reviews* **2004,** *56*, 241-274.

(11) Serajuddin, A. T. M. Salt formation to improve drug solubility. *Advanced Drug Delivery Reviews* **2007,** *59*, 603-616.

(12) Kawabata, Y.; Wada, K.; Nakatani, M.; Yamada, S.; Onoue, S. Formulation design for poorly water-soluble drugs based on biopharmaceutics classification system: Basic approaches and practical applications. *International Journal of Pharmaceutics* **2011,** *420*, 1-10.

(13) Elder, D. P.; Holm, R.; Diego, H. L. d. Use of pharmaceutical salts and cocrystals to address the issue of poor solubility. *International Journal of Pharmaceutics* **2013,** *453*, 88-100.

(14) Almarsson, O.; Zaworotko, M. J. Crystal engineering of the composition of pharmaceutical phases. Do pharmaceutical co-crystals represent a new path to improved medicines? *Chemical Communications* **2004**, 1889-1896.

(15) Qiao, N.; Li, M.; Schlindwein, W.; Malek, N.; Davies, A.; Trappitt, G. Pharmaceutical cocrystals: An overview. *International Journal of Pharmaceutics* **2011,** *419*, 1-11.

(16) Thakuria, R.; Delori, A.; Jones, W.; Lipert, M. P.; Roy, L.; Rodr ́guez-Hornedo, N. Pharmaceutical cocrystals and poorly soluble drugs. *International Journal of Pharmaceutics* **2013,** *453*, 101-125.

(17) Childs, S. L.; Hardcastle, K. I. Cocrystals of Piroxicam with Carboxylic Acids. *Crystal Growth & Design* **2007,** *7*, 1291-1304.

(18) Roy, L.; Lipert, M. P.; Rodriguez-Hornedo, N. Co-crystal Solubility and Thermodynamic Stability. In *Pharmaceutical Salts and Co-crystals*, Wouters, J.; Qu ́r ́é, L., Eds. The Royal Society of Chemistry: 2012; pp 247-279.

(19) Good, D. J.; Rodríguez-Hornedo, N. Cocrystal Eutectic Constants and Prediction of Solubility Behavior. *Crystal Growth & Design* **2010,** *10*, 1028-1032.

(20) Trask, A. V.; van de Streek, J.; Motherwell, W. D. S.; Jones, W. Achieving Polymorphic and Stoichiometric Diversity in Cocrystal Formation: Importance of Solid-State Grinding, Powder X-ray Structure Determination, and Seeding. *Crystal Growth & Design* **2005,** *5*, 2233-2241.

(21) Jayasankar, A.; Reddy, L. S.; Bethune, S. J.; Rodríguez-Hornedo, N. Role of Cocrystal and Solution Chemistry on the Formation and Stability of Cocrystals with Different Stoichiometry. *Crystal Growth & Design* **2009,** *9*, 889-897.

(22) Alhalaweh, A.; George, S.; Boström, D.; Velaga, S. P. 1:1 and 2:1 Urea−Succinic Acid Cocrystals: Structural Diversity, Solution Chemistry, and Thermodynamic Stability. *Crystal Growth & Design* **2010,** *10*, 4847-4855.

(23) Guo, K.; Sadiq, G.; Seaton, C.; Davey, R.; Yin, Q. Co-Crystallization in the Caffeine/Maleic Acid System: Lessons from Phase Equilibria. *Crystal Growth & Design* **2010,** *10*, 268-273.

(24) Bevill, M. J.; Vlahova, P. I.; Smit, J. P. Polymorphic Cocrystals of Nutraceutical Compound p-Coumaric Acid with Nicotinamide: Characterization, Relative Solid-State Stability, and Conversion to Alternate Stoichiometries. *Crystal Growth & Design* **2014,** *14*, 1438-1448.

(25) He, H.; Jiang, L.; Zhang, Q.; Huang, Y.; Wang, J.-R.; Mei, X. Polymorphism observed in dapsone-flavone cocrystals that present pronounced differences in solubility and stability. *CrystEngComm* **2015,** *17*, 6566-6574.

(26) Sarma, B.; Reddy, L. S.; Nangia, A. The Role of π-Stacking in the Composition of Phloroglucinol and Phenazine Cocrystals. *Crystal Growth & Design* **2008,** *8*, 4546-4552.

(27) Zhang, S.-W.; Harasimowicz, M. T.; de Villiers, M. M.; Yu, L. Cocrystals of Nicotinamide and (R)-Mandelic Acid in Many Ratios with Anomalous Formation Properties. *Journal of the American Chemical Society* **2013,** *135*, 18981-18989.

(28) Good, D. J.; Rodr ́guez-Hornedo, N. Solubility Advantage of Pharmaceutical Cocrystals. *Crystal Growth & Design* **2009,** *9*, 2252-2264.

(29) Bethune, S. J.; Huang, N.; Jayasankar, A.; Rodr ́guez-Hornedo, N. Understanding and Predicting the Effect of Cocrystal Components and pH on Cocrystal Solubility. *Crystal Growth & Design* **2009,** *9*, 3976-3988.

(30) Saikia, B.; Bora, P.; Khatioda, R.; Sarma, B. Hydrogen Bond Synthons in the Interplay of Solubility and Membrane Permeability/Diffusion in Variable Stoichiometry Drug Cocrystals. *Crystal Growth & Design* **2015,** *15*, 5593-5603.

(31) Grzesiak, A. L.; Lang, M.; Kim, K.; Matzger, A. J. Comparison of the four anhydrous polymorphs of carbamazepine and the crystal structure of form I. *Journal of Pharmaceutical Sciences* **2003,** *92*, 2260-2271.

(32) Fleischman, S. G.; Kuduva, S. S.; McMahon, J. A.; Moulton, B.; Bailey Walsh, R. D.; Rodr ́guez-Hornedo, N.; Zaworotko, M. J. Crystal Engineering of the Composition of Pharmaceutical Phases: Multiple-Component Crystalline Solids Involving Carbamazepine. *Crystal Growth & Design* **2003,** *3*, 909-919.

(33) Hickey, M. B.; Peterson, M. L.; Scoppettuolo, L. A.; Morrisette, S. L.; Vetter, A.; Guzmán, H.; Remenar, J. F.; Zhang, Z.; Tawa, M. D.; Haley, S.; Zaworotko, M. J.; Almarsson, Ö. Performance comparison of a co-crystal of carbamazepine with marketed product. *European Journal of Pharmaceutics and Biopharmaceutics* **2007,** *67*, 112-119.

(34) Childs, S. L.; Rodriguez-Hornedo, N.; Reddy, L. S.; Jayasankar, A.; Maheshwari, C.; McCausland, L.; Shipplett, R.; Stahly, B. C. Screening strategies based on

solubility and solution composition generate pharmaceutically acceptable cocrystals of carbamazepine. *CrystEngComm* **2008,** *10*, 856-864.

(35) Kumar, S.; Bhargava, D.; Thakkar, A.; Arora, S. Drug carrier systems for solubility enhancement of BCS class II drugs: a critical review. *Critical reviews in therapeutic drug carrier systems* **2013,** *30*, 217-256.

(36) Gracin, S.; Rasmuson, Å. C. Polymorphism and Crystallization of p-Aminobenzoic Acid. *Crystal Growth & Design* **2004,** *4*, 1013-1023.

(37) McMahon, J. A.; Bis, J. A.; Vishweshwar, P.; Shattock, T. R.; McLaughlin, O. L. Crystal engineering of the composition of pharmaceutical phases. 3. Primary amide supramolecular heterosynthons and their role in the design of pharmaceutical co-crystals Abstract. *Zeitschrift für Kristallographie. Crystalline materials* **2005,** *220*, 340-350.

(38) A CBZ/PABA/water ternary crystal is also known but does not show up in the studies reported here. See reference 30.

(39) Paluch, K. J.; McCabe, T.; Müller-Bunz, H.; Corrigan, O. I.; Healy, A. M.; Tajber, L. Formation and Physicochemical Properties of Crystalline and Amorphous Salts with Different Stoichiometries Formed between Ciprofloxacin and Succinic Acid. *Molecular Pharmaceutics* **2013,** *10*, 3640-3654.

(40) Landenberger, K. B.; Bolton, O.; Matzger, A. J. Two Isostructural Explosive Cocrystals with Significantly Different Thermodynamic Stabilities. *Angewandte Chemie International Edition* **2013,** *52*, 6468-6471.

(41) Qiao, N.; Wang, K.; Schlindwein, W.; Davies, A.; Li, M. In situ monitoring of carbamazepine–nicotinamide cocrystal intrinsic dissolution behaviour. *European Journal of Pharmaceutics and Biopharmaceutics* **2013,** *83*, 415-426.

(42) Svard, M.; Nordstrom, F. L.; Hoffmann, E.-M.; Aziz, B.; Rasmuson, A. C. Thermodynamics and nucleation of the enantiotropic compound p-aminobenzoic acid. *CrystEngComm* **2013,** *15*, 5020-5031.

(43) Ikni, A.; Clair, B.; Scouflaire, P.; Veesler, S.; Gillet, J.-M.; El Hassan, N.; Dumas, F.; Spasojević-de Biré, A. Experimental Demonstration of the Carbamazepine Crystallization from Non-photochemical Laser-Induced Nucleation in Acetonitrile and Methanol. *Crystal Growth & Design* **2014,** *14*, 3286-3299.

Chapter 3. Solid State Studies of a Novel Nitric Oxide Releasing Crystal/Polymer Composite with Enhanced Stability

Wo, Y.; Li, Z.; Brisbois, E. J.; Colletta, A.; Wu, J.; Major, T. C.; Xi, C.; Bartlett, R. H.; Matzger, A. J.; Meyerhoff, M. E. "Origin of Long-Term Storage Stability and Nitric Oxide Release Behavior of CarboSil Polymer Doped with S-Nitroso-N-acetyl-D-penicillamine" *ACS App. Mater. Interfaces*, **2015**, *7* (40), pp 22218-22227 (collaboration)

All solid state analysis in this chapter, including optical microscopy, Raman spectroscopy, PXRD characterization and formula derivation were conducted by the dissertation author. All figures in the chapter except for Figure 3.1, 3.3 and 3.16 are constructed by the dissertation author.

3.1 Introduction

Biomedical devices that will contact with blood, ranging from simple catheters to complex extracorporeal life support systems, are vital in daily medical care.[1] However, complications related to blood/surface interactions, such as pulmonary embolism, stroke and deep vein thrombosis, can be associated with the use of indwelling blood-contacting medical devices.[2] Biofilm associated infections are another issue that can cause increased morbidity and death.[3] Therefore, approaches to reduce the risk of these complications and create nonthrombogenic and antimicrobial prosthetic surfaces should be developed.[2]

It has been discovered that the gaseous signaling molecule, nitric oxide (NO), as an endothelium-derived relaxing factor (EDRF), plays an important role in a series of

physiological processes (Figure 3.1), such as inhibiting platelet activation and adhesion, preventing bacterial growth, reducing smooth cell proliferation, regulating complex biological processes, etc.[4-28] Therefore, the ubiquity and chemical simplicity of NO have made it a promising therapeutic agent. The flux of NO released from a healthy endothelium lining has been estimated to be between 0.5 and 4.0×10^{-10} mol cm^{-2} min^{-1}.[6, 29-31] Due to the high reactivity and short half-life of NO under physiological conditions, developments of NO releasing materials are in need to achieve sustained NO release at the physiological flux level, in order to increase the hemocompatibility of blood-contacting devices.[6, 32]

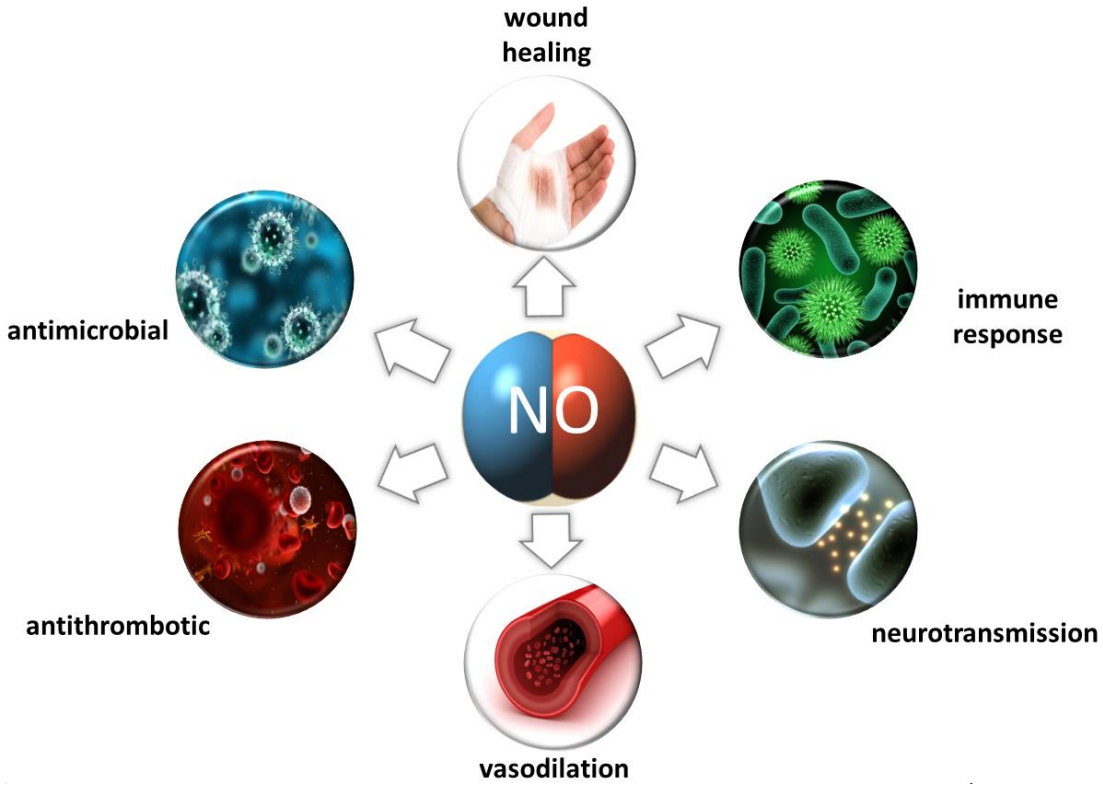

Figure 3. 1 NO plays an important role in a series of physiological processes.

A wide range of NO donors, including *S*-nitrosothiols (RSNO) and *N*-diazeniumdiolates (NONOate), have been studied for NO releasing purposes. These compounds can be incorporated into polymers to provide continuous and localized NO delivery to specific sites of interest.[5, 9, 20, 33] *S*-nitroso-*N*-acetylpenicillamine

(SNAP), a synthetic tertiary RSNO that can decompose and release NO via thermal decomposition, metal ion catalysis and photolysis, is more stable with respect to the loss of NO than other primary and secondary RSNOs, because of the steric hindrance effect imposed by the gem methyl group on the dimerization of the radicals that leads to the formation of the sulfur bridge, as well as the hindered rotation of the R-S-N-O linkage.[5, 6, 15, 34, 35] Based on literature, the acetamide group in SNAP also helps to increase the S-NO bond strength and reduce the NO liability.[36] The overall reaction of SNAP decomposition can be expressed as

$$2\text{SNAP} \rightarrow 2\text{NO} + \text{NAP disulfide}$$

(a) 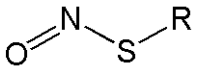

(b) 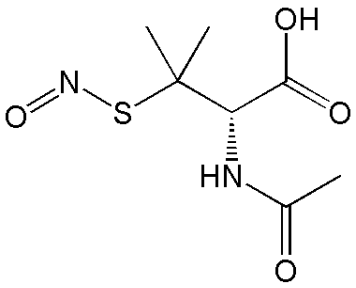

Figure 3. 2 Chemical structures of (a) RSNO and (b) SNAP.

The Meyerhoff lab has achieved stabilization of SNAP by doping SNAP within low water uptake polymers, for instance Elast-eon E2As, a siloxane-base polyurethane elastomer.[6] The polymer film doped with SNAP, produced by the solvent evaporation method, exhibits relatively high stability during shelf-life studies, with 82% of the initial SNAP remaining after 2 months of dry storage at 37 °C. Such polymers can be coated onto the shelf biomedical devices to improve their hemocompatibility. However, studies on the microstructure of such polymer films have not been conducted, and the details of the film solid state chemistry and SNAP decomposition in the polymer remain unclear. Previously, one hypothesized mechanism of the SNAP stabilization and extended NO release has been proposed based on the cage effect of the polymer viscosity on the S-NO bond cleavage and radical pair formation. With mobility restricted by the polymer matrix, the primary radicals formed by the soluble

SNAP molecules in the polymer microenvironment might be favored to recombine rather than to escape from the solvent cage.

CarboSil 20 80A (CarboSil) is a thermoplastic silicone polycarbonate-urethane with a mix of soft segments of poly(dimethylsiloxane) and polycarbonate as well as a hard segment of methylene diphenyl isocyanate, combines the biocompatibility and biostability of silicone elastomers and processing capability and toughness of carbonate-urethanes. In this work, SNAP has been doped onto three selected biomedical grade polymers with low water uptake, and among all the samples SNAP-doped CarboSil film shows most exceptional performance in shelf-life and NO release study: 10 wt% CarboSil films maintain 91.8 ± 3.2% of the initial SNAP after ethylene oxide sterilization, compared to 82.7 ± 3.8% for the Elast-eon 5-325 (E5-325, a silicone based polyurethane elastomer) films and 78.7 ± 3.1% for the silicone rubber (SR, polydimethylsiloxane) films (Figure 3.3). Therefore, SNAP-doped CarboSil has been selected as the model to investigate the stability mechanism of SNAP doped in polymers. A series of solid state characterization experiments have been conducted, and a crystallization based mechanism has been proposed to account for stability and controlled release.

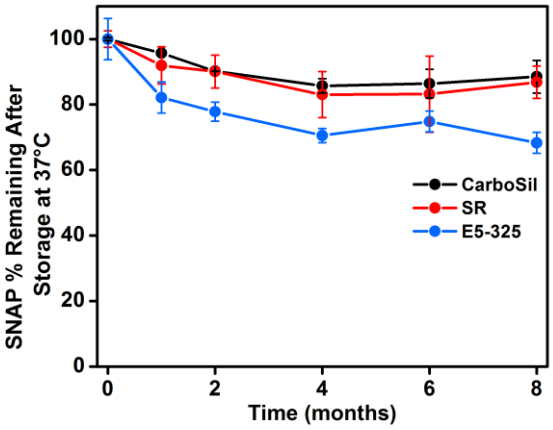

Figure 3. 3 Shelf-life study of 10 wt% SNAP-doped CarboSil, SR and E5-325 films stored dry (with desiccant) in the dark at 37 ℃. The SNAP remaining in the films after various time points is determined and compared with the initial level. Data are mean ± SEM (n=3).

3.2 Results and Discussion

3.2.1 Crystalline SNAP in CarboSil

Under a polarized light microscope, distinguishable crystalline patterns were detected in films of 5 wt % SNAP-doped CarboSil films, while such patterns could not be found within the blank CarboSil references (Figure 3.4). Therefore, it was proposed that SNAP crystallized in the polymer matrix during the solvent evaporation process, as opposed to all dissolving in the polymer and forming a homogeneous matrix as previously believed.

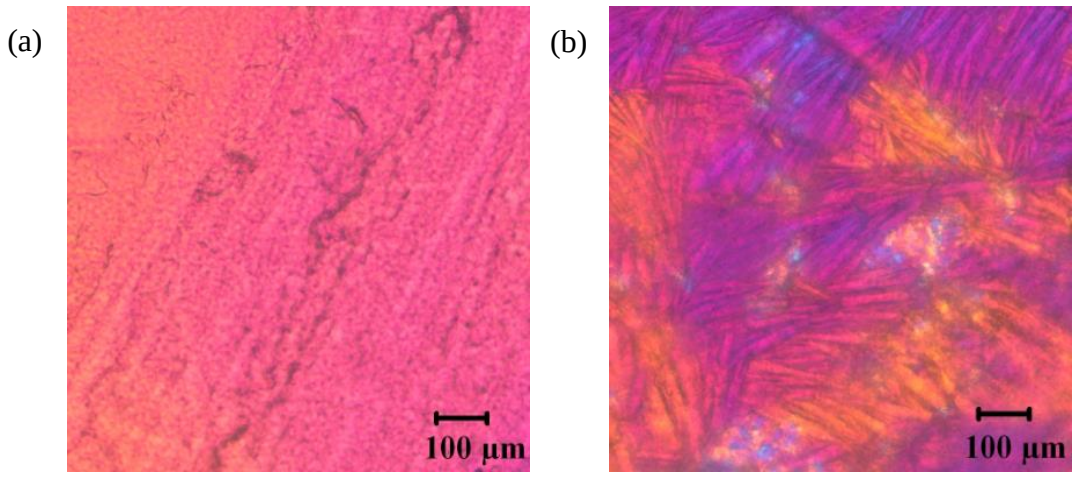

Figure 3. 4 Optical image of (a) blank CarboSil and (b) 5 wt% SNAP-doped CarboSil film surface taken under crossed polarizers in combination with a quarter-wave plate. The 5 wt% film clearly shows patterns which suggest the presence of crystalline structures.

Raman spectra of SNAP crystals, blank CarboSil film and 15 wt % SNAP-doped CarboSil film were compared to clarify the constituents within the SNAP-doped CarboSil firms. Characteristic peaks of both CarboSil and crystalline SNAP were detected in the 15 wt % SNAP-doped CarboSil film, which further substantiates the existence of crystalline SNAP within the polymer film (Figure 3.5). Raman spectroscopy provides information of chemical composition in a small area. Since it can be seen from optical images that the distribution of crystalline patterns in the SNAP-doped CarboSil films are not uniform, other techniques that reflect the average behavior of the sample rather than a specific small region are needed for characterization.

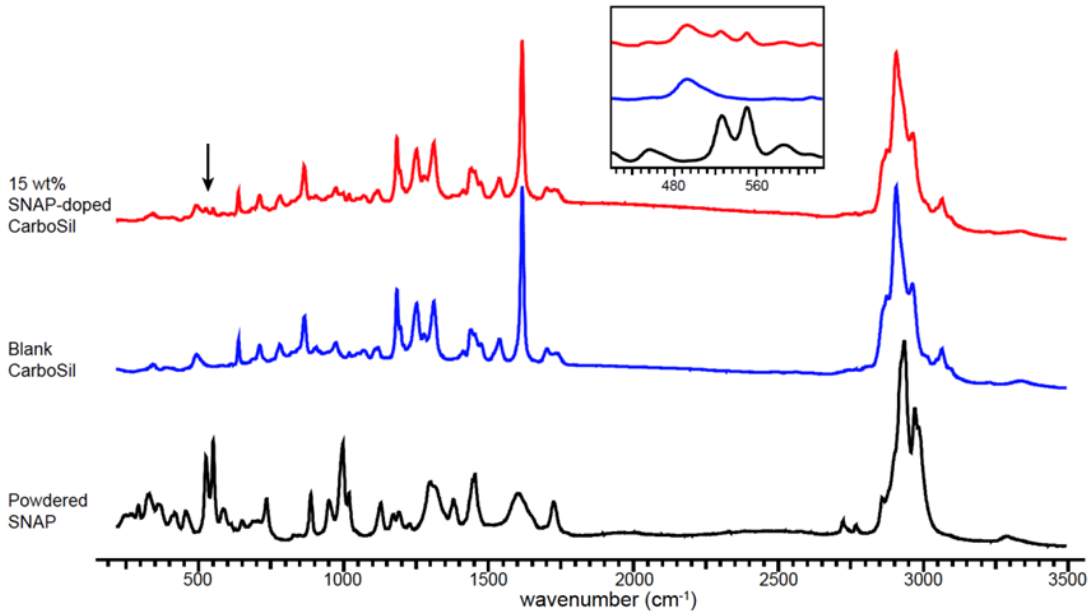

Figure 3. 5 Raman spectra comparison among SNAP powder, blank CarboSil and 15 wt% SNAP-doped CarboSil. The main difference in Raman scattering lies between 500-600 cm^{-1} (see inset), which was used in the static scan for as characteristics for locating the existence of SNAP crystals.

In order to identify the crystalline form of SNAP in CarboSil observed by Raman spectroscopy and to improve the detection limit, PXRD analysis, which is sensitive to the presence of crystals, was applied to samples of SNAP crystals, blank CarboSil and SNAP-doped CarboSil films. There are two polymorphs of SNAP reported in literature: the orthorhombic form and the monoclinic form.[37, 38] The PXRD patterns of synthesized SNAP crystal samples agreed with the simulated pattern of the orthorhombic form (Figure 3.6).

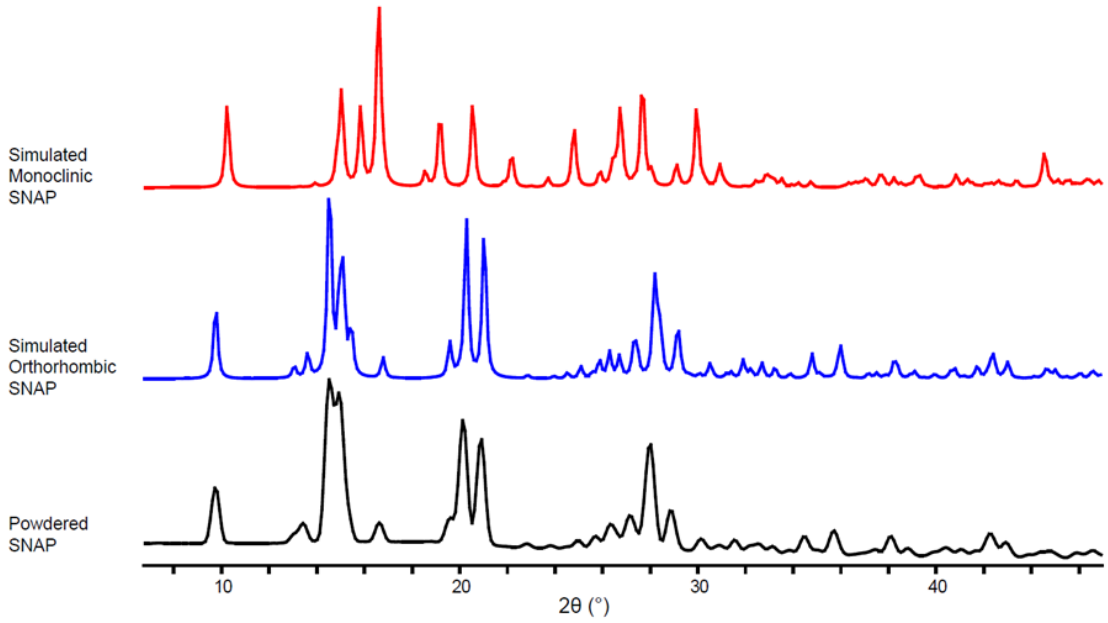

Figure 3. 6 PXRD pattern comparison for grounded SNAP powder, simulated orthorhombic SNAP and simulated monoclinic SNAP. The powdered SNAP used for this study is the orthorhombic polymorph.

For SNAP-doped films with greater than 4 wt % SNAP loading, the obtained PXRD patterns present a convolution of blank CarboSil and the orthorhombic SNAP patterns (Figure 3.7). It has been suggested that, in orthorhombic SNAP, all SNAP molecules are symmetry equivalent. Each SNAP molecule is connected to surrounding SNAP molecules by hydrogen bonding formed by the carboxyl and the amide groups, which build up infinite sheet layers of SNAP (Figure 3.8).[37] Therefore, SNAP molecules become stabilized in such packing motif.

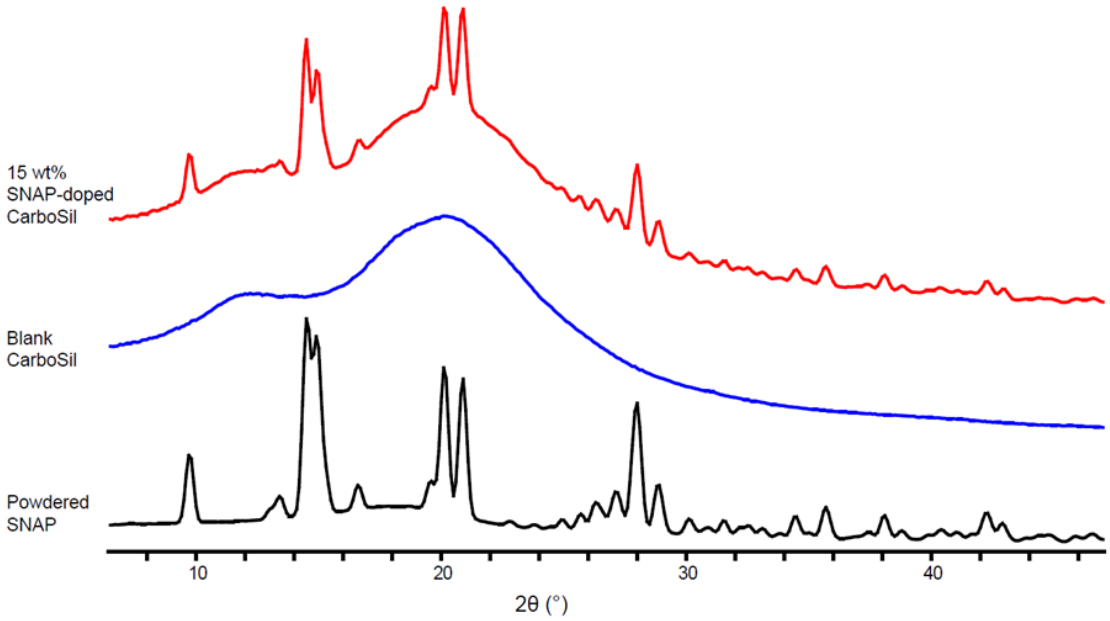

Figure 3. 7 PXRD patterns of SNAP powder, blank CarboSil and 15 wt% SNAP-doped CarboSil film samples. The pattern of the 15 wt% SNAP/CarboSil film demonstrates the existence of orthorhombic SNAP crystals imbedded in the polymer.

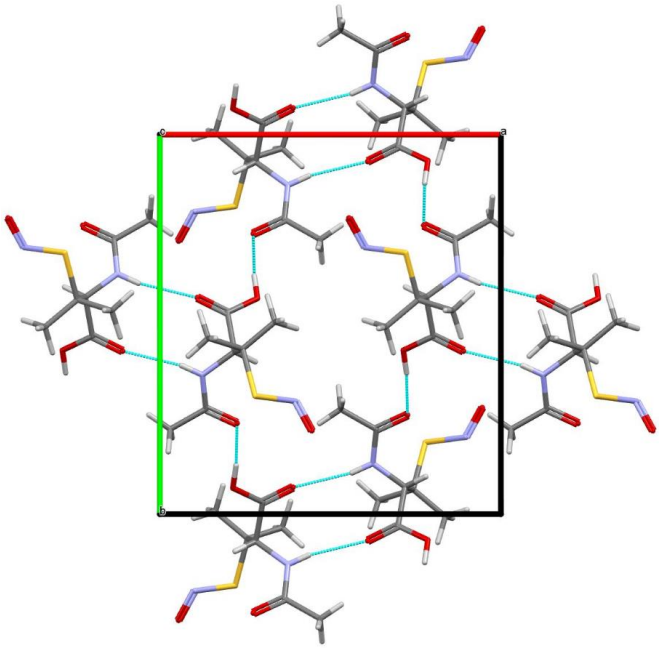

Figure 3. 8 Packing of orthorhombic SNAP crystals. All SNAP molecules are symmetry equivalent, being connected to each other by hydrogen bonds between the carboxyl group and the amide group.

3.2.2 A Crystallization Based Stability Mechanism

The PXRD patterns of SNAP-doped CarboSil samples suggested that, for films with greater than 4 wt % SNAP, as the amount of doped SNAP in polymer increased within the range of detection, the intensity of orthorhombic SNAP peaks in the obtained PXRD pattern is enhanced, indicating an increased amount of crystalline SNAP rather than solubilized SNAP within the polymer films. However, for samples with doped SNAP smaller than 4 wt % loading, SNAP peaks could barely by detected in PXRD patterns (Figure 3.9). Since all SNAP-doped CarboSil films, including those with SNAP loading lower than 4 wt %, present a light green color corresponding to the existence of SNAP, while crystalline SNAP can only be found in samples above certain threshold, it is speculated that SNAP can be partially dissolved in the polymer and forms a homogeneous polymer solution. When the SNAP loading is beyond the polymer solubility limit, excess SNAP crystallizes in the orthorhombic form during the solvent evaporation process and embeds in the polymer (Figure 3.10). This hypothesis is in agreement with the Raman spectroscopy and PXRD characterization results that crystalline SNAP can be detected only when the SNAP concentration exceeds the threshold.

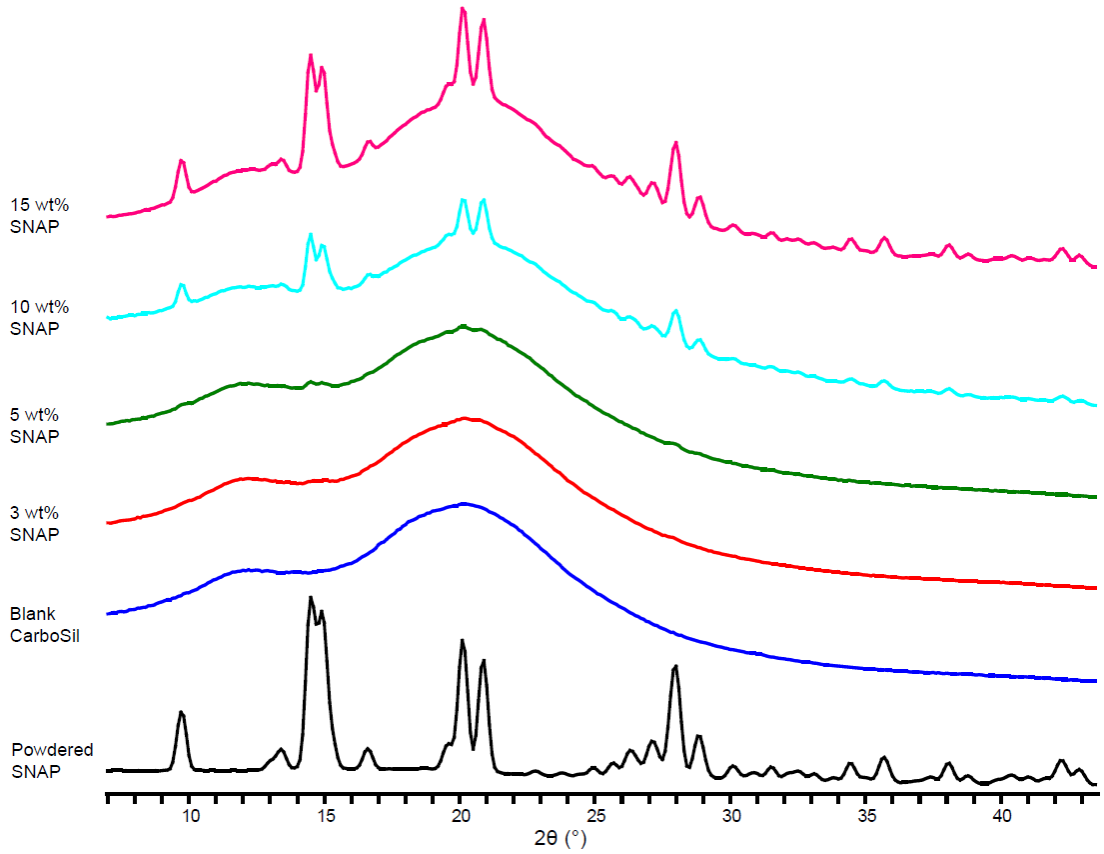

Figure 3. 9 PXRD patterns of SNAP powder, blank CarboSil and SNAP-doped CarboSil film samples of different weight percentages (1-15 wt%) were collected and here are a few typical examples for the patterns. Sample peaks were able to be clearly distinguished when the SNAP weight percentage is no less than 4 wt%.

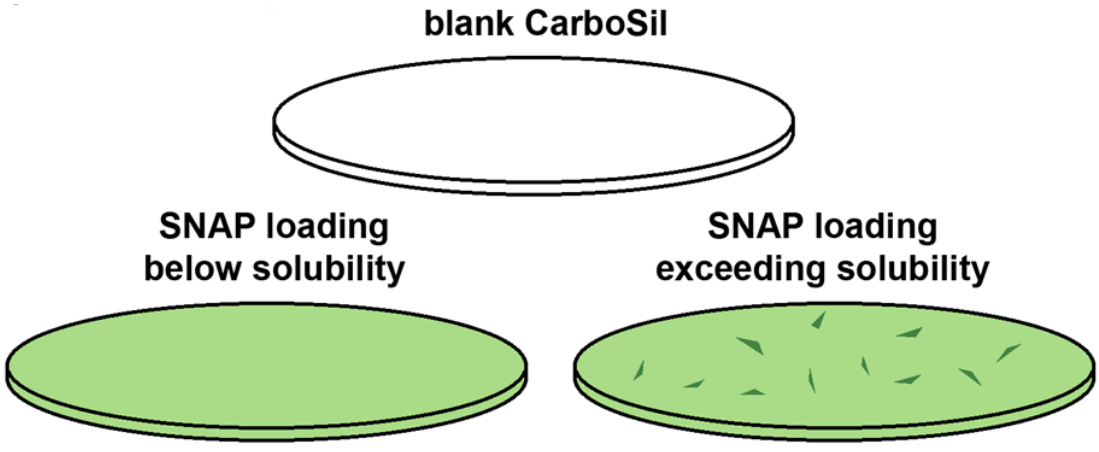

Figure 3. 10 Schematic representation of blank CarboSil and SNAP doped CarboSil with different loadings. Blank CarboSil samples are colorless transparent films. As the SNAP loading increases, SNAP dissolves into CarboSil and forms a polymer solution with higher concentration. Once SNAP loading reaches its solubility limit in CarboSil, excess SNAP forms crystals embedded in the polymer.

To calculate the SNAP solubility in the CarboSil polymer, PXRD analysis was applied to SNAP-doped CarboSil films with various loadings. Based on the following assumption that (1) crystalline SNAP is uniformly distributed in the CarboSil films and that (2) the preferred orientation of SNAP crystals in CarboSil could be eliminated by cutting samples into cubes as well as rotating and oscillating the samples during PXRD characterization, the ratio of peak area of a specific SNAP peak at a chosen 2θ angle over the total area of the obtained pattern would be proportional to the weight percentage of crystalline SNAP in the sample (Figure 3.11). The advantage of using the area ratio as a quantitative representation is to eliminate all the other factor that could affect the peak area (for instance, the volume of the sample irradiated by the X-ray source, the exposure time of sample under the X-ray, etc.), and the only influencing factor would be the proportion of crystalline SNAP in the polymer. Here, we set the doped SNAP weight percentage as x and the ratio of the k^{th} orthorhombic SNAP peak area over the SNAP-doped CarboSil pattern total area as y_k, and then y_k can be calculated as:

$$y_k = \frac{k^{th}\ \text{SNAP peak area}}{\text{total SNAP peaks area} + \text{CarboSil pattern area}} = \frac{a_k(x - x_0)}{a(x - x_o) + b(1 - x)}$$

For a PXRD pattern of a sample with a unit volume and taken with a unit exposure time, a_k, a and b correspond to the area of the k^{th} peak in the orthorhombic SNAP pattern, the total area of all orthorhombic SNAP peaks, and the total area of blank CarboSil pattern, respectively. The term x_o is the SNAP solubility in SNAP-CarboSil solid solution system in the percentage representation. As a result, for any SNAP-doped CarboSil sample, $a_k(x - x_0)$ represents the area of the k^{th} orthorhombic SNAP peak in the pattern, $a(x - x_o)$ represents the area of all signals from orthorhombic SNAP, and $b(1 - x)$ represents the area of all signals from CarboSil in this sample. Since y_k is a ratio of areas, which is independent of sample volume and exposure time, etc., the only factor that influences y_k is the SNAP weight percentage x in the

prepared CarboSil films. By substituting various x and y_k at chosen 2θ angles, a_k, a, b and x_o can be determined.

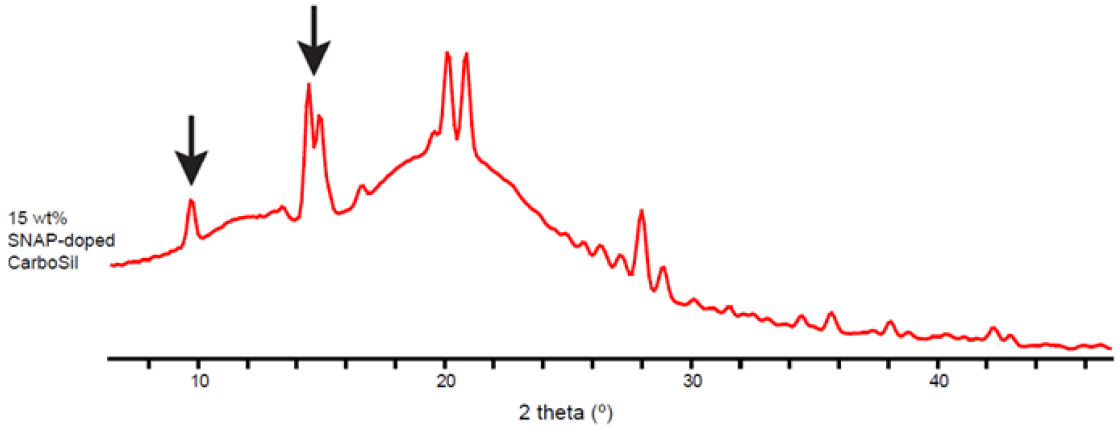

Figure 3. 11 SNAP solubility in CarboSil films prepared by solvent evaporation was calculated based on the ratio of selected SNAP peak area over the total area of the sample pattern.

A linear least-squares regression was conducted using three dominant characteristic peaks (2θ = 9.5, 14.5, 14.9), and the calculated solubility is 3.6, 3.5 and 3.9 wt %, respectively (Figure 3.12). The a values calculated using three different SNAP peaks were 0.099, 0.082 and 0.102, respectively, and the b values were 13.0, 12.9 and 13.0, respectively. As both values are within the error of tolerance, it suggests that the derived equation and the fitting model are successful quantitative representations of the doped polymer system. Allowing the influence of crystal orientation in the sample that could affect the result, the solubility of SNAP in CarboSil was ca. 3.4-4.0 wt %.

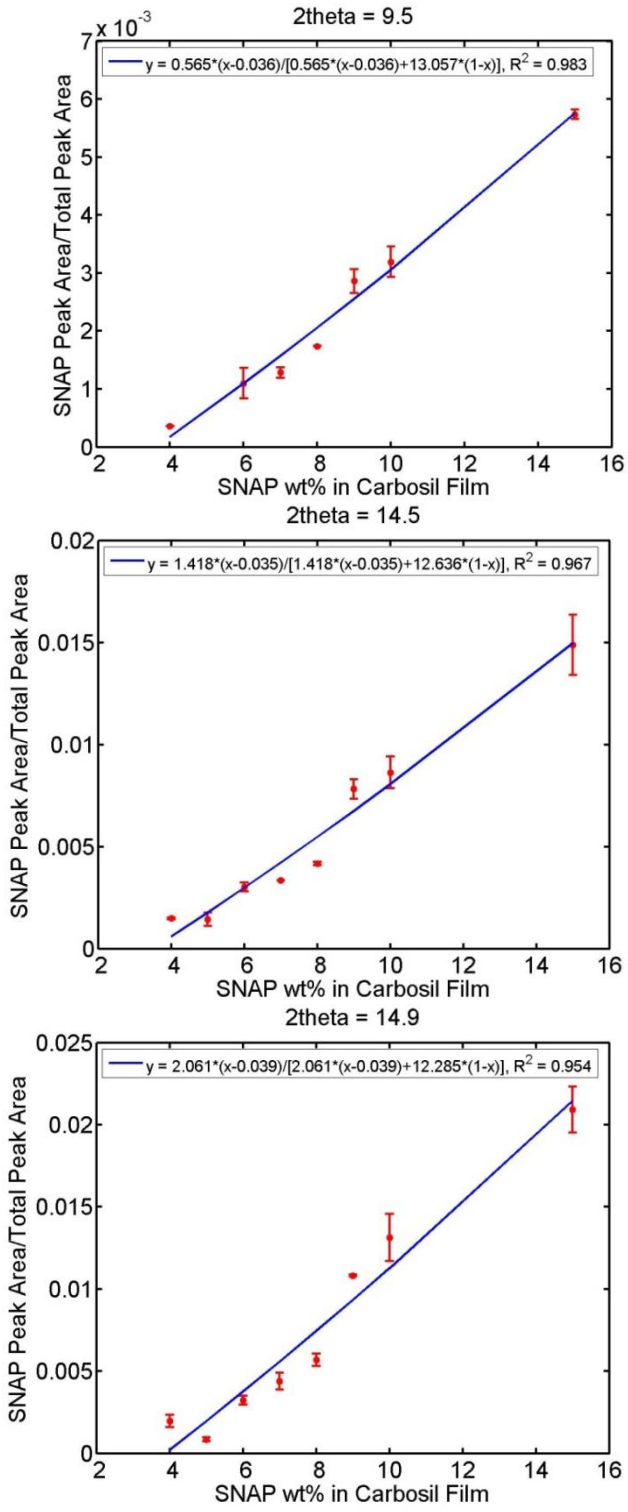

Figure 3. 12 Correlation of data obtained by powder X-ray diffraction for SNAP in CarboSil. Linear regression lines were fitted using least squares approach. The 3 most prominent orthorhombic SNAP peaks were chosen to do the fitting (2θ = 9.5, 14.5 and 14.9) and the calculated SNAP solubility in CarboSil polymer was 3.6 wt%, 3.5 wt% and 3.9 wt%, respectively.

In this crystalline based hypothesis, the crystal lattice energy of the crystalline form is the key for the improved SNAP stability. It is proposed that the solubilized SNAP behaves as a solute, which is more reactive at ambient conditions than the crystalline SNAP. As the solubilized SNAP in the polymer decomposes and releases NO, the SNAP crystals embedded in the CarboSil are driven to gradually dissolve into the polymer layer (Figure 3.13). Characterizing the stabilities of SNAP-doped CarboSil films further verifies the hypothesis that solubilized SNAP decomposes faster. PXRD analysis was conducted for freshly prepared 5 and 15 wt % SNAP-doped CarboSil samples as well as the samples stored under ambient light at room temperature for 10 days under the same conditions. For 5 wt % fresh samples, most of the SNAP added during the film preparation is dissolved in the polymer, which is liable and more likely to decompose via thermal decomposition and photolysis. However, for the 15 wt % SNAP films, most of the SNAP in the film (ca. 11-12 wt %) stays in the crystalline state and is stabilized by the intermolecular interactions in the orthorhombic form. After 10 days, the 5 wt % sample faded from green color to pale green corresponding to the loss of SNAP, while there was no obvious change in color for the 15 wt % sample. The percentage of SNAP remaining in the 5 and 15 wt % films after 10 days under ambient light is 19.8 and 83.2 wt % of the initial amount, respectively, which corresponds to the approximate initial amount of crystalline SNAP in each fresh sample. The attenuation of orthorhombic SNAP peaks of the SNAP-doped CarboSil films relative to the fresh samples is minor compared to the total loss (Figure 3.14). The results validate that the lost SNAP is mainly the SNAP dissolved in CarboSil. The decrease of SNAP remaining in the 15 wt % sample is less significant than that in the 5 wt %, is the result of the greater proportion of SNAP crystals in the 15 wt % sample that hinders the photolysis of solubilized SNAP.

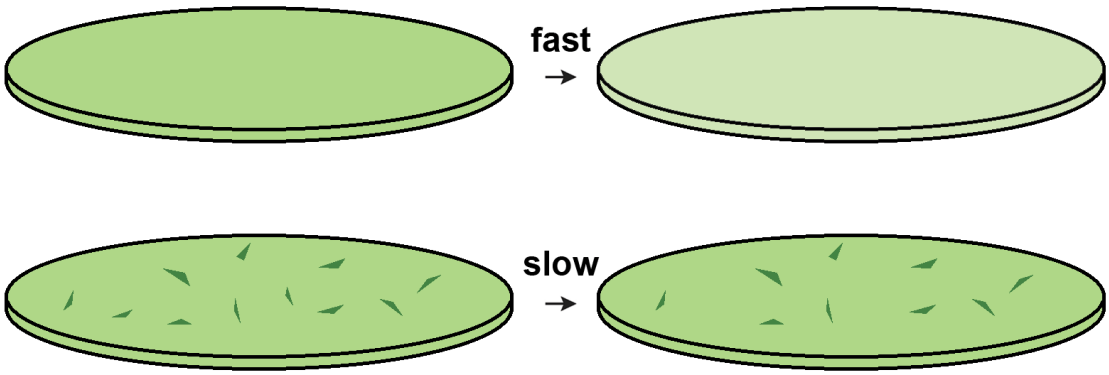

Figure 3. 13 Schematic diagram of SNAP decomposition in CarboSil. In CarboSil films with low SNAP loading, most SNAP molecules are dissolved in polymer and decomposes fast. In CarboSil films with high SNAP loading, greater proportion of SNAP is in the crystalline state, which undergoes slow decomposition process.

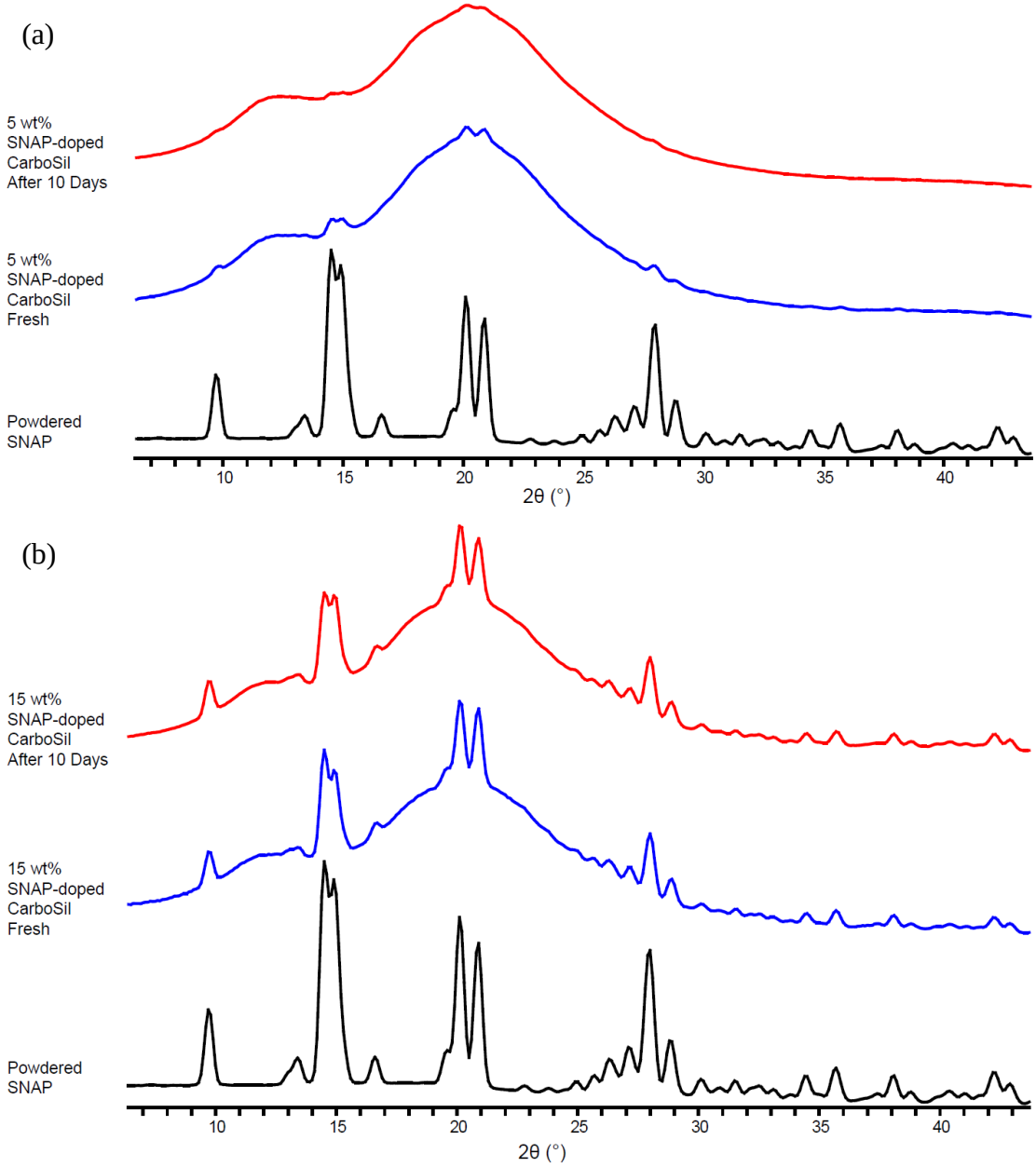

Figure 3. 14 PXRD patterns of (a) 5 wt % and (b) 15 wt % SNAP-doped CarboSil samples freshly prepared and stored under ambient light at room temperature for 10 days under the same conditions.

Raman mapping characterization using static scans was employed to determine the 2D representation of the SNAP crystal distribution inside of the 3 and 5 wt % SNAP-doped CarboSil films (Figure 3.15). The green regions represent regions with signal corresponding to crystalline SNAP, which are found in large quantities only in

the 5 wt % SNAP/CarboSil films, but not in 3 wt % films. This finding correlates with the PXRD peak area fitting results which indicate that the solubility of SNAP in polymer is 3.4-4.0 wt %. However, the exact grain sizes of the SNAP crystals could not yet be quantified by this method because the focal depth of the laser is likely to exceed the grain size of the crystal. Thus, the crystalline SNAP signal could represent crystals from both the surface and deeper within the polymer phase, which results in difficulty in distinguishing any individual crystal from overlaid crystals.

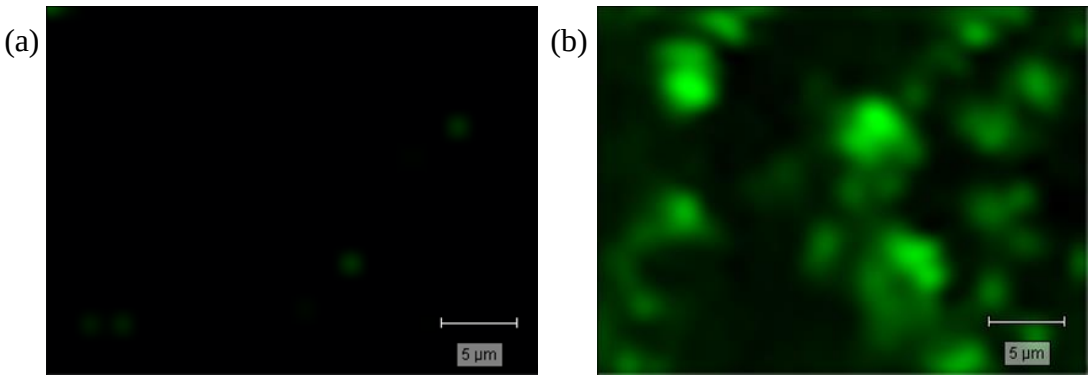

Figure 3. 15 Raman mapping results for fitting of cross section of (a) 3 wt% and (b) 5 wt% SNAP-doped Carbosil films with pure orthorhombic SNAP spectrum as the reference under 100× objective. Green represents areas fitting the crystalline SNAP spectrum.

3.2.3 Solid State Analysis of SNAP-doped PVC/DEHP Polymer Systems

The crystallization based mechanism of SNAP stability in doped polymers is also supported by studies in a SNAP-doped polyvinyl chloride (PVC)/di-2-ethylhexyl phthalate (DEHP) composite. Terumo Sarns™ cannulae is a commercial catheter used in medical applications such as cardiac surgery where it removes de-oxygenated blood, sends it to the heart-lung machine, and returns oxygenated blood to the patient. It is manufactured using PVC plasticized with DEHP. Adding SNAP to this polymer in order to create an NO releasing surface has the potential to improve the hemocompatibility of the catheter by reducing platelet activation and bacterial adhesion. The shelf-life study of SNAP-doped PVC/DEHP films demonstrated that samples with

3.6wt% SNAP were stable; after 1 month of storage, 98.1 ±0.8% at room temperature and 88 ±0.5% at 37 ℃ of the initial SNAP was retained in the sample (Figure 3.16). In contrast, samples doped with 1.3 wt% SNAP were less stable overall, retaining approximately 70.4 ±8.3% and 60.4 ±10.3% of the initial SNAP at room temperature and 37 ℃, respectively. Such result indicates that retaining a higher loading of the initial SNAP is critical to maintaining effective NO release levels needed for potential biomedical applications, which agrees with our previous stability study of SNAP-doped CarboSil films. Therefore, solid state characterization has been conducted on SNAP doped PVC-DEHP films.

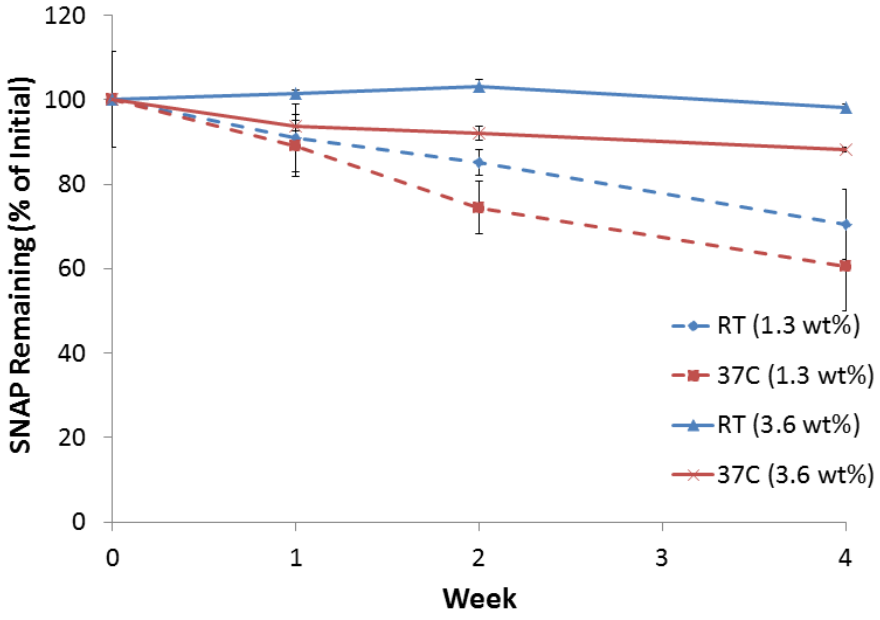

Figure 3. 16 Stability of 1.3 and 3.6 wt% SNAP in the PVC-DEHP polymer matrix, where samples were stored dry either at room temperature (RT, 25 °C) or 37 °C with desiccant. Samples were dissolved in DMAc to rapidly determine the amount of SNAP remaining at various times (compared to the initial SNAP amount) using UV-Vis at 340 nm. Data are the mean ± SEM (n=4).

The existence of crystals was again confirmed by the crystalline patterns in the SNAP-doped PVC/DEHP films in comparison with the blank PVC/DEHP film under an optical microscope equipped with polarizers (Figure 3.17). With 5 wt% SNAP

loading, the crystalline patterns in PVC/DEHP appeared to be denser than that in CarboSil, which can imply a lower SNAP solubility in PVC/DEHP that leads to higher proportion of crystalline SNAP for the same degree of SNAP loading. Raman spectra of 10 wt% SNAP-doped PVC/DEHP films presented characteristic peaks of both PVC/DEHP and orthorhombic SNAP crystal (Figure 3.18), which verifies the crystallization of SNAP in PVC/DEHP into the orthorhombic form. Similar to the case of SNAP doped CarboSil, for PVC/DEHP samples with low SNAP loading, due to the strong polymer background, characteristic peaks of SNAP are concealed by the PVC/DEHP signal. Therefore, PXRD analysis has been applied to estimate the proportion of crystalline SNAP in the polymer films.

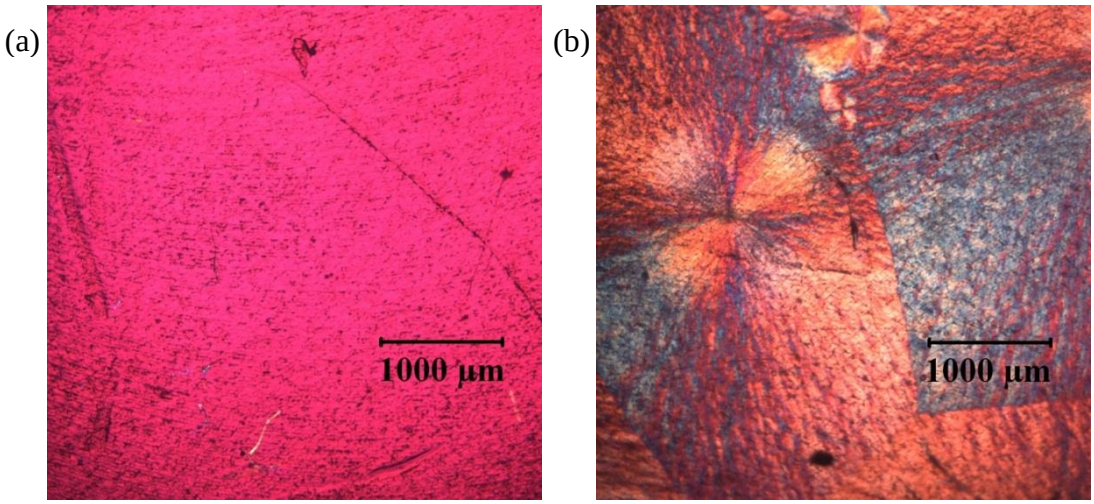

Figure 3. 17 Optical image of (a) blank PVC/DEHP and (b) 5 wt% SNAP-doped PVC/DEHP film surface taken under crossed polarizers in combination with a quarter-wave plate. The 5 wt% film clearly shows patterns which suggest the presence of crystalline structures.

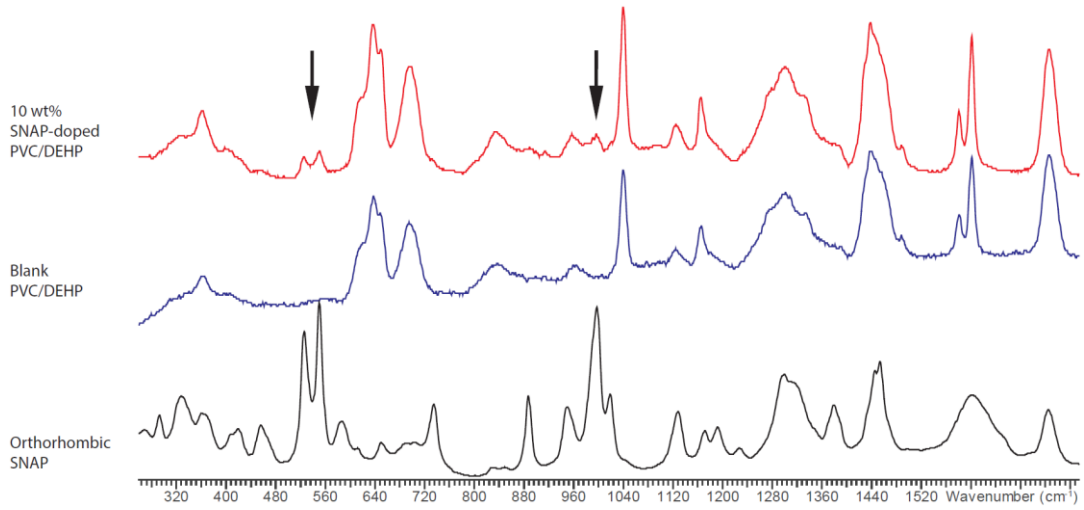

Figure 3. 18 Raman spectra comparison of orthorhombic SNAP (black), blank PVC/DEHP (blue) and 10 wt% SNAP-doped PVC/DEHP film (red). The existence of SNAP crystals in SNAP-doped PVC/DEHP is verified by the characteristic peaks of crystalline SNAP between 500-600 cm^{-1} and 950-1050 cm^{-1}.

PXRD patterns of SNAP-doped PVC/DEHP composites with various SNAP loadings agree with the Raman spectra in which the features of both orthorhombic SNAP and PVC/DEHP are presented. Similar to the SNAP/CarboSil films, as the initial loading of SNAP decreases, the intensity of orthorhombic SNAP characteristic peaks declines until those peaks become indistinguishable under certain threshold of SNAP loading (Figure 3.19). The crystal/polymer composite theory that explains the increased stability of SNAP doped within CarboSil can still be applied to this SNAP-doped PVC/DEHP system. At weight percentages lower than the solubility, all SNAP dissolves in the polymer and forms a homogenous film. When the SNAP weight percentage exceeds its solubility in PVC/DEHP polymer, the undissolved portion crystallizes as solvent evaporates, and remains as the thermodynamically most stable orthorhombic form in the polymer. The lattice energy of crystallization SNAP in polymer prevents SNAP from fast degradation, thus allows long-term NO storage and releasing.

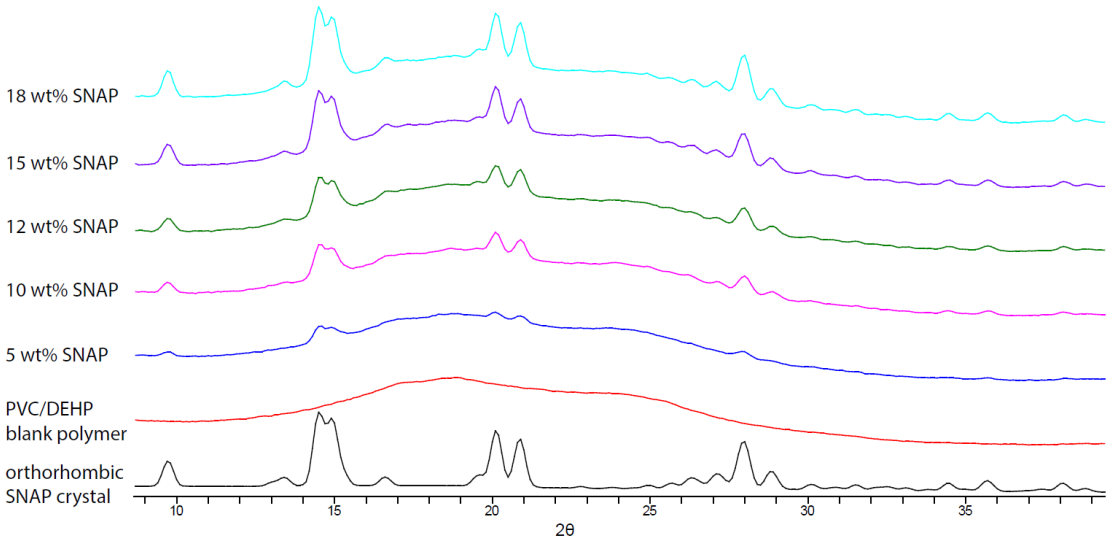

Figure 3. 19 Representative PXRD patterns of orthorhombic SNAP crystal, PVC/DEHP blank polymer, and SNAP-doped PVC/DEHP film samples of different weight percentages (5-18 wt%). Peak intensity of crystalline SNAP increased with higher loading of SNAP in polymer.

Due to the differences in PXRD patterns of CarboSil and PVC/DEHP that impeded the integration of pattern area, the height rather than the area of characteristic peaks is utilized for solubility calculation. Based on the following assumption that (1) crystalline SNAP is uniformly distributed in PVC/DEHP and that (2) the preferred orientation of SNAP crystals in PVC/DEHP could be eliminated by cutting samples into cubes and rotating the samples during data collection, at a chosen 2θ angle, the ratio of a specific SNAP PXRD peak height over the polymer PVC/DEHP signal height would be proportional to the ratio of crystalline SNAP weight percentage over the polymer weight percentage in the sample. By using the height ratio for quantification, all the other factors that can potentially influence the peak intensity (e.g., the volume of the sample irradiated by the X-ray source, the exposure time of sample under the X-ray, etc.) can be eliminated. Here, the solubility of SNAP in PVC/DEHP, represented as x_o, can be calculated from $y_{2\theta}$, the height ratio of the SNAP peak over the polymer peak at 2θ:

$$y_{2\theta} = \frac{I_{SNAP2\theta}}{I_{PVC/DEHP2\theta}} = \frac{a(x - x_o)}{b(1 - x)}$$

where $I_{SNAP2\theta}$ and $I_{PVC/DEHP2\theta}$ are the signal intensity of SNAP and PVC/DEHP in a SNAP-polymer sample at 2θ obtained from the measurement. For a PXRD pattern of a unit volume sample taken with a unit exposure time, a and b correspond to the peak height of pure orthorhombic crystal and blank PVC/DEHP pattern at 2θ, respectively. Consequently, for any SNAP-doped PVC/DEHP sample with the doped SNAP weight percentage of x, $y_{2\theta}$ as the height ratio of SNAP peak over PVC/DEHP signal at 2θ, which is independent of sample volume and exposure time, etc., is proportional to the weight percentage ratio of the undissolved orthorhombic SNAP crystal $(x - s)$ over the PVC/DEHP $(1 - x_o)$. By substituting various x and $y_{2\theta}$ at chosen 2θ angles, the solubility s can be determined. Based on calculation, the solubility of SNAP in PVC/DEHP is 1.8 ± 0.1 wt%. The height based equation has been also applied to all previously collected PXRD patterns of SNAP doped CarboSil films, and the calculated solubility of SNAP in CarboSil is 4.3 ± 0.3 wt%. The lower solubility of SNAP in PVC/DEHP compared with CarboSil is in agreement with the denser crystalline patterns in the light image of 5 wt% SNAP. Based on the crystallization theory, the low solubility of SNAP in PVC/DEHP explains the shelf-life study result of SNAP doped PVC/DEHP; the proportion of solubilized SNAP is small (the measured solubility in PVC/DEHP is even smaller than that in CarboSil), and most SNAP molecules are stabilized by the crystal lattice energy of orthorhombic SNAP.

3.2.4 SNAP-Impregnated CarboSil Composite

Sustained NO release has been achieved by composites of SNAP crystal and biomedical grade polymers, and the crystal distribution in SNAP-doped polymer films prepared by solvent evaporation method present is relatively uniform. However, like

many NO donors, SNAP or its analogs are sensitive to high temperatures, which are used during industrial catheter extrusion processes. As a result, alternative doping methods rather than solvent evaporation are needed to dope SNAP after polymer molding. In order to apply NO release to any pre-made or off the shelf biomedical devices, Colletta et al. developed a simple solvent impregnation method to load SNAP into commercially available silicone Foley urinary tract catheters under mild condition (room temperature).[26] In this approach, SNAP is dissolved in an organic solvent that can swell the polymer to a great extent without dissolving it, and as the polymer uptakes the solvent, the NO donors are loaded into the polymers. After drying to remove the solvent, the resulting polymer contains a stabilized form of the SNAP or analog of SNAP. As an example, commercial silicone Foley catheters were swelled in a SNAP solution prepared in tetrahydrofuran (THF) (125 mg/mL) for 24 h, resulting in SNAP impregnation of 5.43 ± 0.15 wt% SNAP in the final dried catheter. This level of SNAP loading enabled the catheters to achieve stable NO release above physiological levels for more than 4 weeks.

To investigate the properties of SNAP/CarboSil films prepared by different methods, the characterization methods utilized for films made by solvent evaporation were applied to films made by impregnation. Under polarized microscope, it was observed that the distribution of crystals on the surfaces of SNAP impregnated samples was not as uniform as the films prepared by evaporation (Figure 3.20). For samples with low SNAP loading, crystalline patterns were mainly discovered in some regions on the surface of the films despite the uniform dark green color of SNAP over the sample. The non-uniformity of the crystals may exhibit depth dependence by which the crystalline SNAP can be incorporated into the polymer thin film; crystallization merely on the surface would suggest unsuccessful impregnation. Therefore, optical images of the cross section of CarboSil impregnated with 5 wt% SNAP were taken under polarized light microscope. The results demonstrated that crystals were distributed randomly in the polymer interior rather than aggregated near to the surface

(Figure 3.21). The differences in crystal distribution (depth in the polymer) and grain sizes between polymers prepared by diverse methods can lead to variety in performance, which requires further NO release study to illustrate potential correlation.

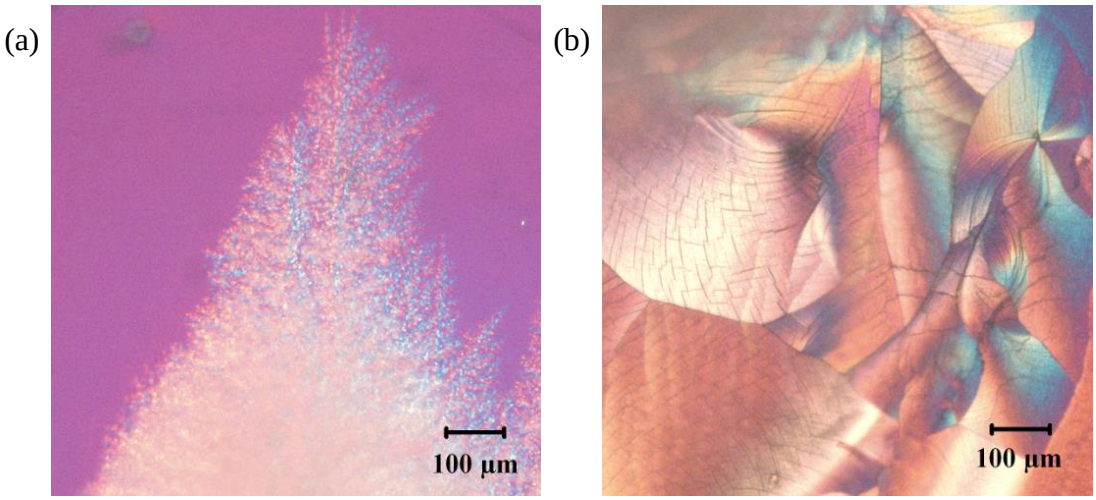

Figure 3. 20 Optical image of different regions of 5 wt% SNAP-impregenated CarboSil film surface taken under crossed polarizers in combination with a quarter-wave plate. The 5 wt% films presented crystalline patterns of various distribution and morphology.

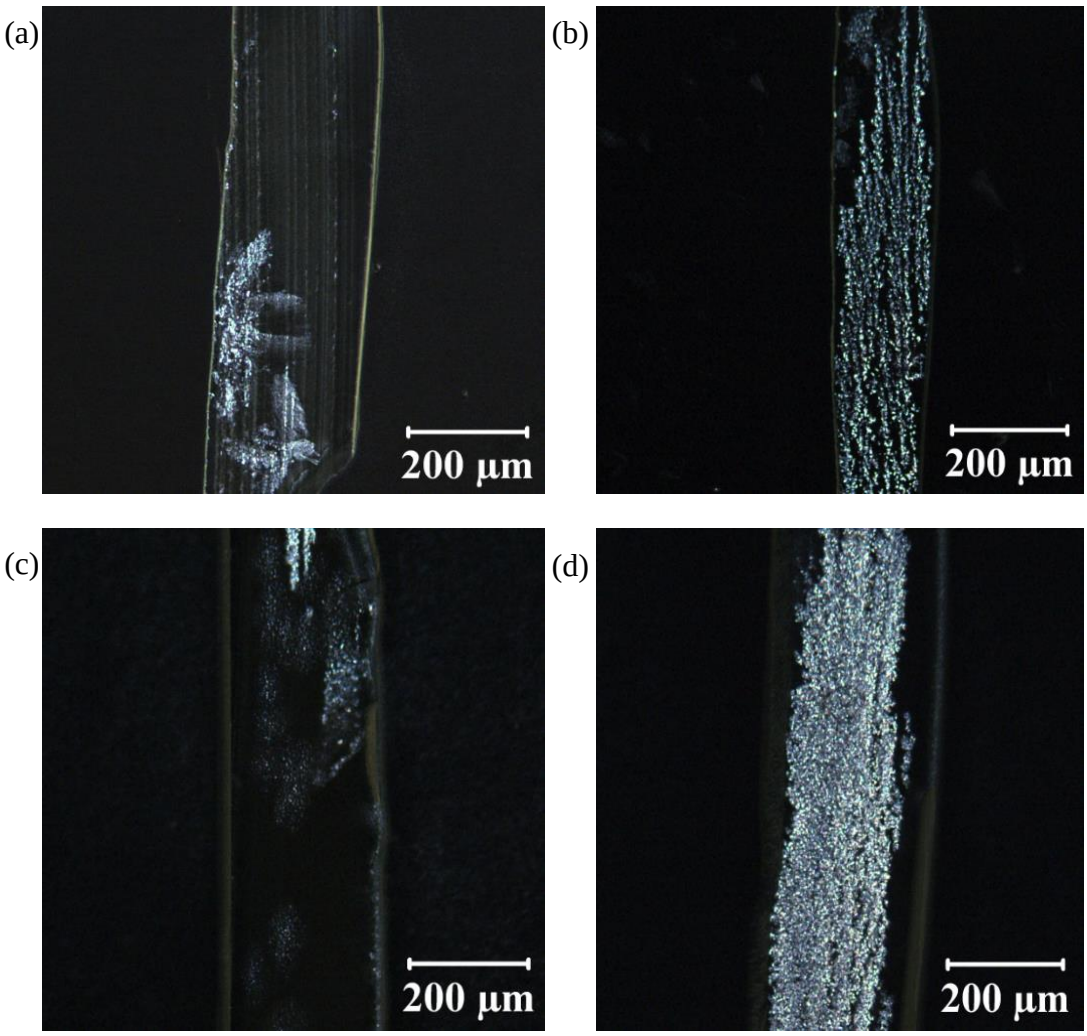

Figure 3. 21 Optical images of the cross section of CarboSil samples impregnated with SNAP taken under polarized light microscope. All samples were with 5 wt% SNAP loading and treated by microtome. The crystal grain sizes and distribution appeared to be random and uncorrelated with film thickness.

StreamLine High Resolution (HR) Raman mapping characterization was utilized to elucidate the chemical constituent of crystals inside of the SNAP-impregnated CarboSil in combination with the 2D representation of crystal distribution (Figure 3.22). Similar to what was observed in CarboSil doped with SNAP by solvent evaporation, in SNAP-impregnated CarboSil films, the regions with visible crystalline patterns under polarizer presented characteristic peaks between 500-600 cm^{-1} that matched with SNAP crystals. Despite the differences in crystal morphology observed

under optical microscope, PXRD analysis indicated that these SNAP crystals were still in the orthorhombic form. Therefore, SNAP has been successfully impregnated into premade polymers, and the differences between such prepared composites and those by solvent evaporation lie in crystal grain sizes and distribution.

(a)

(b)

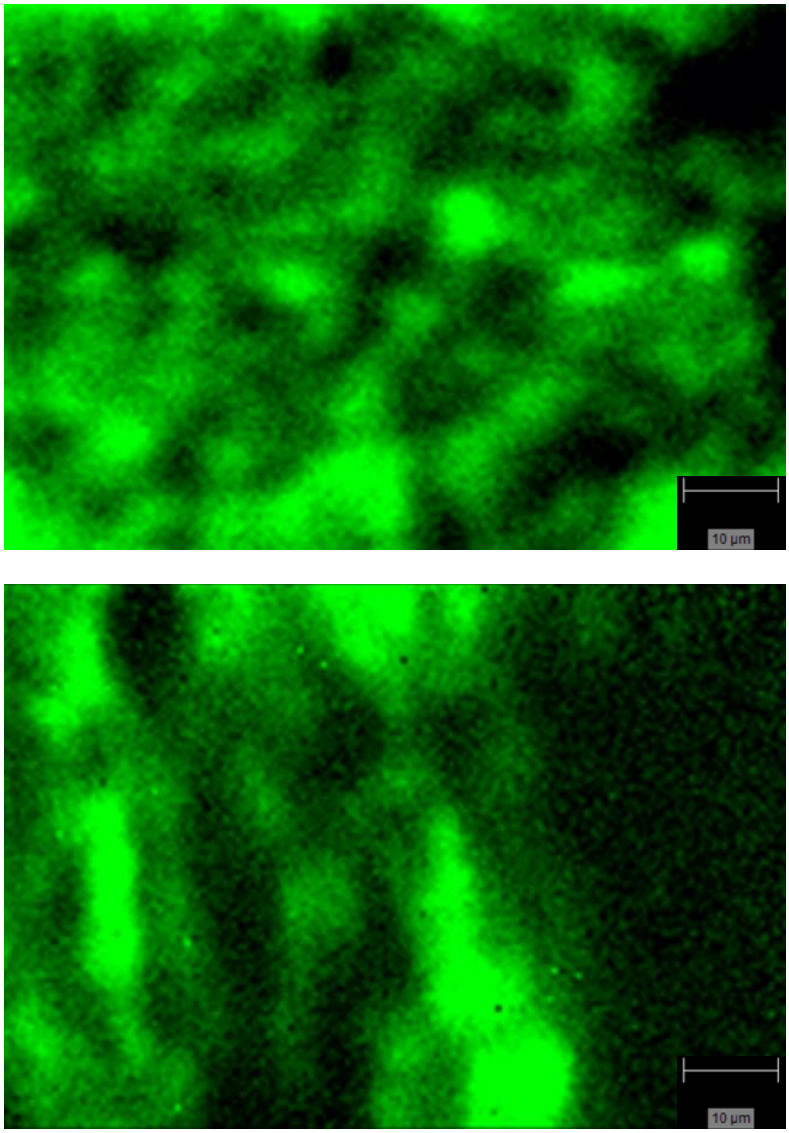

Figure 3. 22 StreamLine HR Raman mapping results for fitting of cross section of CarboSil samples 5 wt% SNAP loading prepared by (a) solvent evaporation and (b) impregnation with pure orthorhombic SNAP spectrum as the reference under 50× objective. Green represents areas fitting the spectrum of orthorhombic SNAP. The distribution of crystalline SNAP in the impregnated sample is less uniform.

In principle, SNAP solubility in CarboSil should be constant regardless of preparation methodology. PXRD patterns of the CarboSil films impregnated with various loading

of SNAP were collected (Figure 3.23), and the "solubility" of impregnated SNAP in CarboSil was calculated by applying the peak intensity based equations. The obtained "solubility" was 2.4 ± 0.1 wt%, significantly lower than the 4.3 ± 0.3 wt% result of films made by evaporation.

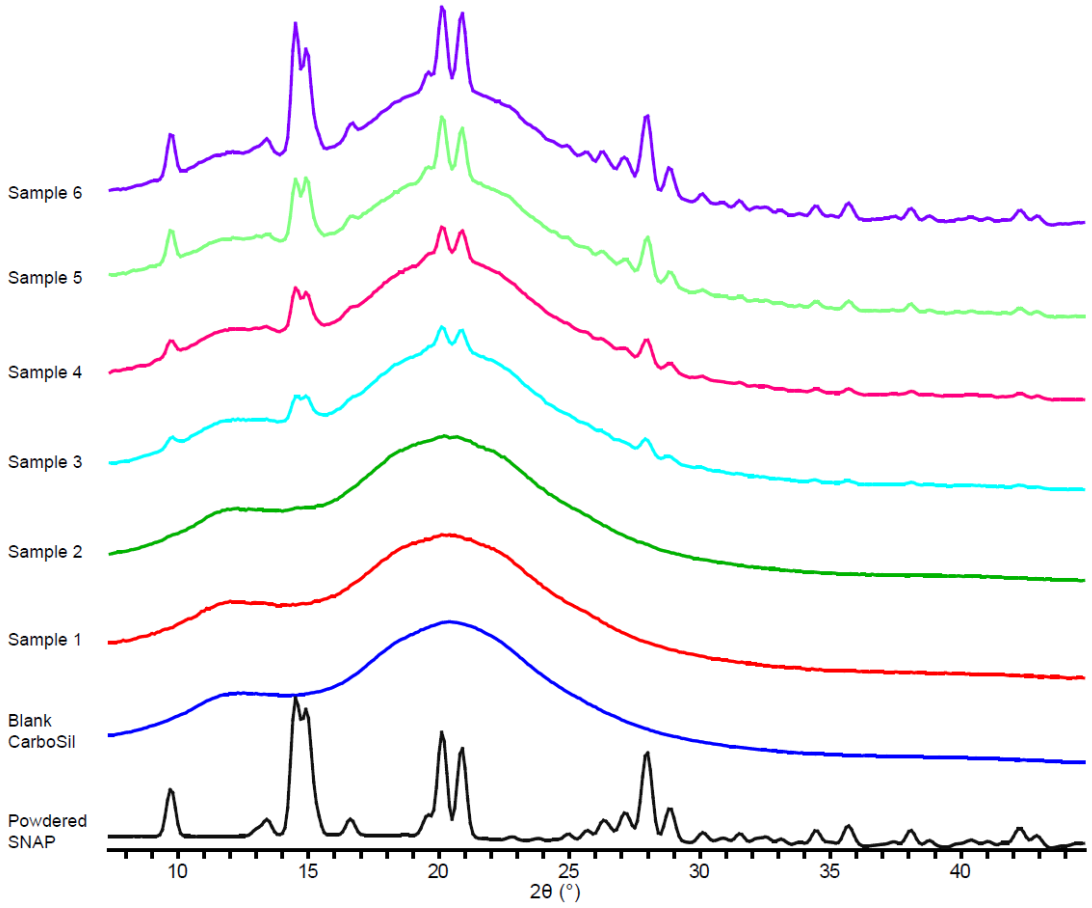

Figure 3. 23 Representative PXRD patterns of orthorhombic SNAP crystal, CarboSil blank polymer, and CarboSil impregnated with SNAP of different weight percentages. Characteristic peaks of orthorhombic SNAP were detected in samples. Peak intensity of crystalline SNAP increased with higher loading of SNAP in polymer. The SNAP loadings on Sample 1 to 6 in the figure were 1.2, 3.2, 4.7, 6.4, 10.7 and 13.5 wt%, respectively. Crystalline patterns of orthorhombic SNAP started to appear in Sample 2.

The decrease in calculated SNAP solubility can be attributed to insufficient "dissolution" of impregnated SNAP to reach the solubility equilibrium in premade polymer, which leads to higher proportion of insolubilized SNAP in the impregnated

composites compared to samples prepared by evaporation. Opposed to low SNAP loading samples prepared by solvent evaporation, where SNAP and CarboSil molecules were initially mixed well in solvent, that after solvent evaporation SNAP molecules are uniformly dispersed in the polymer matrix to form a solid polymer solution before reaching the solubility limit (Figure 3.24 (a)), impregnated samples were prepared by "inserting" SNAP molecules into the interspace between CarboSil chains in the premade polymers swelled by the THF solvent. The diffusion of SNAP molecules in solid polymers may be less efficient compared to that by the evaporation method. In addition, the swelling effect of THF can be varied for different segments in the polymer: the space in the soft segments may be expanded more and allow impregnation of more SNAP molecules, resulting in local SNAP crystallization (Figure 3.24 (b)). According to the previous crystallization based stability theory, the increased percentage of crystalline SNAP in polymer is beneficial for SNAP stability. The overall NO release performance of the impregnated composites, which need to be further investigated, can be affected synthetically by crystal grain size, distribution and proportion of crystallized SNAP.

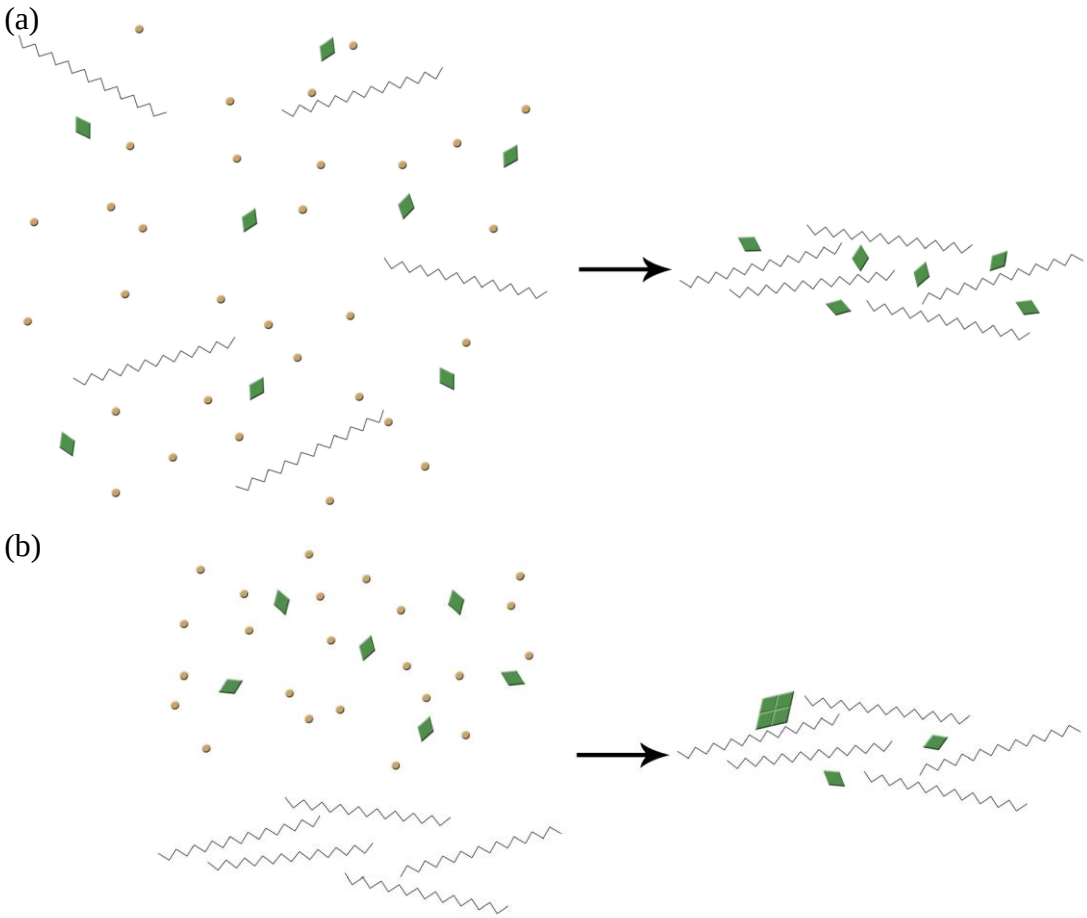

Figure 3. 24 Schematic diagram of SNAP distribution in CarboSil films prepared by (a) solvent evaporation and (b) impregnation. Chains correspond to CarboSil. Diamonds correspond to SNAP. Dots correspond to solvent.

3.3 Conclusions

A synthetic tertiary RSNO, SNAP, can be doped onto low water uptake polymers by solvent evaporation to achieve excellent stability and long term NO release capability, which shows great potential in application of biomedical device manufacture. Solid state studies of such SNAP-doped polymer system have been conducted to elucidate the mechanism under improved SNAP stability. Crystalline SNAP in the orthorhombic form has been detected in the polymer by polarized optical microscopy, Raman spectroscopy and PXRD analysis. Based on the discovery, a crystallization based theory has been proposed that SNAP can be partially dissolved in the polymer

and which forms a homogeneous "solid solution" with the polymer, while excess SNAP beyond the polymer solubility limit crystallizes in the orthorhombic form during the solvent evaporation process and embeds in the polymer. It is proposed that the lattice energy of crystalline SNAP is the key to the stability improvement, while the solubilized SNAP behaves as a solute, which is more reactive at ambient conditions that decomposes and releases NO. A 3.4-4.0 wt% solubility of SNAP in CarboSil has been determined by the ratio of selected orthorhombic SNAP peak area over the PXRD pattern total area of CarboSil with various SNAP loading. Comparison of SNAP stability in CarboSil films with 5 wt% and 15 wt% SNAP loading indicated that SNAP in the samples with lower loading decomposed much faster. In other word, the solubilized SNAP is the main portion that decomposed within 10 days, which verified the hypothesis that a greater proportion of crystalline SNAP is beneficial for stabilization.

This crystallization based stability hypothesis has been demonstrated in another system: SNAP-doped PVC/DEHP, a composite material for commercial catheters with desired stability presented in shelf-life study. Similar crystallization behavior was detected, and a 1.75 ± 0.13 wt% SNAP solubility in PVC/DEHP has been calculated based on the height ratio of selected orthorhombic SNAP peak over the signal of polymer at corresponding 2θ in PXRD analysis of CarboSil with various SNAP loading. The data agrees with the high crystal density and SNAP stability of this composite.

Impregnation is an alternative approach that can dope SNAP onto premade polymers, avoiding thermal decomposition in the catheter extrusion process which undergoes high temperature. Despite a less uniform distribution, it has been demonstrated in solid state studies that SNAP has been successfully impregnated into CarboSil. A 2.41 ± 0.09 wt% solubility of SNAP has been calculated, which is lower than the

result in films prepared by solvent evaporation. The higher proportion of crystalline SNAP in impregnated samples may be attributed to insufficient “dissolution” of SNAP in CarboSil in this method.

3.4 Experimental

3.4.1 Materials

N-acetyl-D-penicillamine (NAP), sodium nitrile and tetrahydrofuran (THF) were purchased from Sigma-Aldrich (St. Louis, MO). CarboSil 20 80A was obtained from DSM Biomedical Inc. (Berkeley, CA). SNAP was synthesized by equimolar NAP and sodium nitrite in a 1:3 mixture of water and methanol with 2M H_2SO_4 and 2M HCl following the literature procedure.[38]

3.4.2 Preparation of SNAP Films

Polymer films with different wt% SNAP prepared by solvent evaporation were made based on the previously reported method: selected polymers were dissolved in THF, followed by the addition of SNAP. The well mixed solution were cast in Teflon wells and allowed to dry overnight under ambient conditions.

For preparing SNAP-impregnated films, blank CarboSil films were impregnated in SNAP-containing methanol and methyl ethyl ketone (30:70 v/v) solvent mixtures for 2 h at room temperature. Various concentrations of SNAP solutions were employed to achieve different SNAP loading in the polymer. Then the films were removed from the solutions and dried in ambient conditions and protected from light exposure before use. 5 wt% SNAP-impregnated CarboSil films were embedded in optical cutting temperature (OCT) compound and allowed to be solidified at -20 ℃. Then the films

samples were cut into 30 μm thick slides in the cryostat microtome **(Leicia 3050S Cryostat)** and attached onto glass slides for Raman spectroscopy analysis.

3.4.3 Polarized Optical Microscopy

SNAP-doped Polymer films with 5 wt% SNAP loading and blank reference film of corresponding polymer, both without topcoats, were prepared as described above. Optical images were captured by a Leica DMLP polarization microscope equipped with an N Plan 10× objective under crossed polarizers in combination with a quarter-wave plate, and were then taken with a SPOT Flex Mosaic 15.2 camera using SPOT 5.2 Software from Diagnostic Instruments, Inc. For SNAP-impregnated CarboSil slides prepared by microtome, the quarter-wave plate was not utilized.

3.4.4 Raman Spectroscopy Characterization

Raman spectra were collected by using a Renishaw inVia Raman microscope equipped with a Leica microscope, a RenCam CCD detector and a 633nm laser employing an 1800 lines/nm grating and a 50 μm slit. Spectra were obtained using the WiRE 3.4 software package. Calibration was performed using a silicon standard in static mode. Full spectra of blank polymers (without SNAP), pure SNAP crystals and SNAP-doped polymer composites were collected through an Olympus SLMPlan 20× objective in extended scan mode in the range of 100-4000 cm^{-1} and further analyzed by ACD/SpecManager Version 12.01 software from Advanced Chemistry Development, Inc. For Raman mapping characterization, SNAP-doped CarboSil samples were cut into thin strips and laid down on the stage with the cross section facing upwards. Raman cross-section mapping data were obtained by using an Olympus SLMPlan 100× objective in combination with an automatic Renishaw MS20 encoded stage in static scan mode. The mapping data were analyzed using the Wire 3.4 software package component direct classical least squares (DCLS) analysis routines with the full spectra of blank CarboSil and pure SNAP crystals as references.

StreamLine HR Raman Mapping experiments were conducted by using a Renishaw inVia Raman microscope equipped with a Leica microscope, a RenCam CCD detector and a 785nm laser employing an 1200 lines/nm grating and a 50 μm slit.

3.4.5 Powder X-ray Diffraction Measurements

SNAP-doped Polymer films with 1-15 wt% SNAP loading and blank reference film of corresponding polymer, all without topcoats, were prepared as described in Section 3.4.2. Powder X-ray diffraction (PXRD) patterns were collected at room temperature using a Rigaku R-Axis Spider diffractometer with an image plate detector and graphite monochromated Cu-Kα radiation (λ = 1.54187Å) at 40 kV and 44 mA. Synthesized SNAP crystals were finely ground to eliminate preferred orientation, whereas blank CarboSil and SNAP-doped CarboSil samples were cut into cubes with dimensions of approximately 250 μm. All samples were mounted on a CryoLoop™ using heavy mineral oil, and images were collected for 15 min with a 0.3 mm collimator. The ω-axis was oscillated between 120° and 180° at 1°/sec, the ϕ-axis was rotated at 10°/sec, and χ-axis was fixed at 45°. The obtained images were integrated from 2.5 to 70° with a 0.1° step size in AreaMax 2.0 software from Rigaku. All powder patterns were processed using Jade 9 XRD Pattern Processing, Identification & Quantification analysis software from Materials Data, Inc. The simulated powder patterns of monoclinic and orthorhombic SNAP crystals were calculated in Mercury 3.3 from the CCDC and were compared with the experimental SNAP powder pattern in Jade 9. Linear least squares regression for quantitation of peak area ratios versus doped-SNAP weight percentage was performed in MATLAB. Linear least squares regression for quantitation of peak intensity ratios versus doped-SNAP weight percentage was performed in KaleidaGraph 3.5.

The 5 wt% and 15 wt% SNAP-doped samples were stored under ambient environment at room temperature for 10 days, assuming that the amount of dissolved

SNAP decompose after 10 d was comparable for both films. PXRD measurements of 5 wt% and 15 wt% SNAP/CarboSil film (both fresh and old) were taken and compared.

3.5 References

(1) Ratner, B. D. The catastrophe revisited: Blood compatibility in the 21st Century. *Biomaterials* **2007,** *28*, 5144-5147.

(2) Suchyta, D. J.; Handa, H.; Meyerhoff, M. E. A Nitric Oxide-Releasing Heparin Conjugate for Delivery of a Combined Antiplatelet/Anticoagulant Agent. *Molecular Pharmaceutics* **2014,** *11*, 645-650.

(3) Otto, M. Staphylococcal Infections: Mechanisms of Biofilm Maturation and Detachment as Critical Determinants of Pathogenicity. *Annual Review of Medicine* **2013,** *64*, 175-188.

(4) Kolluru, G. K.; Shen, X.; Kevil, C. G. A tale of two gases: NO and H(2)S, foes or friends for life?(). *Redox Biology* **2013,** *1*, 313-318.

(5) Genevieve, E. G.; Matthew, N.; Megan, C. F. S-Nitroso- N -acetyl-D-penicillamine covalently linked to polydimethylsiloxane (SNAP–PDMS) for use as a controlled photoinitiated nitric oxide release polymer. *Science and Technology of Advanced Materials* **2011,** *12*, 055007.

(6) Brisbois, E. J.; Handa, H.; Major, T. C.; Bartlett, R. H.; Meyerhoff, M. E. Long-Term Nitric Oxide Release and Elevated Temperature Stability with S-Nitroso-N-acetylpenicillamine (SNAP)-Doped Elast-eon E2As Polymer. *Biomaterials* **2013,** *34*, 6957-6966.

(7) Kiedrowski, M. R.; Horswill, A. R. New approaches for treating staphylococcal biofilm infections. *Annals of the New York Academy of Sciences* **2011,** *1241*, 104-121.

(8) Kolluru, G. K.; Yuan, S.; Shen, X.; Kevil, C. G. Chapter Fifteen - H2S Regulation of Nitric Oxide Metabolism. In *Methods in Enzymology*, Enrique, C.; Lester, P., Eds. Academic Press: 2015; Vol. Volume 554, pp 271-297.

(9) Shishido, S. l. M.; Seabra, A. B.; Loh, W.; Ganzarolli de Oliveira, M. Thermal and photochemical nitric oxide release from S-nitrosothiols incorporated in Pluronic

F127 gel: potential uses for local and controlled nitric oxide release. *Biomaterials* **2003,** *24*, 3543-3553.

(10) Hofler, L.; Koley, D.; Wu, J.; Xi, C.; Meyerhoff, M. E. Electromodulated release of nitric oxide through polymer material from reservoir of inorganic nitrite salt. *RSC Advances* **2012,** *2*, 6765-6767.

(11) Ren, H.; Colletta, A.; Koley, D.; Wu, J.; Xi, C.; Major, T. C.; Bartlett, R. H.; Meyerhoff, M. E. Thromboresistant/anti-biofilm catheters via electrochemically modulated nitric oxide release. *Bioelectrochemistry* **2015,** *104*, 10-16.

(12) Ren, H.; Wu, J.; Xi, C.; Lehnert, N.; Major, T.; Bartlett, R. H.; Meyerhoff, M. E. Electrochemically Modulated Nitric Oxide (NO) Releasing Biomedical Devices via Copper(II)-Tri(2-pyridylmethyl)amine Mediated Reduction of Nitrite. *ACS Applied Materials & Interfaces* **2014,** *6*, 3779-3783.

(13) Bohl, K. S.; West, J. L. Nitric oxide-generating polymers reduce platelet adhesion and smooth muscle cell proliferation. *Biomaterials* **2000,** *21*, 2273-2278.

(14) Brisbois, E. J.; Bayliss, J.; Wu, J.; Major, T. C.; Xi, C.; Wang, S. C.; Bartlett, R. H.; Handa, H.; Meyerhoff, M. E. Optimized polymeric film-based nitric oxide delivery inhibits bacterial growth in a mouse burn wound model. *Acta Biomaterialia* **2014,** *10*, 4136-4142.

(15) Brisbois, E. J.; Davis, R. P.; Jones, A. M.; Major, T. C.; Bartlett, R. H.; Meyerhoff, M. E.; Handa, H. Reduction in thrombosis and bacterial adhesion with 7 day implantation of S-nitroso-N-acetylpenicillamine (SNAP)-doped Elast-eon E2As catheters in sheep. *Journal of Materials Chemistry B* **2015,** *3*, 1639-1645.

(16) Frost, M. C.; Reynolds, M. M.; Meyerhoff, M. E. Polymers incorporating nitric oxide releasing/generating substances for improved biocompatibility of blood-contacting medical devices. *Biomaterials* **2005,** *26*, 1685-1693.

(17) Reynolds, M. M.; Frost, M. C.; Meyerhoff, M. E. Nitric Oxide-Releasing Hydrophobic Polymers: Preparation, Characterization, and Potential Biomedical Applications. *Free Radical Biology and Medicine* **2004,** *37*, 926-936.

(18) Reynolds, M. M.; Saavedra, J. E.; Showalter, B. M.; Valdez, C. A.; Shanklin, A. P.; Oh, B. K.; Keefer, L. K.; Meyerhoff, M. E. Tailored synthesis of nitric oxide-releasing polyurethanes using O2-protected diazeniumdiolated chain extenders. *Journal of Materials Chemistry* **2010,** *20*, 3107-3114.

(19) Reynolds, M. M.; Hrabie, J. A.; Oh, B. K.; Politis, J. K.; Citro, M. L.; Keefer, L. K.; Meyerhoff, M. E. Nitric Oxide Releasing Polyurethanes with Covalently Linked Diazeniumdiolated Secondary Amines. *Biomacromolecules* **2006,** *7*, 987-994.

(20) Simões, M. M. d. S. G.; de Oliveira, M. G. Poly(vinyl alcohol) films for topical delivery of S-nitrosoglutathione: Effect of freezing–thawing on the diffusion properties. *Journal of Biomedical Materials Research Part B: Applied Biomaterials* **2010,** *93B*, 416-424.

(21) Seabra, A. B.; Fitzpatrick, A.; Paul, J.; De Oliveira, M. G.; Weller, R. Topically applied S-nitrosothiol-containing hydrogels as experimental and pharmacological nitric oxide donors in human skin. *British Journal of Dermatology* **2004,** *151*, 977-983.

(22) Li, Y.; Lee, P. I. Controlled Nitric Oxide Delivery Platform Based on S-Nitrosothiol Conjugated Interpolymer Complexes for Diabetic Wound Healing. *Molecular Pharmaceutics* **2010,** *7*, 254-266.

(23) Keyaerts, E.; Vijgen, L.; Chen, L.; Maes, P.; Hedenstierna, G.; Van Ranst, M. Inhibition of SARS-coronavirus infection in vitro by S-nitroso-N-acetylpenicillamine, a nitric oxide donor compound. *International Journal of Infectious Diseases* **2004,** *8*, 223-226.

(24) Hetrick, E. M.; Schoenfisch, M. H. Analytical Chemistry of Nitric Oxide. *Annual Review of Analytical Chemistry* **2009,** *2*, 409-433.

(25) Riccio, D. A.; Schoenfisch, M. H. Nitric oxide release: Part I. Macromolecular scaffolds. *Chemical Society Reviews* **2012,** *41*, 3731-3741.

(26) Colletta, A.; Wu, J.; Wo, Y.; Kappler, M.; Chen, H.; Xi, C.; Meyerhoff, M. E. S-Nitroso-N-acetylpenicillamine (SNAP) Impregnated Silicone Foley Catheters: A Potential Biomaterial/Device To Prevent Catheter-Associated Urinary Tract Infections. *ACS Biomaterials Science & Engineering* **2015,** *1*, 416-424.

(27) Carpenter, A. W.; Schoenfisch, M. H. Nitric Oxide Release Part II. Therapeutic Applications. *Chemical Society reviews* **2012,** *41*, 3742-3752.

(28) Coneski, P. N.; Schoenfisch, M. H. Nitric oxide release: Part III. Measurement and reporting. *Chemical Society Reviews* **2012,** *41*, 3753-3758.

(29) Handa, H.; Brisbois, E. J.; Major, T. C.; Refahiyat, L.; Amoako, K. A.; Annich, G. M.; Bartlett, R. H.; Meyerhoff, M. E. In vitro and in vivo study of sustained nitric oxide release coating using diazeniumdiolate-doped poly(vinyl chloride) matrix with poly(lactide-co-glycolide) additive. *Journal of Materials Chemistry B* **2013,** *1*, 3578-3587.

(30) Handa, H.; Major, T. C.; Brisbois, E. J.; Amoako, K. A.; Meyerhoff, M. E.; Bartlett, R. H. Hemocompatibility comparison of biomedical grade polymers using rabbit thrombogenicity model for preparing nonthrombogenic nitric oxide releasing surfaces. *Journal of Materials Chemistry B* **2014,** *2*, 1059-1067.

(31) Vaughn, M. W.; Kuo, L.; Liao, J. C. Estimation of nitric oxide production and reactionrates in tissue by use of a mathematical model. *American Journal of Physiology - Heart and Circulatory Physiology* **1998,** *274*, H2163-H2176.

(32) Hakim, T. S.; Sugimori, K.; Camporesi, E. M.; Anderson, G. Half-life of nitric oxide in aqueous solutions with and without haemoglobin. *Physiological Measurement* **1996,** *17*, 267.

(33) Coneski, P. N.; Schoenfisch, M. H. Synthesis of nitric oxide-releasing polyurethanes with S-nitrosothiol-containing hard and soft segments. *Polymer Chemistry* **2011,** *2*, 906-913.

(34) Wang, P. G.; Xian, M.; Tang, X.; Wu, X.; Wen, Z.; Cai, T.; Janczuk, A. J. Nitric Oxide Donors: Chemical Activities and Biological Applications. *Chemical Reviews* **2002,** *102*, 1091-1134.

(35) Lin, C.-E.; Richardson, S. K.; Wang, W.; Wang, T.; Garvey, D. S. Preparation of functionalized tertiary thiols and nitrosothiols. *Tetrahedron* **2006,** *62*, 8410-8418.

(36) de Oliveira, M. G.; Shishido, S. M.; Seabra, A. B.; Morgon, N. H. Thermal Stability of Primary S-Nitrosothiols: Roles of Autocatalysis and Structural Effects on the Rate of Nitric Oxide Release. *The Journal of Physical Chemistry A* **2002,** *106*, 8963-8970.

(37) Arulsamy, N.; Bohle, D. S.; Butt, J. A.; Irvine, G. J.; Jordan, P. A.; Sagan, E. Interrelationships between Conformational Dynamics and the Redox Chemistry of S-Nitrosothiols. *Journal of the American Chemical Society* **1999,** *121*, 7115-7123.

(38) Chipinda, I.; Simoyi, R. H. Formation and Stability of a Nitric Oxide Donor: S-Nitroso-N-acetylpenicillamine. *The Journal of Physical Chemistry B* **2006,** *110*, 5052-5061.

Chapter 4 Cocrystallization Driven by Introducing Soluble Polymers to Adjust Metastable Zone Width

Unpublished Work

4.1 Introduction

Energetic materials, including propellants, explosives and pyrotechnics, are a class of compounds with a large amount of stored chemical energy that can be released in a short period of time (Figure 4.1). Due to the rigorous requirements in properties including explosive power, oxygen balance, sensitivity and cost of synthesis, implementing new synthetic chemistry for explosives applications is risky and costly. A substitute is to explore polymorphism of existing materials to seek for forms with desired shock sensitivity, density, melting point or reactivity, due to the high dependence of explosive power on solid-state density. When no polymorph meets the application requirement, cocrystallization can be an alternative strategy to optimized existing energetic chemical entities.[1-7]

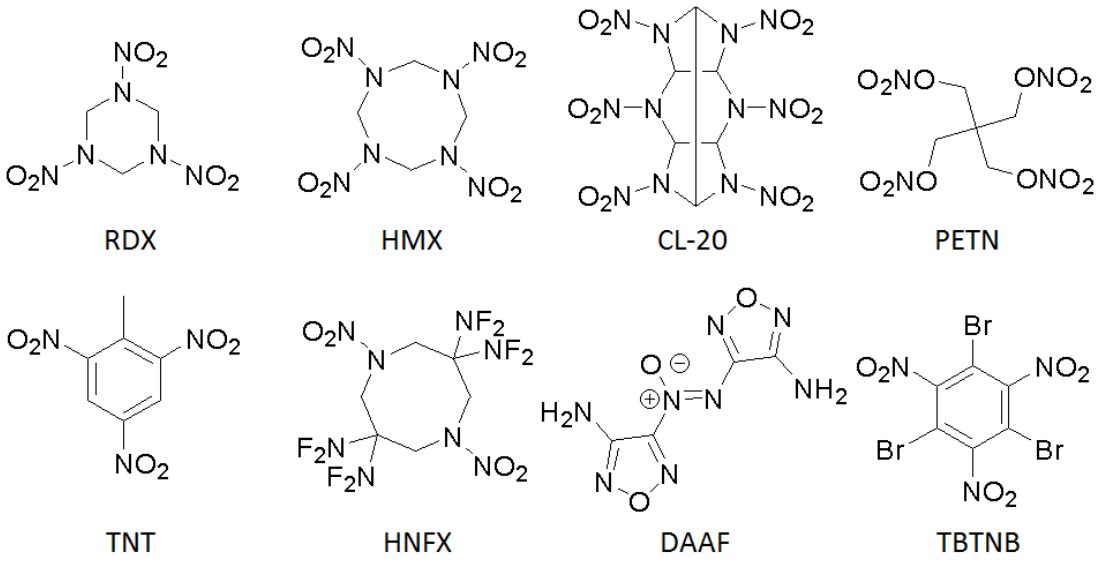

Figure 4. 1 Chemical structures of some energetic materials.

Cocrystallization has been widely applied in the field of pharmaceuticals. However, for energetic compounds, the functional groups in most active pharmaceutical ingredients that allow predictable interactions (eg: hydrogen bonding) for cocrystal formation are not always available. Landenberger et al. have successfully cocrystallized 2,4,6-trinitrotoluene (TNT), an energetic compound that has an electron-poor aromatic ring, with a wide range of coformers possessing electron-rich benzene rings.[1] The donor-acceptor π-π interactions between aromatic rings of both components are a reliable supramolecular synthon for cocrystal formation. Instead of the edge-to-face stacking seen in both polymorphs of TNT and most of the coformers in their pure form, in the obtained cocrystals face-to-face π-stacking was preferred due to the donor-acceptor π-π interactions.

However, not all electron-rich systems readily cocrystallize with TNT. Five compounds, including iminostilbene, triphenylamine, dibromobiphenyl, methyl-4-iodobenzoate and 1,3,5-tribromobenzene, have been selected as candidates to cocrystallize with TNT. The electrostatic potential surfaces of the five

cocrystallization candidates have been calculated (Figure 4.2). It can be seen that, similar to reported coformers that successfully cocrystallized with TNT, these compounds all possess relatively electron-rich aromatic rings, which are expected to introduce donor-acceptor π-π interactions with the electron-poor benzene ring in TNT.[1] Despite the π-rich systems, cocrystals consisting of TNT and these compounds appear to be less accessible. Following the same solvent evaporation crystallization method that successfully produced the reported TNT cocrystals, separate single component crystals of TNT and the selected candidates rather than cocrystals were obtained. Failure in cocrystallization can result from kinetic barriers: an example is the caffeine/benzoic acid cocrystal, which is thermodynamically stable but only cocrystallized in presence of nuclei.[8] Since π-π interaction synthon is available to form cocrystals, there can be other factors that hinder potential TNT cocrystallization.

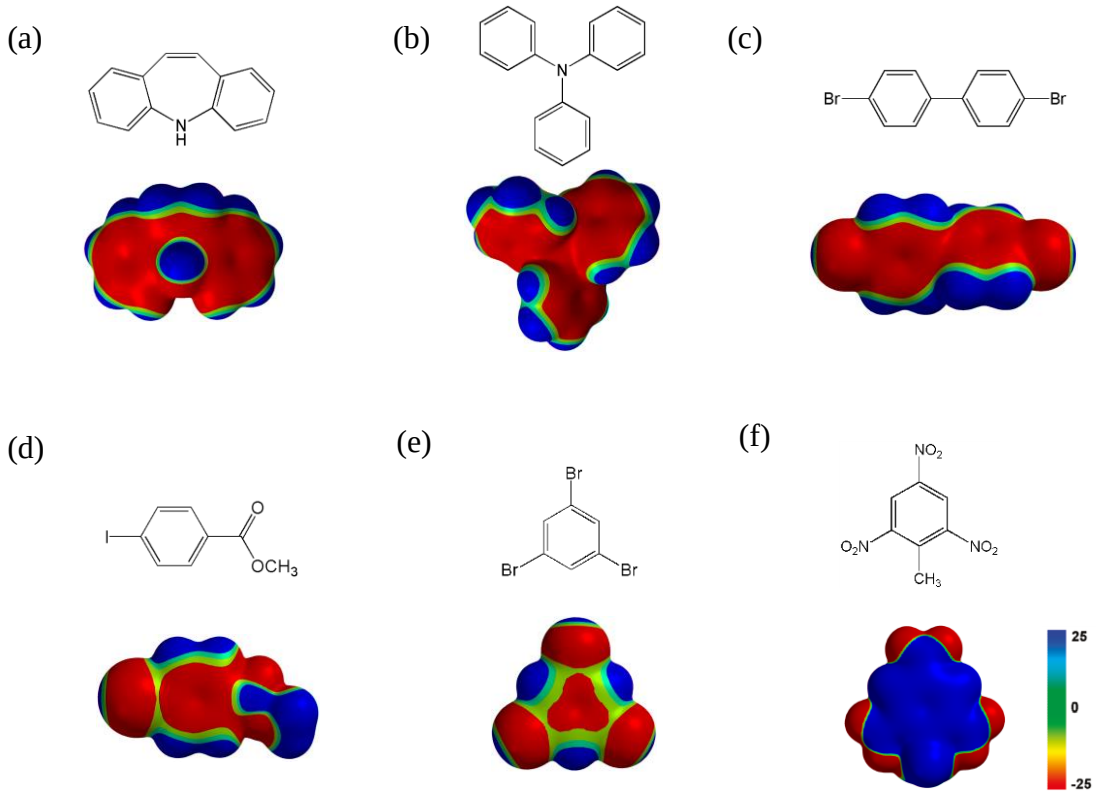

Figure 4. 2 Chemical structure and electrostatic potential surfaces of (a) iminostilbene, (b) triphenylamine, (c) 4,4'-dibromobiphenyl, (d) methyl-4-iodobenzoate, (e) 1,3,5-tribromobenzene and (f) TNT. Electrostatic potential surfaces were calculated using the semiempirical methods and the AM1 model. Red surfaces correspond to

electron rich regions. Blue surfaces correspond to electron poor regions. Surfaces are normalized between -25 and 25 kJ/mol. Electron-rich aromatic rings in (a) to (e) are expected to build up donor-acceptor π-π interactions with the electron-poor benzene ring in TNT that leads to cocrystallization.

As one of the decisive factors in solvent evaporation crystallization, solubility of all crystallizing components involved in this TNT cocrystallization issue, either those that succeeded or failed in forming cocrystals, were evaluated in search for factors that can impede potential cocrystallization. It was discerned that the solubility of most coformers that successfully cocrystallize with TNT are relatively high, accompanied by a broad metastable zone, which is the region between the solubility curve and the curve of the maximum supersaturation, referring to the range of concentration and temperature where crystallization is viable (Figure 4.3). On the other hand, failed candidates are usually less soluble, processing a narrow metastable zone width (MSZW). MSZW is defined as the temperature difference between the clear point (the point at which all suspended solid material disappears from solution during heating solution, corresponding to the solubility) and the cloud point (the point at which solids first appear in solution during cooling solution, corresponding to the maximum supersaturation) for a given concentration (Figure 4.3).[9, 10] It is hypothesized that the low solubility and narrow MSZW of the coformer with electron-rich aromatic rings favors single component crystallization, and the formed single component crystals compete with cocrystal formation. Therefore, increasing MSZW of the poorly soluble components or decreasing MSZW of the components with relatively high solubility is proposed as a new strategy to facilitate cocrystallization.

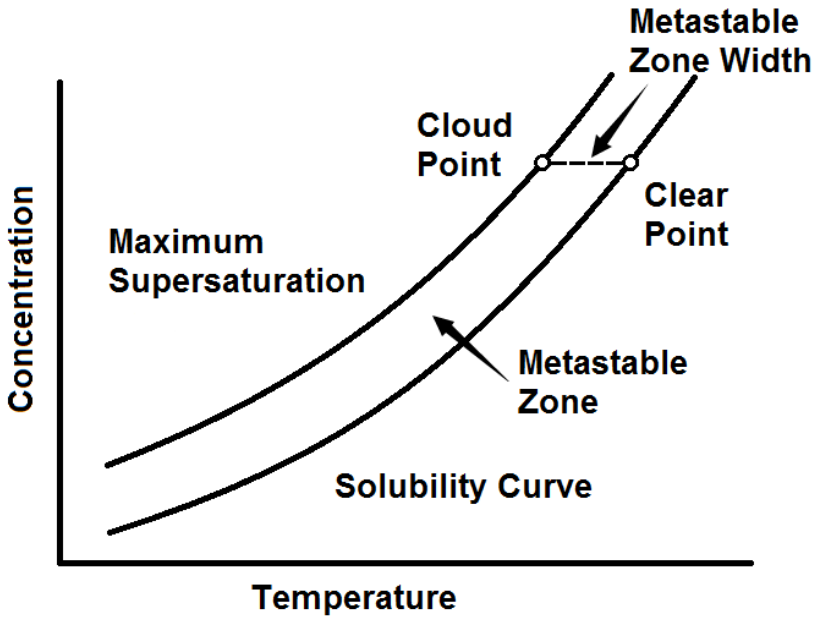

Figure 4. 3 Solubility curve and the metastable zone. Crystallization occurs in the metastable zone, where compounds are supersaturated in solution.

The proposed methodology to adjust the MSZW is to apply polymeric additives into the cocrystallizing solution. Polymers have been utilized to successfully suppress crystallization of poorly soluble drugs in amorphous solid dispersion formulations.[11-16] Furthermore, if a soluble additive efficiently inhibits crystal growth on specific crystal faces in solution, the strong interaction between the functional groups can be utilized to decrease the induction time of crystal appearance by incorporating the soluble additives into insoluble polymers.[17, 18] From the view of metastable zone based crystallization theory, polymeric inhibitors can broaden the MSZW by increasing the maximum degree of supersaturation. Here we propose that for components with significant difference in solubility that leads to formation of single component crystals independently, cocrystallization can be facilitated by introducing polymer additives to adjust the MSZW. By selectively suppressing crystallization of the less soluble compound, a higher concentration of this component can be achieved, which can be necessary for both components to crystallize simultaneously and form a cocrystal (Figure 4.4).

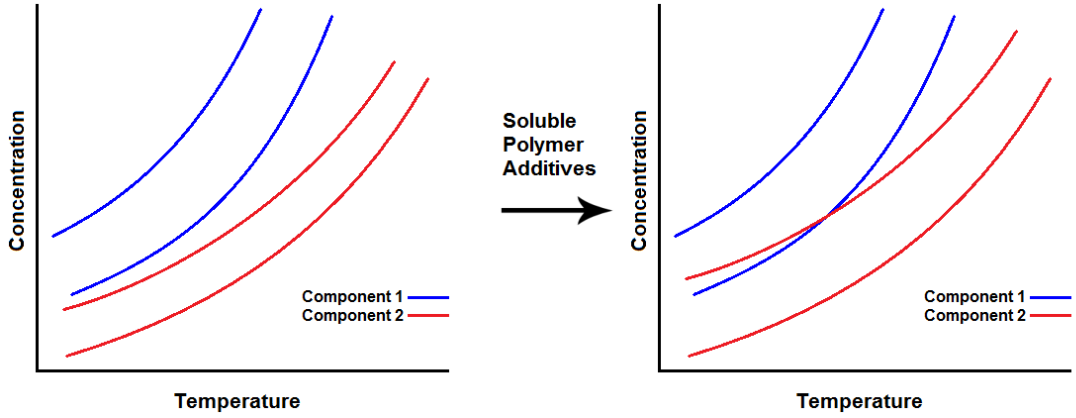

Figure 4. 4 Schematic plot of cocrystallization promoted by polymeric additives. The MSZW of crystallizing components can be adjusted by soluble polymeric additives. With metastable zones of both components included in the region where cocrystallization is viable, simultaneous crystallization of both components that forms a cocrystal rather than single component crystals can be favored.

4.2 Results and Discussion

4.2.1 Cocrystallization Failure in Poorly Soluble π -rich Systems

According to the calculated electrostatic potential surfaces of TNT and five selected cocrystallization candidates (Figure 4.5), it is possible for these π-rich compounds to pack into cocrystals with TNT by the donor-acceptor π-π interactions. In search for differences between the five selected compounds and those coformers reported in literature that can lead to cocrystallization failure, the widely used solvent evaporation method applied here has attracted attention.[1]

Products of solvent evaporation crystallization are highly dependent on the solubility of crystallizing compound in the corresponding solvent. This especially holds for cocrystallization systems with multiple components in presence. In order to elucidate factors that may impede cocrystallization, solubility and the metastable limit (the

maximum compound concentration in solution before crystal appearance) of the five candidates as well as several coformers that successfully cocrystallized with TNT in ethanol at 25 °C were measured (Table 4.1). All five candidates presented relatively low solubility. In molarity representation, only methyl-4-iodobenzoate is more soluble than TNT. On the other hand, solubility does not appear to be a limitation for those reported coformers. Since donor-acceptor π-π interactions have been shown to be a reliable synthon for TNT cocrystallization with the electron-rich systems, there should be supramolecular interactions available between selected candidates and TNT that enable cocrystal formation. It is therefore speculated that the unsuccessful cocrystallization is a kinetic result of the low solubility in ethanol rather than the inherent chemical structure of the candidate. Due to the low solubility in ethanol, the candidates precipitated in their single component crystalline states before they reached the requisite concentration for target cocrystallization, which acted as a strong competitor of the cocrystal pathway, leading to single component crystals of both the candidates and TNT as the final product.

Table 4. 1 Solubility and metastable limit of TNT and compounds applied for TNT cocrystallization in ethanol at 25 °C

Compound	Solubility (mg/mL)	Metastable Limit (mg/mL)	Solubility (mmol/mL)	Metastable Limit (mmol/mL)
TNT	16.6	24.1	0.074	0.106
iminostilbene	6.8	9.1	0.035	0.047
triphenylamine	10.5	17.1	0.043	0.070
4,4’-dibromobiphenyl	6.8	8.4	0.022	0.027
methyl-4-iodobenzoate	22.3	58.3	0.085	0.222
1,3,5-tribromobenzene	12.9	27.9	0.041	0.089

naphthalene	94.7	151.7	0.739	1.184
phenanthrene	31.6	47.8	0.177	0.268
phenothiazine	25.5	37.0	0.128	0.186
dibenzothiophene	25.5	30.5	0.120	0.166
1,2-phenylenediamine	77.9	142.8	0.721	1.321
2-aminobenzoic acid	123.2	267.0	0.898	1.947
4-aminobenzoic acid	88.6	133.5	0.646	0.973

The five compounds failed to form TNT cocrystal present relatively low solubility, whereas the coformers successfully cocrystallized with TNT are generally more soluble.

4.2.2 Adjusting Metastable Zone Width by Soluble Polymeric Additives

The most common way to solve poor solubility issues is to alter solvent. However, exploring the inhibitor effect can be another option. This method is advantageous because the conditions required to form multicomponent crystals can be highly specific so that the traditional strategy of changing solvent and temperature may not be applicable. By introducing soluble polymers with functional groups that can strongly interact with the target compound, a higher degree of supersaturation can be attained.

Eight polymers soluble in ethanol were selected as additives: hydroxypropyl cellulose, methyl vinyl ether/maleic acid copolymer, methyl vinyl ether/maleic anhydride copolymer, poly (acrylic acid), poly (vinyl butyral), poly (vinyl pyrrolidone), styrene/allyl alcohol copolymer, and vinyl alcohol/vinyl butyral copolymer. Solubility and metastable limit of five candidates as well as TNT in ethanol in the presence of 0 wt%, 0.01 wt%, 0.1 wt%, and 1 wt% polymer additives were measured following the

same characterization process. Apart for the situations where little polymeric additive effect was observed, there were three types of influences that can be introduced by the addition of soluble polymers.

Significant enhancement of metastable limit without corresponding solubility improvement was detected in several combinations. A typical example is iminostilbene in ethanol. As the weight percentage of specific soluble polymers (poly (acrylic acid), poly (vinyl butyral), styrene/allyl alcohol copolymer and vinyl alcohol/vinyl butyral copolymer) increased, iminostilbene crystallization was impeded (Figure 4.5). Similar behavior was detected in triphenylamine crystallization in presence of poly (vinyl butyral), styrene/allyl alcohol and vinyl alcohol/vinyl butyral copolymers, as well as 4,4'-dibromobiphenyl crystallization in presence of methyl vinyl ether/maleic acid and styrene/allyl alcohol copolymers. In these combinations, the polymeric additives successfully inhibited the formation of undesirable crystals. By enlarging MSZW, the poorly soluble candidates are present in solution at a high degree of supersaturation which is beneficial for cocrystallization. On the other hand, significant increase in TNT metastable limit at high temperature was observed in presence of poly (acrylic acid), which is a disadvantage for TNT cocrystallization with the poorly soluble compounds.

(a)

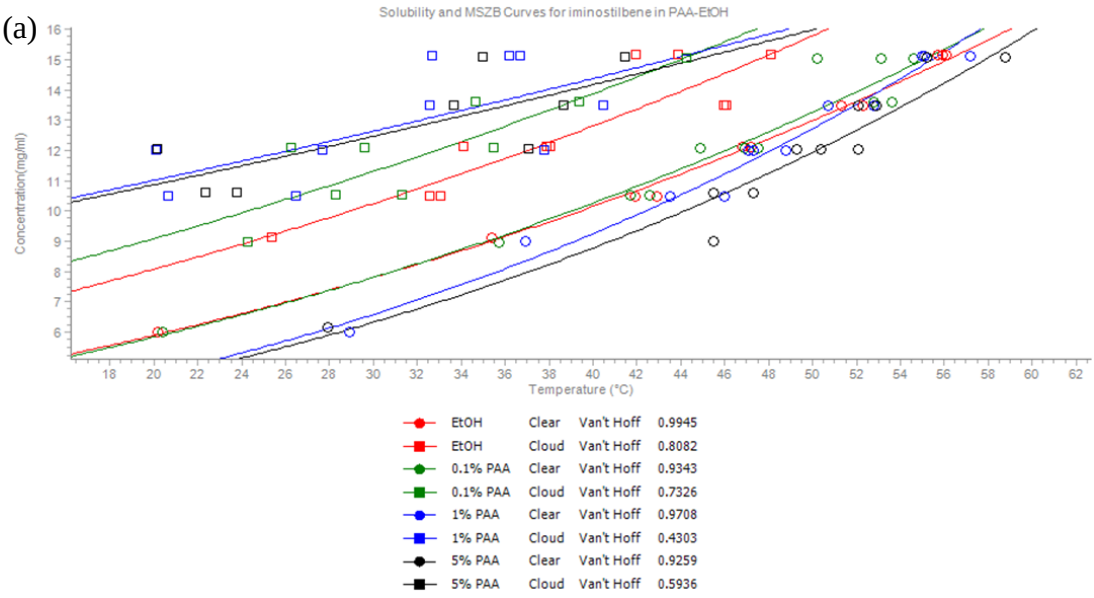

EtOH	Clear	Van't Hoff	0.9945
EtOH	Cloud	Van't Hoff	0.8082
0.1% PAA	Clear	Van't Hoff	0.9343
0.1% PAA	Cloud	Van't Hoff	0.7326
1% PAA	Clear	Van't Hoff	0.9708
1% PAA	Cloud	Van't Hoff	0.4303
5% PAA	Clear	Van't Hoff	0.9259
5% PAA	Cloud	Van't Hoff	0.5936

(b)

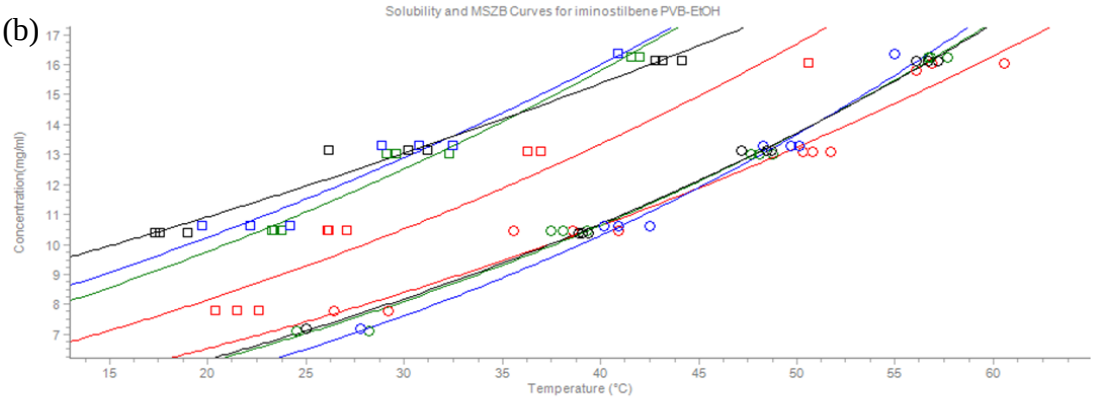

EtOH	Clear	Van't Hoff	0.9672
EtOH	Cloud	Van't Hoff	0.9288
0.01%PVB	Clear	Van't Hoff	0.9917
0.01%PVB	Cloud	Van't Hoff	0.9681
0.1%PVB	Clear	Van't Hoff	0.9793
0.1%PVB	Cloud	Van't Hoff	0.9507
1%PVB	Clear	Van't Hoff	0.9968
1%PVB	Cloud	Van't Hoff	0.9776

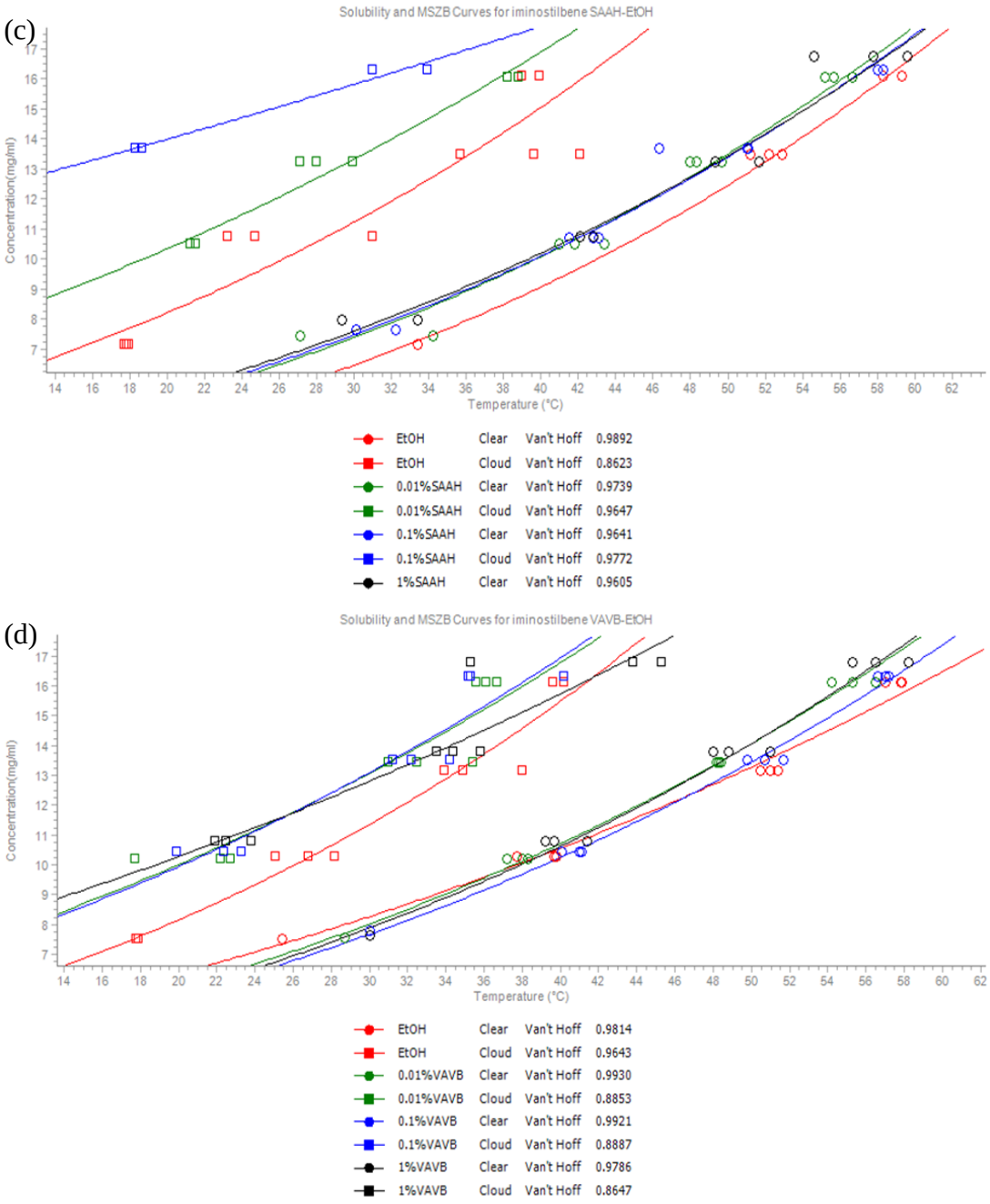

Figure 4. 5 Solubility and metastable limit of iminostilbene in ethanol solution in presence of (a) poly (acrylic acid), (b) poly (vinyl butyral), (c) styrene/allyl alcohol copolymer and (d) vinyl alcohol/vinyl butyral copolymer. Metastable limit was enhanced with the soluble polymer additives, allowing for higher degrees of supersaturation.

For the second type of candidate-additive combinations, both solubility and metastable limit of compound are improved the polymeric additives. Such behavior was detected in 4,4'-dibromobiphenyl in presence of hydroxypropyl cellulose and poly (vinyl butyral) (Figure 4.6), as well as 1,3,5-tribromobenzene in presence of poly (acrylic acid) and poly (vinyl pyrrolidone). In this case, MSZW of the compound was not guaranteed to increase. However, the metastable zone of poorly soluble compound was promoted to higher concentration, which can be beneficial for cocrystallization as well.

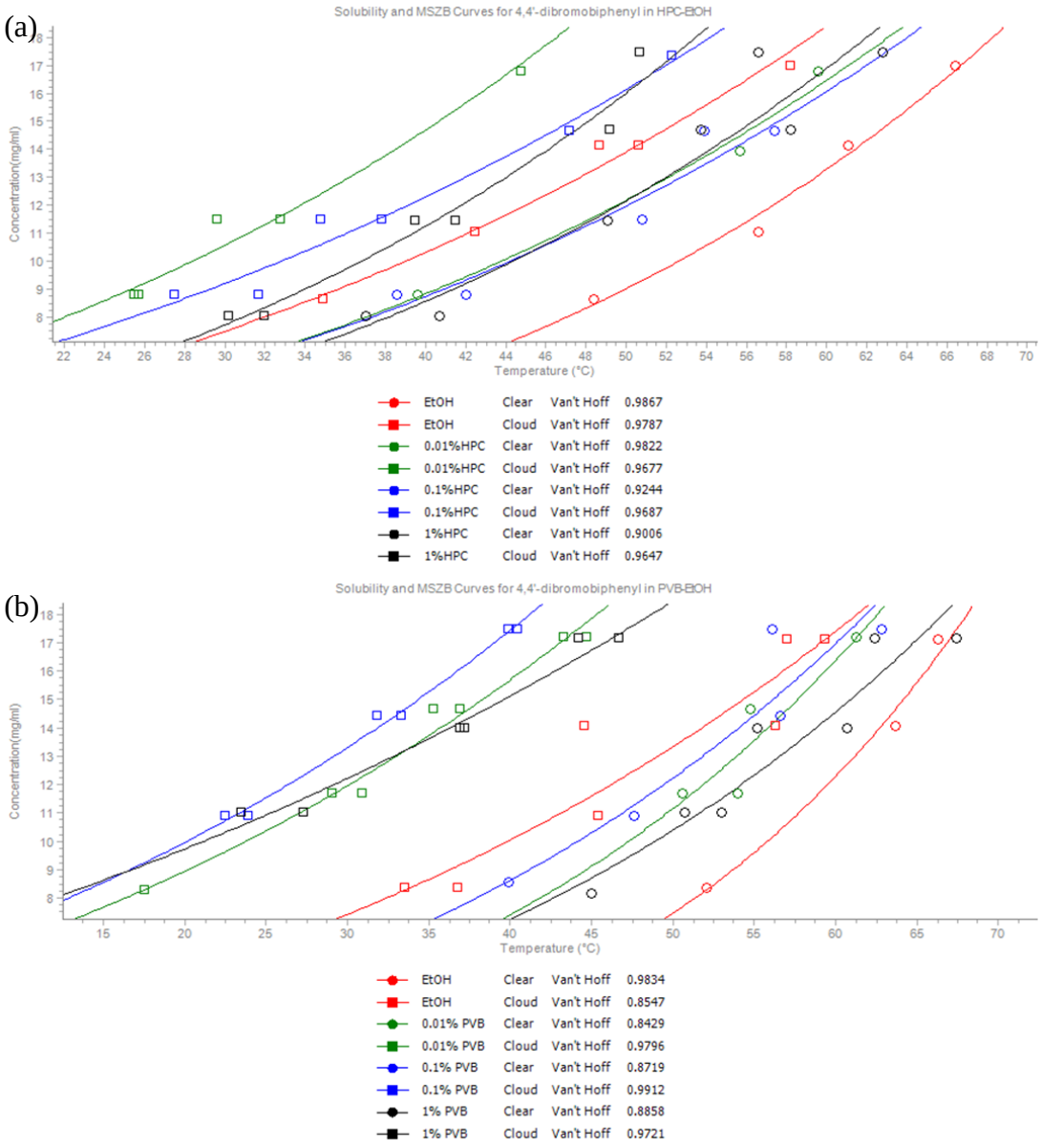

Figure 4. 6 Solubility and metastable limit of 4,4'-dibromobiphenyl in ethanol solution in presence of (a) hydroxypropyl cellulose and (b) poly (vinyl butyral). Both solubility and metastable limit increased in presence of the soluble polymer additives, allowing for higher degrees of supersaturation.

In the third scenario, single component crystallization can be promoted by polymer additives. In presence of hydroxypropyl cellulose or methyl vinyl ether/maleic anhydride copolymer, the metastable limit of iminostilbene decreased (Figure 4.7). As a result, MSZW of iminostilbene was reduced, and cocrystallization became less

likely. From the aspect of poorly soluble coformers, this promotion effect may not be helpful for simultaneous crystallization of both components to form cocrystals. However, it can be useful to promote a soluble component to crystallize at lower concentration, leading to the formation of cocrystals with poorly soluble coformers.

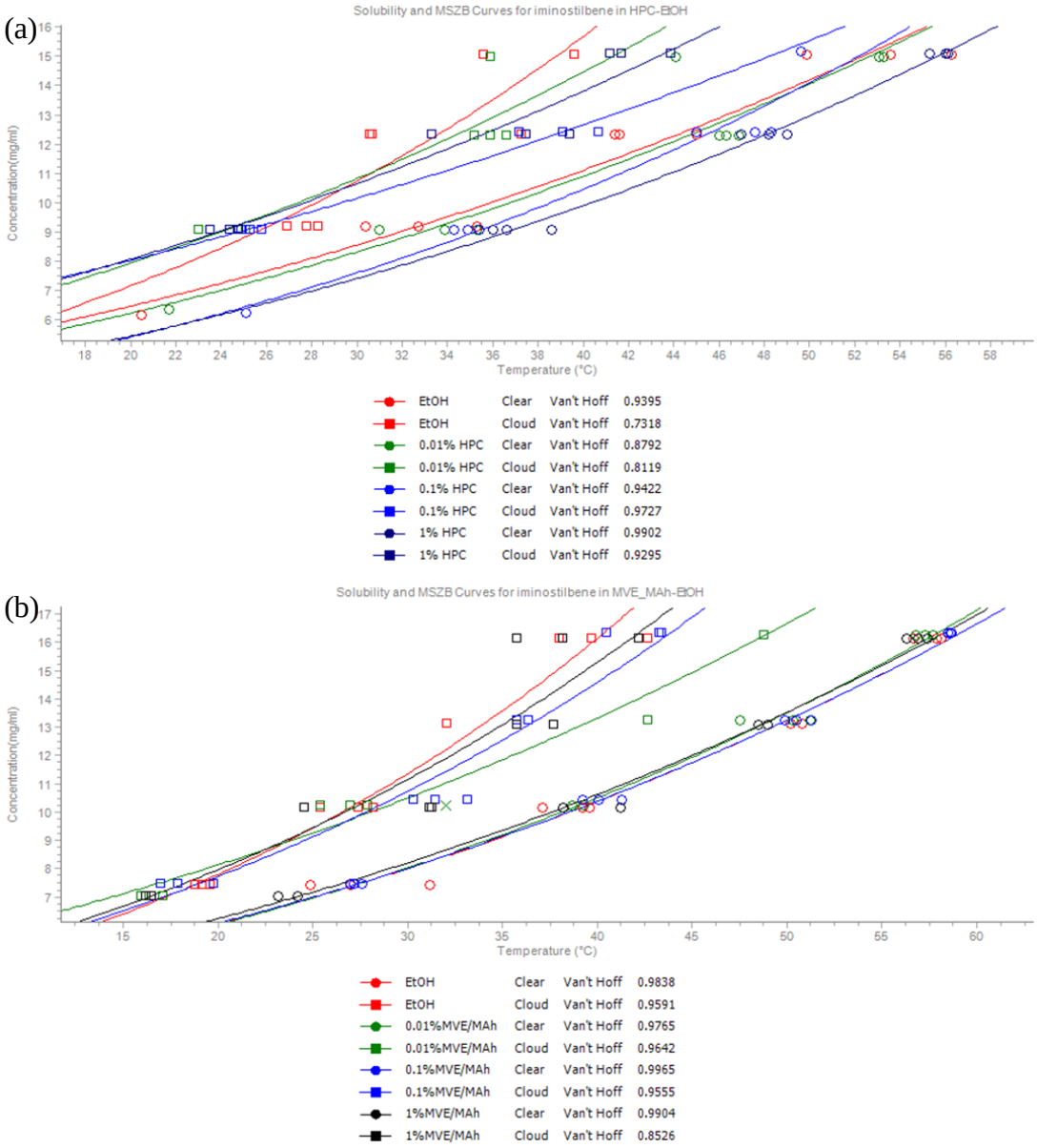

Figure 4. 7 Solubility and metastable limit of iminostilbene in ethanol solution in presence of (a) hydroxypropyl cellulose and (b) methyl vinyl ether/maleic anhydride copolymer. Metastable limit decreased with the soluble polymer additives, resulting in reduced MSZW.

4.2.3 Cocrystallization Experiments in the Presence of Polymeric Additives

In the presence of polymers that can increase the metastable limit of the selected poorly soluble compounds, crystallization experiments were conducted in order to obtain corresponding TNT cocrystals. The solvent evaporation method reported in literature was applied.[1] Instead of the reported pure ethanol solvent, ethanol solution with 0.01 wt%, 0.1 wt% and 1 wt% polymer additives was used as the crystallizing medium. Various volumes of the TNT solution and a different coformer solution were dispensed throughout 96 well polypropylene plates to obtain mixtures of different coformer ratios. After slow evaporation of ethanol, crystals were obtained. Known TNT cocrystals, TNT/naphthalene and TNT/4-aminobenzoic acid, were grown under this condition, which verified that cocrystallization would not be impeded by the polymeric additives. However, for the five selected candidates, despite the differences in morphology between crystals grown in the absence or presence of polymers, no cocrystals were discovered. In all trials of TNT cocrystallization with iminostilbene, triphenylamine, 4,4'-dibromobiphenyl and 1,3,5-tribromobenzene by solvent evaporation, only single component crystals of TNT and the corresponding coformer candidates were detected by Raman spectroscopy and PXRD analysis. It was noticed that due to the inhibition effect of polymeric additives, TNT became more reluctant to crystallize as the polymer weight percentage in solution increased. As a result, in many trials, only the coformer candidate crystallized. Therefore, tailor-made additives, the ones that can selectively interact with the poorly soluble coformer without disturbing crystallization of the soluble TNT, will be the ideal options.[18]

To avoid the formation of solid polymers that could act as heteronuclei in solvent evaporation, solution cooling method was also utilized in trials of TNT cocrystallization. In an ethanol solution with 1 wt% effective polymer additives, TNT and coformer candidates were dissolved under high temperature to form a uniform solution. Crystallization was then allowed at room temperature. Again the products

are identified as physical mixture of single component crystals of both crystallizing components by Raman spectroscopy and PXRD characterization. Failure to see cocrystals may be caused by the chosen concentration of both TNT and the selected compound; although several degrees of supersaturation of individual coformers was explored, without knowing the solubility of the (hypothetical) cocrystal the cocrystal region in the phase diagram may never be entered. Additionally, TNT cocrystals can be kinetic cocrystals, which easily convert to single component forms in the solvent medium.[5, 19]

Finally, it is possible that for the selected compounds, cocrystallization with TNT was not accessible due to their inherent properties: iminostilbene, triphenylamine and 4,4'-dibromobiphenyl are not planar molecules, and donor-acceptor π-π interactions may not be strong enough to overcome this steric hindrance, while methyl-4-iodobenzoate and 1,3,5-tribromobenzene are not as typical π-rich systems as the other three candidates. These properties are not kinetic issues that can be overcome by polymer additives.

4.3 Conclusions

Five compounds with electron-rich aromatic rings were expected to cocrystallize with TNT according to the calculated electrostatic potential surface indicating possible donor-acceptor π-π interactions. However, physical mixtures of single component crystals rather than cocrystals were obtained in cocrystallization trials by solvent evaporation method. In solubility comparison with coformer successfully cocrystallized with TNT, it is speculated that the failure in cocrystal formation can be due to the low solubility and narrow metastable zone of the selected compounds, which leads to formation of single component crystals.

In order to retain a high degree of supersaturation in solution favorable for cocrystallization, soluble polymer additives are proposed. Eight polymers soluble in ethanol were selected. With the presence of polymeric additives, the metastable zone width of compounds in solution can be efficiently altered. For the selected poorly soluble compounds, additives that increase the metastable limit are desirable for inhibiting single component crystal formation and promoting cocrystallization. Oppositely, for soluble coformers, polymer additives can lower the metastable zone, resulting in a cocrystallization region.

Although no new cocrystals were discovered in the trials of TNT cocrystallization in presence of soluble polymers, strong influence of polymeric additives on solubility and metastable limit has been verified in the metastable zone study. Therefore, adjusting the metastable zone width of cocrystalling components is be a potential strategy to grow previously unattainable cocrystals, and the utilization of polymer additives is a feasible approach to this tactic.

4.4 Experimental

4.4.1 Materials

TNT was synthesized and purified according to the published procedures.[10] Iminostilbene, triphenylamine and 4,4'-dibromobiphenyl were purchased from Acros Organics (New Jersey, USA). Methyl-4-iodobenzoate, and 1,3,5-tribromobenzene were purchased from Matrix Scientific (Columbic, SC). Hydroxypropyl cellulose, methyl vinyl ether/maleic acid copolymer, methyl vinyl ether/maleic anhydride copolymer, poly (acrylic acid), poly (vinyl butyral), poly (vinyl pyrrolidone), styrene/allyl alcohol copolymer, and vinyl alcohol/vinyl butyral copolymer were

purchased from Scientific Polymer Products, Inc (Ontario, New York). Ethanol was purchased from Decon Laboratories, Inc.

4.4.2 Solubility and Metastable Limit Measurement

All solubility and metastable limit data in chapter 4.2.1 and 4.2.2 were collected on a Crystal Breeder. Compounds were weighed in 8 mm clear round bot crimp vials. The vials were sealed after the addition of 100 μL of ethanol or polymer solution. The program was set to start at 20 °C, increase temperature at a 0.2 °C/min rate, hold at 65 °C for 30 min, and then decrease temperature at a 0.2 °C/min rate. Dissolution was facilitated by stirring. The existence of crystals was evaluated by turbidity.

All data listed in Chapter 4.2.1 Table 4.1 were obtained in ethanol. In Chapter 4.2.2 the solubility and metastable limit of iminostilbene, triphenylamine, 4,4'-dibromobiphenyl, methyl-4-iodobenzoate, 1,3,5-tribromobenzene and TNT were measured in ethanol and ethanol solution with 0.01 wt%, 0.1 wt%, and 1 wt% soluble polymer. For each compound, effect of eight polymers (hydroxypropyl cellulose, methyl vinyl ether/maleic acid copolymer, methyl vinyl ether/maleic anhydride copolymer, poly (acrylic acid), poly (vinyl butyral), poly (vinyl pyrrolidone), styrene/allyl alcohol copolymer, and vinyl alcohol/vinyl butyral copolymer) have been tested.

4.4.3 Cocrystallization Methods

Cocrystallization by solvent evaporation was performed in 96 well polypropylene plates. 0.02 M solution of TNT and cocrystallizing compound in ethanol or solution with 0.01 wt%, 0.1 wt%, and 1 wt% soluble polymer were prepared. Solutions were dispensed into the plates using a Gilson 215 liquid handler. The volumes of TNT

solution dispensed across each row were 0, 4, 5, 6, 7, 8, 10, 12, 13, 14, 15, and 16 μL. The volumes of coformer solution dispensed across each row were 20, 16, 15, 14, 13, 12, 10, 8, 7, 6, 5, and 4 μL. The resulting ratios of TNT to coformer were 0:1, 1:4, 1:3, 3:7, 7:13, 2:3, 1:1, 3:2, 13:7, 7:3, 3:1, and 4:1. After solution dispensing, the plates were covered by aluminum foil for slow solvent evaporation.

Cocrystallization in solution was performed by sealing both components as well as 50 μL ethanol or ethanolic solution with 1 wt% selected soluble polymer according to Section 4.2.2 results into 8 mm clear round bot crimp vials to create 2×, 3×, 4× and 5×component supersaturation. The solutions were heated to dissolve all solids, and cooled to room temperature to allow crystal formation.

4.4.4 Calculations

Calculations of the electrostatic potential energy density maps were performed. using semi-empirical methods with the AM1 model available in Spartan ’08 version 1.2.0 (Wavefunction, Inc.). All maps were normalized between -25 and 25 kJ/mol.

4.5 References

(1) Landenberger, K. B.; Matzger, A. J. Cocrystal Engineering of a Prototype Energetic Material: Supramolecular Chemistry of 2,4,6-Trinitrotoluene. *Crystal Growth & Design* **2010,** *10,* 5341-5347.

(2) Bolton, O.; Matzger, A. J. Improved Stability and Smart-Material Functionality Realized in an Energetic Cocrystal. *Angewandte Chemie International Edition* **2011,** *50,* 8960-8963.

(3) Landenberger, K. B.; Matzger, A. J. Cocrystals of 1,3,5,7-Tetranitro-1,3,5,7-tetrazacyclooctane (HMX). *Crystal Growth & Design* **2012,** *12,* 3603-3609.

(4) Bolton, O.; Simke, L. R.; Pagoria, P. F.; Matzger, A. J. High Power Explosive with Good Sensitivity: A 2:1 Cocrystal of CL-20:HMX. *Crystal Growth & Design* **2012,** *12,* 4311-4314.

(5) Landenberger, K. B.; Bolton, O.; Matzger, A. J. Two Isostructural Explosive Cocrystals with Significantly Different Thermodynamic Stabilities. *Angewandte Chemie International Edition* **2013,** *52,* 6468-6471.

(6) Landenberger, K. B.; Bolton, O.; Matzger, A. J. Energetic–Energetic Cocrystals of Diacetone Diperoxide (DADP): Dramatic and Divergent Sensitivity Modifications via Cocrystallization. *Journal of the American Chemical Society* **2015,** *137,* 5074-5079.

(7) Bennion, J. C.; McBain, A.; Son, S. F.; Matzger, A. J. Design and Synthesis of a Series of Nitrogen-Rich Energetic Cocrystals of 5,5′-Dinitro-2H,2H′-3,3′-bi-1,2,4-triazole (DNBT). *Crystal Growth & Design* **2015,** *15,* 2545-2549.

(8) Bucar, D.-K.; Day, G. M.; Halasz, I.; Zhang, G. G. Z.; Sander, J. R. G.; Reid, D. G.; MacGillivray, L. R.; Duer, M. J.; Jones, W. The curious case of (caffeine)[middle

dot](benzoic acid): how heteronuclear seeding allowed the formation of an elusive cocrystal. *Chemical Science* **2013,** *4*, 4417-4425.

(9) Kadam, S. S.; Kulkarni, S. A.; Coloma Ribera, R.; Stankiewicz, A. I.; ter Horst, J. H.; Kramer, H. J. M. A new view on the metastable zone width during cooling crystallization. *Chemical Engineering Science* **2012,** *72*, 10-19.

(10) Wang, L.; Feng, H.; Peng, J.; Dong, N.; Li, W.; Dong, Y. Solubility, Metastable Zone Width, and Nucleation Kinetics of Sodium Dichromate Dihydrate. *Journal of Chemical & Engineering Data* **2015,** *60*, 185-191.

(11) Trasi, N. S.; Taylor, L. S. Effect of polymers on nucleation and crystal growth of amorphous acetaminophen. *CrystEngComm* **2012,** *14*, 5188-5197.

(12) Ilevbare, G. A.; Liu, H.; Edgar, K. J.; Taylor, L. S. Impact of Polymers on Crystal Growth Rate of Structurally Diverse Compounds from Aqueous Solution. *Molecular Pharmaceutics* **2013,** *10*, 2381-2393.

(13) Ilevbare, G. A.; Liu, H.; Edgar, K. J.; Taylor, L. S. Maintaining Supersaturation in Aqueous Drug Solutions: Impact of Different Polymers on Induction Times. *Crystal Growth & Design* **2013,** *13*, 740-751.

(14) Marks, J. A.; Wegiel, L. A.; Taylor, L. S.; Edgar, K. J. Pairwise Polymer Blends for Oral Drug Delivery. *Journal of Pharmaceutical Sciences* **2014,** *103*, 2871-2883.

(15) Van Eerdenbrugh, B.; Taylor, L. S. Small Scale Screening To Determine the Ability of Different Polymers To Inhibit Drug Crystallization upon Rapid Solvent Evaporation. *Molecular Pharmaceutics* **2010,** *7*, 1328-1337.

(16) Wegiel, L. A.; Mauer, L. J.; Edgar, K. J.; Taylor, L. S. Crystallization of Amorphous Solid Dispersions of Resveratrol during Preparation and Storage—Impact of Different Polymers. *Journal of Pharmaceutical Sciences* **2013,** *102*, 171-184.

(17) López-Mejías, V.; Knight, J. L.; Brooks, C. L.; Matzger, A. J. On the Mechanism of Crystalline Polymorph Selection by Polymer Heteronuclei. *Langmuir* **2011,** *27*, 7575-7579.

(18) Pfund, L. Y.; Price, C. P.; Frick, J. J.; Matzger, A. J. Controlling Pharmaceutical Crystallization with Designed Polymeric Heteronuclei. *Journal of the American Chemical Society* **2015,** *137*, 871-875.

(19) Li, Z.; Matzger, A. J. Influence of Coformer Stoichiometric Ratio on Pharmaceutical Cocrystal Dissolution: Three Cocrystals of Carbamazepine/4-Aminobenzoic Acid. *Molecular Pharmaceutics* **2016,** *13*, 990-995.